Frequency Dependent Heat Generation during Vibrothermographic Testing of Composite Materials

by

Shiang-Shin Lin

Dissertation submitted to the Faculty of the
Virginia Polytechnic Institute and State University
in partial fulfillment of the requirements for the degree of
Doctor of Philosophy
in
Engineering Mechanics

APPROVED:

Edmund G. Henneke, II, Chairman

Kenneth L. Reifsnider

Wayne W. Stinchcomb

Mark S. Cramer

McIntyre R. Louthan, Jr.

August, 1987

Blacksburg, Virginia

Frequency Dependent Heat Generation during Vibrothermographic Testing of Composite Materials

by

Shiang-Shin Lin

Edmund G. Henneke, II, Chairman

Engineering Mechanics

(ABSTRACT)

This investigation concerns the frequency dependent heat generation behavior and the heat generation mechanisms for the thermal patterns of delamination in fiber reinforced composites during a vibrothermographic test, which uses real time thermography as a nondestructive evaluation of a structure or a component excited with mechanical vibration. A local resonance model was proposed in the past to describe the frequency dependent heat generation behavior during a vibrothermographic test, and this model was used as a basis for writing software for calculating the natural frequencies of a plate with the size of delamination. Vibrothermographic tests were performed on three glass-epoxy panels that each contained four different sized simulated delaminations. Comparison between the observed vibrothermal peak frequencies and the natural frequencies predicted by the local resonance model, and investigations of the thermoelastic emission field in the delamination region using SPATE, were made to determine the validity of the local resonance model. A significant conclusion of the results is that the local resonance is indeed the mechanics model for the frequency dependent heat generation behavior.

A careful measurement of the degree of heating of both sides of $[0_5]$ glass-epoxy panel with delaminations on the 2-3 ply interface, and comparison between the predicted heat patterns generated from a finite difference heat transfer program and observed heat patterns, was made to identify the heat generation mechanism. The results show that the majority of heat generation during vibrothermographic testing results from higher stresses or strains due to local resonance. The heat generation was affected by the combination of the principal strains and shear strain for the lower modes of resonant vibration, and was dominated by the shear strain for the higher modes of resonant vibration.

Impact damaged graphite-epoxy panels were also inspected constituting an application of vibrothermography on real damaged components. The degree of heating of the damage were measured through a frequency range, and the damage severity was inspected by ultrasonic C-scan and edge replication. From comparison of two plots of the degree of heating versus exciting frequency, either the area under the curve or the number of vibrothermal peak frequencies, the severity of the damage can be qualitatively identified.

Acknowledgements

The author wishes especially to thank Dr. Edmund G. Henneke, II for the patience, advice, assistance, and encouragement he received during his years at Virginia Tech.

Also appreciation and sincere thanks to:

- Dr. K. L. Reifsnider, Dr. W. W. Stinchcomb, Dr. M. S. Cramer, and Dr. M. R. Louthan, Jr. for their advice and for serving on his committee.
- Dr. H. P. Day, Jr. for his advice and for serving on his preliminary examination committee.
- Mr. R. L. Davis, Mr. George Lough, Mr. G. K. McCauley, Mr. Mike DeBusk for their assistance in the laboratory.
- Mr. Chuck Bakis and Mrs. Barbara Wengert for their assistance.
- His wife Hui-Chun for her support and encouragement during this endeavor.

Table of Contents

List of Illustrations

List of Tables

1. INTRODUCTION

In the past decade, composite materials have been used more and more often. However, most of the nondestructive testing methods used today were originally developed for detecting flaws in metals. Because of the complex nature of high performance composite materials, the interpretation of the results obtained from the nondestructive testing are more difficult.

Among the most widely used NDT methods is ultrasonics; however, one disadvantage of this technique is the tedious scanning procedures required to inspect large surface areas. This disadvantage leads to the research of the thermographic infrared technique as an alternate method for the detection of flaws. Video thermography can inspect large surface areas of the advanced composite material in a fraction of a second.

Thermography is the technique used to visualize surface temperature of an object, and generally refers to the thermal image pattern of a full-field temperature distribution rather than one selected surface point. The thermal image

is generally presented as isothermal lines on the surface and can be obtained by either of two methods: chemical imaging (contact method) or electronic imaging (noncontact method) .

To apply a chemical imaging method, a temperature-sensitive coating must be placed upon the surface of the test object to be examined. A change in temperature is evidenced by a change in color or appearance of the coating due to a temperature-sensitive chemical or physical change. An example of this is the use of a liquid crystal coating on the surface as a temperature sensor. This technique needs preparation of the surface before the liquid crystal coating can be applied. The temperature difference between isotherms varies and must be calibrated with each liquid crystal application. The biggest disadvantage is that for different ranges of temperatures, different sets of liquid crystals must be selected. The most widely used electronic imaging system is a real time scanning infrared camera. Although more costly, this system is much more flexible, requiring little surface preparation, and allowing one to change the range of isotherms while a test is being performed. Additional details may be found in the survey presented in Ref. 1. In this study, an AGA Thermovision infrared camera is used.

Thermal-field generation can be accomplished in two ways, termed 'passive' and 'active' heating. In passive heating, a portion of the surface or the whole surface to be examined is heated by an external heat source. Different thermal conductivities in the regions of defects in the material then can produce thermal gradients on the material surface which can be used to characterize the defects. In the second type of thermal excitation, active heating, the heat is

produced actively in the specimen by transformation processes which occur while the test object is being subjected to a normal operating, testing, or loading condition. For example, stress sensitive hysteresis effects in the material are used to generate heat internally in the material during cyclic loading. Other phenomena, such as crack-surface rubbing, can also produce heat locally. The technique to transform mechanical energy into thermal energy to produce an heat image, is also termed vibrothermography. This method can be divided into at least two classes: large displacement-low frequency mechanical excitation (cyclic loading) and small displacement-high frequency excitation (excited ultrasonically).

Wilson and Charles[2] used a passive thermographic technique to detect the regions of disbond in graphite-epoxy and E glass-epoxy panels. They used a liquid crystal coating as the thermal sensor and applied heat on the other side of the panel. The regions of disbond were shown as cool regions because of the poor thermal conductivity due to the disbonding.

McLaughlin and coworkers[3] used two different passive heating techniques to identify various geometries of delamination in graphite-epoxy and glass-epoxy panels. They found that for the conduction heating technique it is hard to obtain thermal gradients for some lay-ups, and that the radiation/convection heat application technique was better. In Ref. 4, they also performed an experiment to determine the effect of surface finish. They found that paint thickness on the surface also resulted in thermal gradients which could be confused with material defects.

Pye and Adams[5] used an AGA Thermovision scanner to locate shear cracks in carbon and glass fiber reinforced plastic (CFRP and GFRP respectively) bars. The bars were under resonant torsional vibration. They found that there are minimum detectable crack lengths for both GFRP and CFRP. In Ref. 6, they used resonant excitation on tube and plate GFRP specimens in axial and bending modes, respectively. They located simulated damage as hot spots. The frequencies they used caused a global structure resonance, therefore the stresses in a vibrating plate varied with positions in any particular mode. They also did the same test on CFRP plate but failed to detect the damage, probably due to the higher thermal conductivities in the direction of the fibers.

1.1 Frequency-Dependent Heat Image during a Vibrothermographic Test

Duke and Russell[7] used vibrothermography and other NDT techniques to investigate the imperfections in sheet molding compound. They concluded that ultrasonic C-scanning and vibrothermography appeared to provide complementary information which allowed for the location and selection of the most significant of the imperfections.

Henneke and Russell[8] used several NDT techniques to detect impact damage in graphite-epoxy panels. It was shown that the vibrothermography technique easily discriminated the region of impact damage from the remainder

of the panel for the higher impact energy levels. Also, the greater the damage, the greater the temperature rise which occurred during mechanical vibration. It was revealed that there was a strong correlation between the impact energy level and the degree of heating of the damaged region. But for the lower impact energy levels, vibrothermography could not detect the impact damage while the ultrasonic C-scan method could.

In Refs. 7 and 8, it was found that conditions for the generation of a heat pattern were strongly dependent on the frequency of excitation for a vibrothermographic test of composite materials. This frequency related behavior has been studied in Refs. 9 and 10. Two models were proposed to explain the frequency dependent heat patterns generated during vibrothermography. First, a local resonance model was postulated using analytical dynamic examination of a delamination in a panel. The delamination was modeled as two plates, one on either side of the delamination, free to resonate with their own dynamics, and clamped together along the boundary of the delamination. Based upon the equations in Ref. 11 and the Rayleigh-Ritz approximation used in Ref. 12, Russell and Henneke[9] developed a model for local resonant frequency prediction. Details of the analysis of this model are included in Ref. 10. It was assumed that heating would occur when the local plates began resonating.

Second, a structural resonance model was proposed. Here, the natural frequencies were calculated for the entire specimen. It was assumed that heating would occur when local strain field increased in value due to the structural resonating conditions. During a structural resonance, a damage region may or may

not develop heating, depending upon the location of the damage in the structure relative to the modes of resonance. The standing wave or mode shapes in the structure determine where the strain energy is distributed and hence determine if a particular damage region in a certain location will develop heating to an extent detectable by the thermographic camera.

From the experimental results obtained in Ref. 10, it was found that the vibrothermal peak frequencies of simulated delamination in an $[0_2]$ glass-epoxy coupon correlated with the predicted local natural frequencies very well. It was also found that the vibrothermal peak frequencies of two simulated delaminations in $[0_4]$ glass-epoxy panel did not correlate with the predicted local natural frequencies. It was concluded that the global structural resonance predominated for the thicker laminate.

The same $[0_4]$ panel was tested again and it was found that even after a year of resting in the laboratory, the specimen displayed the same frequency-heating peaks as previously. An ultrasonic C-scan was then performed carefully by the present author and it was found that the sizes of the simulated delaminations were larger than the mylar squares which had been inserted during manufacture, probably due to the separation of the adhesive tape surrounding the mylar. When the newly observed sizes of the delamination were input to the numerical program of the local resonance model, the calculated resonant frequencies were found to correlate well with the observed vibrothermal peak frequencies. It has thus been shown that the size and geometry of the delamination significantly affects the observed frequencies for developing a heat pattern. It is

thus suggested that local resonance is indeed the mechanism that is responsible for the frequency dependent heat generation behavior. More experiments should be performed on multi-angle ply laminates to determine a more definitive answer.

The software program which was written in Ref. 10 had a few errors, was inefficient, and was primarily written for 0-degree unidirectional laminates. In particular, it can not treat an off-axis unidirectional and multi-directional laminate. Only the parameters K_n ($K_n^2 = \rho\omega_n^2 b^4/D_{11}$), which are related to the eigenvalues of the governing equations and which are functions of material density ρ, delamination dimension b, natural frequencies ω_n, and the 11 term of D-matrix (the bending stiffness) D_{11} , can be obtained from the previous program. Once these are obtained, the natural frequencies have to be calculated from K_n by hand. For a 0-degree unidirectional laminate, D_{11} is easy to calculate, but for a multi-directional laminate, D_{11} is much more difficult to calculate by hand.

In this study, a new software program, based upon the concepts developed by the program in Ref. 10, is written to calculate the natural frequencies of a mid-plane symmetric, multi-angle ply anisotropic laminate. Experiments are then performed to check on the predictions made by this more general analysis. The development of the theory of the local resonance model and the calculation of the natural frequencies are presented in the following chapter.

1.2 Heat Generation Mechanism and Heat Image Simulation during a Vibrothermographic Test

In order to use the vibrothermographic technique for evaluation of composite materials, appropriate physical models must be found for interpretation of the mechanical to heat transformation process.

Henneke, Reifsnider, and Stinchcomb[13] used an AGA thermographic camera to monitor fatigue damage and to locate delaminations by vibrothermography. The stress distribution and heat pattern of a methyl methacrylate specimen with a center hole under cyclic loading were compared. The temperature pattern around the hole is more similar to the shear stress distribution than to the hydrostatic stress distribution. The damage development during fatigue was monitored for $[0/\pm 45/0]_s$ laminates of boron-epoxy and boron-aluminum with a center hole. The thermographic pattern changed with fatigue damage which occurred before any visual surface damage could be detected, and the sites of damage initiation corresponded to those points of highest surface temperature. A comparison of the stress field with the thermographic heat pattern revealed a strong similarity to the interlaminar shear stress in the 45° ply.

In Refs. 14 and 15, Reifsnider, Henneke, and Stinchcomb discussed the mechanics and physical models which could be responsible for stress related thermal emission and the limitation of using a scanning infrared detection system.

For a nondestructive scheme, they categorized those heat generation mechanisms as anelastic effects, viscoelastic effects and structural dissipation. At low stress levels, anelastic effects including the various relaxation phenomena (atomic diffusion, order-disorder processes, thermal diffusion, etc.) are common. The object of anelasticity is to study the material itself as a bulk substance, and to establish the character of certain internal features by their relaxation spectra. While these events may be prominent in the small strain range, the heat produced by them is not significant because of the low ratios of dissipated-to-input energy, the low levels of input energy, and the low frequencies at which these events are commonly excited. Including viscoelastic and anelastic effects, only the dissipation produced by the relaxation mechanism in long chain polymers is of practical importance to the vibrothermographic technique. The structural dissipation mechanism which is related to local vibration is the clapping or rubbing of the defect surfaces. Therefore, likely heat generation mechanisms during vibrothermographic testing are heat dissipation of nonconservative deformation, or heat dissipation due to clapping or rubbing of the defect surfaces. These mechanisms have never been qualified, and it has been believed that the latter one is the main mechanism responsible for the heat generation.

In order to qualify the heat generation mechanism during vibrothermographic testing, the following hypothesis will be tested. If local resonance dominates the vibrothermographic behavior, and there are different plates on each side of the simulated delamination in a panel, the delamination spot should heat up at both sets of the predicted natural frequencies calculated from

two sides of the delamination. If the heat generation is due to delamination surface interactions (clapping or rubbing), then it would be expected that the degree of heating would be always greater on the side of the laminate corresponding to the thinner plate, each time a frequency corresponding to a resonance of either plate is applied to the laminate. This hypothesis is based upon the idea that if heat generation is due to some surface interaction, then, since the delaminated surface is closer to the laminate surface on the side of the thinner plate, this side should always appear hotter than the other side at a resonance frequency of either plate, or at least the temperatures of both sides would be the same. On the other hand, if heating is caused by a nonconservative deformation dependent upon local stresses, the side of laminate containing the plate which is under a natural resonance should heat up more than the side which is not resonating at a particular applied frequency. The hypothesis can be tested by embedding a non-mid-plane delamination in a laminated panel and subjecting the panel to a range of excitation frequencies. This is an approach taken to meet the objectives of the present work.

Whitcomb[16] used the temperature measured with an infrared camera as the boundary condition in a finite element heat transfer program and calculated the fatigue damage zones. The calculated damage zones were compared with other NDT technique results and it was shown that the analysis was effective in locating the boundaries of the fatigue damage zones. Henneke and Jones[17] developed a finite difference heat transfer model to predict the heat pattern of a known defect. Details of the finite difference heat transfer model and the pro-

gram are included in Ref. 18. Simulated flaws were fabricated into a graphite-epoxy laminate panel. Subjected to high frequency-low displacement excitation, the heat patterns developed correlated with the predictions very well and the pattern indicated the shapes of the simulated flaws.

For the present work, a finite difference heat transfer program, based upon the work done in Ref. 18, was written to calculate the temperature distribution of the heat pattern due to the delamination in the panel and compared with the observed heat pattern. In Ref. 18, a software program was written for an 8-ply symmetric laminate with 10 × 10 nodal points and with damage symmetric to the mid-plane also. The heat generation was assumed to be a constant temperature increase at the delamination layer. This is an unrealistic assumption. In this study, the program was modified and rewritten for any kind of layup and damage location and the nodal points can be defined as necessary and required. The heat generation is assumed to be either a constant heat input or proportional to either the displacement field or the strain field for each mode of the local resonant vibration. Which of the latter two assumptions to use depends on what the heat generation mechanism is. If the heat generation mechanism is heat dissipation due to nonconservative deformation, the heat generation is more likely proportional to the strain field. If the heat generation mechanism is either clapping or rubbing of the delamination surfaces, the heat generation is more likely proportional to the displacement field.

In the preliminary run of the program, the heat input was assumed to be proportional to the displacement field of each mode. The predicted heat pattern

outputs in this case are more circular or elliptical in form, while the actual delamination dimensions are rectangular. For some modes, the center part of the elliptical heat pattern has a long axis either in the x-direction or y-direction depending on the mode. This result is close to the observed heat pattern generated during a vibrothermographic test. But, with a constant heat input, the predicted heat pattern generated by the program is more rectangular in form. The phenomenon shown above indicates that the heat generation is dependent on the vibration mode and is proportional to either the displacement field or the strain field.

1.3 Objectives

The objectives of this study are as follows:

1. To determine the validity of the local resonance model, which was proposed to describe the frequency dependent heat generation behavior during a vibrothermographic test.
2. To identify the heat generation mechanism of vibrothermal heat patterns of the delamination.
3. To apply vibrothermography to impact damaged graphite-epoxy panels which are real damaged components.

Computer software, based upon the local resonance model, was written to calculate natural modes of vibration for mid-plane symmetric anisotropic plates.

In the previous work performed by Russell, Ref. 10, the local resonance model was proposed to describe the frequency dependent heat generated pattern during a vibrothermographic test. In his work the experimental results were inconclusive concerning whether or not the local resonance model dominates the frequency dependent heat generation. In this study, the local resonance model was used as a basis for writing a software program for the mid-plane symmetric anisotropic laminate, and the model was verified via several experimental means.

The work done by Jones in Ref. 18 provides a direction for the simulation of the heat pattern during a vibrothermographic test. The heat input assumption used by Jones was unrealistic and the software program which was written was restricted to certain specific conditions. Actually, the shape of the predicted heat pattern did not quite match the observed heat pattern. The finite difference heat transfer program, based upon the work done in Ref. 18, was rewritten for a more general and realistic simulation of the heat pattern generated during a vibrothermographic test, and the predicted heat pattern will be compared with the observed heat pattern.

Previous work concerning the heat generation mechanisms during a vibrothermographic test proposed several likely heat generation mechanisms without being qualified, and it was believed that the clapping or rubbing between the delamination surfaces is the main mechanism responsible for heat generation. In this study, the frequency dependent heat generation mechanism will be quali-

fied, developing more understanding of the phenomenon responsible for the vibrothermography technique.

2. THEORETICAL BACKGROUND

2.1 Local Resonance Model

For development of a dynamic model of a delamination or an in-plane crack in a plate subjected to vibrothermographic inspection, it is assumed heat generation is related to the dynamic displacements, stresses, or velocities of the material in the flaw. Two models, the local resonance model and the structure resonance model, were proposed in Ref. 10. As already noted, the experimental results suggested that the local resonance is indeed the mechanism responsible for the frequency dependent heat generation behavior, but were unable to show this conclusively. Therefore, only the local resonance model is discussed in this study.

As postulated in Ref. 10, a panel is divided into two parts, one containing a single delamination, and the other containing the remainder of the panel, as shown in Fig. 1. The delamination is modeled as two plates, one on either side

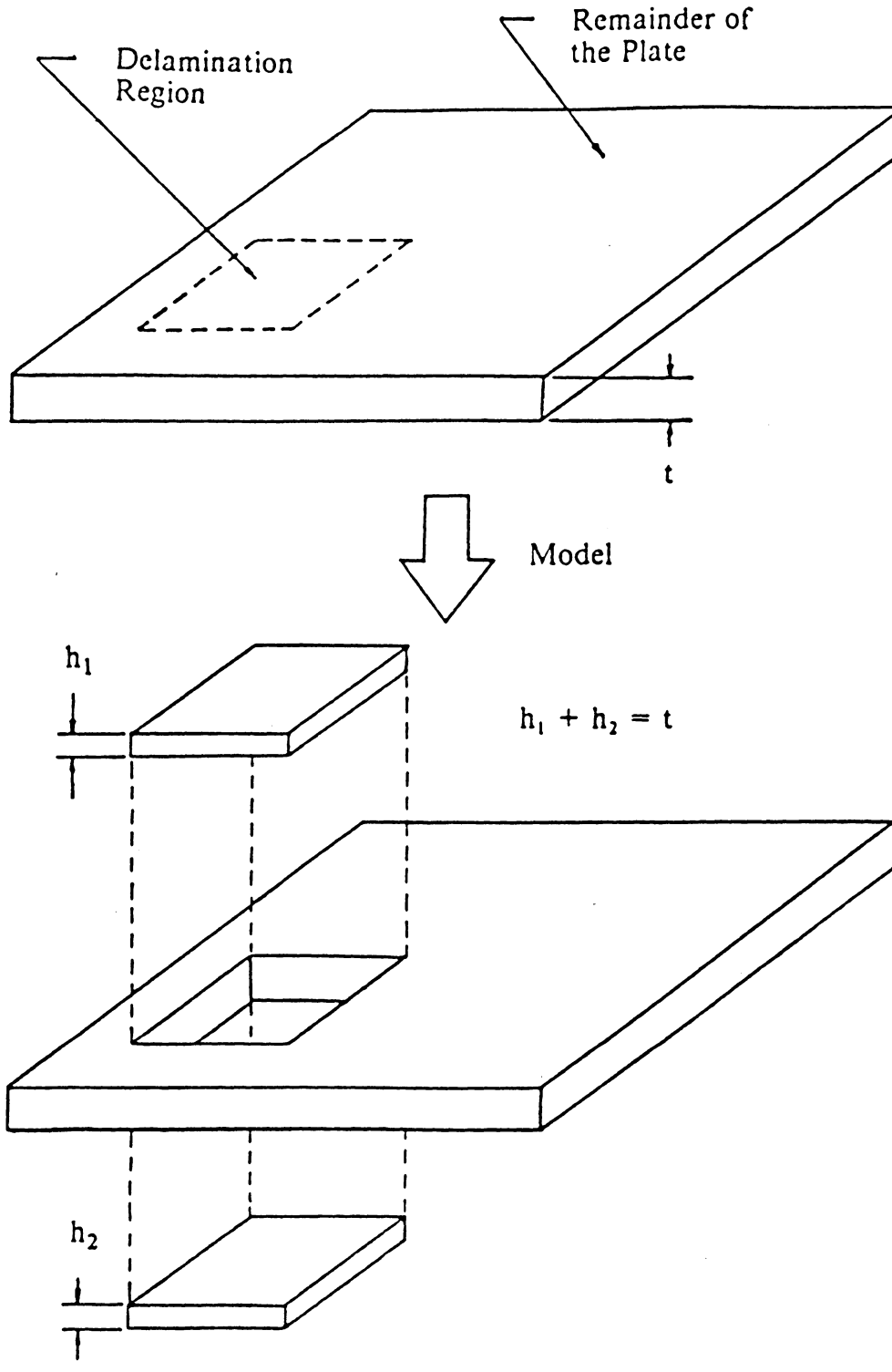

Figure 1. Model of in-plane delamination in a panel.

of the delamination, free to resonate with their own dynamics, and clamped together along the boundary of the delamination by the remainder of the panel. During a vibrothermographic test, the vibration of the panel provides the boundary conditions for the forced vibration of those two plates in the delamination region. From the geometry stated above, the boundary conditions of free vibration for those two plates in the delamination region would appear to be modeled by a clamped condition. In this study, only one plate, either the top one or the bottom one of those two plates in the delamination region, will be considered at one time.

The boundary value problem and the manner to solve it has been stated and discussed in Ref. 10. For the local resonance model, the natural frequencies, ω_k, of the free vibration of the small plate determines the resonance of the plate, and hence the heating of the delamination. Therefore, the focus here is to solve the natural frequencies of the free vibration of the plate in the delamination region. The development of the procedure for obtaining the natural frequencies of a clamped mid-plane symmetric anisotropic laminate, based upon Refs. 11 and 12, will be discussed below.

For a rectangular mid-plane symmetric anisotropic laminate, the energy criterion governing the free vibration is given by Ref. 11 as

$$\frac{1}{2}\int_0^a\int_0^b \{D_{11}\left[\frac{\partial^2 v}{\partial x^2}\right]^2 + 2D_{12}\frac{\partial^2 v}{\partial x^2}\frac{\partial^2 v}{\partial y^2} + D_{22}\left[\frac{\partial^2 v}{\partial y^2}\right]^2 + 4D_{66}\left[\frac{\partial^2 v}{\partial x \partial y}\right]^2 + 4D_{16}\frac{\partial^2 v}{\partial x^2} + 4D_{26}\frac{\partial^2 v}{\partial x \partial y}\frac{\partial^2 v}{\partial y^2} - \omega^2 \rho v^2\}\, dxdy \quad (2.1.1)$$

$$= \text{stationary value}$$

where ω is the natural frequency, ρ is the material density, v is the out-of-plane displacement, x and y are the global coordinates, and D_{ij} are the components of the bending stiffness matrix which is defined as

$$D_{ij} = \int_{\frac{-h}{2}}^{\frac{h}{2}} \overline{Q}_{ij}^{k}\ (z)\ z^2\ dz \tag{2.1.2}$$

For a laminate of thickness h, and for the k^{th} layer lamina

$$\begin{Bmatrix} \sigma_x \\ \sigma_y \\ \sigma_{xy} \end{Bmatrix}^{k} = \left[\overline{Q}_{ij}\right]^{k} \begin{Bmatrix} \varepsilon_x \\ \varepsilon_y \\ \varepsilon_{xy} \end{Bmatrix}^{k} \tag{2.1.3}$$

where σ_x, σ_y, σ_{xy}, ε_x, ε_y, ε_{xy} are the in-plane stresses and strains, and $\overline{Q}_{ij}$ are the transformed reduced stiffness in the global coordinate system (refer to Ref. 11). In the material coordinate system, the reduced stiffness are defined in terms of the engineering constants as

$$\left[Q_{ij}^{\cdot}\right] = \begin{bmatrix} \dfrac{E_1}{1-\nu_{12}\nu_{21}} & \dfrac{\nu_{21}E_1}{1-\nu_{12}\nu_{21}} & 0 \\ \dfrac{\nu_{12}E_2}{1-\nu_{12}\nu_{21}} & \dfrac{E_2}{1-\nu_{12}\nu_{21}} & 0 \\ 0 & 0 & G_{12} \end{bmatrix} \tag{2.1.4}$$

where 1 and 2 are the material coordinates.

Proceeding to solve for the natural modes using the Rayleigh-Ritz procedure used in Ref. 12, the solution is assumed to be in the form of a series with undetermined coefficients:

$$v\ (x,y) = \sum_{i=1}^{m} \sum_{j=1}^{n} a_{ij}\ \varphi_i\ (x)\ \theta_j\ (y) \tag{2.1.5}$$

where $\varphi_i(x)$ and $\theta_j(y)$ satisfy the boundary conditions on the edges x = 0,a and y = 0,b, respectively.

Substituting Eq. (2.1.5) into Eq. (2.1.1) and minimizing with respect to a_{ij}, the equation becomes

$$\begin{aligned}
&\sum_{k=1}^{m} \sum_{l=1}^{n} \{D_{11} \int_0^a \varphi_k''\ (x)\ \varphi_i''\ (x)\ dx \int_0^b \theta_l\ (y)\ \theta_j\ (y)\ dy \\
&+ D_{12} [\int_0^a \varphi_k''\ (x)\ \varphi_i\ (x)\ dx \int_0^b \theta_l\ (y)\ \ddot{\theta}_j\ (y)\ dy \\
&+ \int_0^a \varphi_k\ (x)\ \varphi_i''\ (x)\ dx \int_0^b \ddot{\theta}_l\ (y)\ \theta_j\ (y)\ dy] \\
&+ D_{22} \int_0^a \varphi_k\ (x)\ \varphi_i\ (x)\ dx \int_0^b \ddot{\theta}_l\ (y)\ \ddot{\theta}_j\ (y)\ dy \\
&+ 4D_{66} \int_0^a \varphi_k'\ (x)\ \varphi_i'\ (x)\ dx \int_0^b \dot{\theta}_l\ (y)\ \dot{\theta}_j\ (y)\ dy \\
&+ 2D_{16} [\int_0^a \varphi_k''\ (x)\ \varphi_i'\ (x)\ dx \int_0^b \theta_l\ (y)\ \dot{\theta}_j\ (y)\ dy \\
&+ \int_0^a \varphi_k'\ (x)\ \varphi_i''\ (x)\ dx \int_0^b \dot{\theta}_l\ (y)\ \theta_j\ (y)\ dy] \\
&+ 2D_{26} [\int_0^a \varphi_k'\ (x)\ \varphi_i\ (x)\ dx \int_0^b \dot{\theta}_l\ (y)\ \ddot{\theta}_j\ (y)\ dy \\
&+ \int_0^a \varphi_k\ (x)\ \varphi_i'\ (x)\ dx \int_0^b \ddot{\theta}_l\ (y)\ \dot{\theta}_j\ (y)\ dy] \\
&- \omega^2 \rho \int_0^a \varphi_k\ (x)\ \varphi_i\ (x)\ dx \int_0^b \theta_l\ (y)\ \theta_j\ (y)\ dy\}\ a_{kl} = 0
\end{aligned} \tag{2.1.6}$$

i = 1 to m

j = 1 to n

The prime and the dot denote differentiation with respect to x and y, respectively. From Ref. 11, the functions φ and theta have been chosen to be a characteristic shape corresponding to a beam clamped on each end. Hence φ satisfies

$$\frac{d^4\varphi_k}{dx^4} - \alpha_k^4 \, \varphi_k = 0 \tag{2.1.7}$$

and θ satisfies

$$\frac{d^4\theta_l}{dy^4} - \beta_l^4 \, \theta_l = 0 \tag{2.1.8}$$

with boundary conditions of

$$\varphi_k = \frac{\partial\varphi_k}{\partial x} = 0 \quad \text{at} \quad x = 0,a \tag{2.1.9}$$

and

$$\theta_l = \frac{\partial\theta_l}{\partial y} = 0 \quad \text{at} \quad y = 0,b \tag{2.1.10}$$

The parameters α_k and β_l satisfy

$$[\cos \alpha_k \, a] \, [\cosh \alpha_k \, a] = 1 \tag{2.1.11}$$

$$[\cos \beta_l \, b] \, [\cosh \beta_l \, b] = 1 \tag{2.1.12}$$

Hence the Ritz functions for the clamped plate are

$$\varphi_k(x) = [\sin\alpha_k a - \sinh\alpha_k a][\cosh\alpha_k x - \cos\alpha_k x] - [\cos\alpha_k a - \cosh\alpha_k a][\sinh\alpha_k x - \sin\alpha_k x] \quad (2.1.13)$$

$$\theta_l(y) = [\sin\beta_l b - \sinh\beta_l b][\cosh\beta_l y - \cos\beta_l y] - [\cos\beta_l b - \cosh\beta_l b][\sinh\beta_l y - \sin\beta_l y] \quad (2.1.14)$$

Because of the choice of φ and θ, some of the integrals in Eq. (2.1.6) can be simplified by integrating by parts and then using the boundary conditions as follows:

$$\int_0^a \varphi_k'' \ \varphi_i'' \ dx = \varphi_k' \ \varphi_i'' \Big]_0^a - \varphi_k \ \varphi_i''' \Big]_0^a + \int_0^a \varphi_k \ \varphi_i'''' \ dx \quad (2.1.15)$$

$$\int_0^b \ddot{\theta}_l \ \ddot{\theta}_j \ dy = \dot{\theta}_l \ \ddot{\theta}_j \Big]_0^b - \theta_l \ \dddot{\theta}_j \Big]_0^b + \int_0^b \theta_l \ \theta_j^{IV} \ dy \quad (2.1.16)$$

Hence,

$$\int_0^a \varphi_k'' \ \varphi_i'' \ dx = \alpha^4 \int_0^a \varphi_k \ \varphi_i \ dx \quad (2.1.17)$$

$$\int_0^b \ddot{\theta}_l \ \ddot{\theta}_j \ dy = \beta^4 \int_0^b \theta_l \ \theta_j \ dy \quad (2.1.18)$$

and

$$\int_0^a \varphi_k \ \varphi_i'' \ dx = \varphi_k \ \varphi_i' \Big]_0^a - \int_0^a \varphi_k' \ \varphi_i' \ dx = -\int_0^a \varphi_k' \ \varphi_i' \ dx \quad (2.1.19)$$

$$\int_0^b \theta_l \ \ddot{\theta}_j \ dy = \theta_l \ \dot{\theta}_j \Big]_0^b - \int_0^b \dot{\theta}_l \ \dot{\theta}_j \ dx = -\int_0^b \dot{\theta}_l \ \dot{\theta}_j \ dx \quad (2.1.20)$$

$$\int_0^a \varphi_k' \ \varphi_i'' \ dx = \varphi_k' \ \varphi_i' \Big]_0^a - \int_0^a \varphi_k'' \ \varphi_i' \ dx = - \int_0^a \varphi_k'' \ \varphi_i' \ dx \quad (2.1.21)$$

$$\int_0^b \dot{\theta}_l \ \ddot{\theta}_j \ dy = \dot{\theta}_l \ \dot{\theta}_j \Big]_0^b - \int_0^b \ddot{\theta}_l \ \dot{\theta}_j \ dx = - \int_0^b \ddot{\theta}_l \ \dot{\theta}_j \ dx \quad (2.1.22)$$

$$\int_0^a \varphi_k \ \varphi_i' \ dx = \varphi_k \ \varphi_i \Big]_0^a - \int_0^a \varphi_k' \ \varphi_i \ dx = - \int_0^a \varphi_k' \ \varphi_i \ dx \quad (2.1.23)$$

$$\int_0^b \theta_l \ \dot{\theta}_j \ dy = \theta_l \ \theta_j \Big]_0^b - \int_0^b \dot{\theta}_l \ \theta_j \ dx = - \int_0^b \dot{\theta}_l \ \theta_j \ dx \quad (2.1.24)$$

Because φ and θ form orthogonal sets

$$\int_0^a \varphi_k \ (x) \ \varphi_i \ (x) \ dx = a \ \delta_{ki} \quad (2.1.25)$$

$$\int_0^b \theta_l \ (y) \ \theta_j \ (y) \ dy = b \ \delta_{lj} \quad (2.1.26)$$

where δ_{ki} (or δ_{lj}) is unity if $k = i$ (or $l = j$) and is zero otherwise.

From the above, the governing equation (Eq. (2.1.6)) can be simplified as

$$\sum_{k=1}^{m}\sum_{l=1}^{n}\{[D_{11}\,\alpha^4 + D_{22}\,\beta^4 - \rho\,\omega^2]\,a\,b\,\delta_{ki}\,\delta_{lj}$$
$$+ [2\,D_{12} + 4\,D_{66}]\int_0^a \varphi_k'(x)\,\varphi_i'(x)\,dx \int_0^b \dot{\theta}_l(y)\,\dot{\theta}_j(y)\,dy$$
$$+ 4D_{16}\int_0^a \varphi_k''(x)\,\varphi_i'(x)\,dx \int_0^b \theta_l(y)\,\dot{\theta}_j(y)\,dy$$
$$+ 4D_{26}\int_0^a \varphi_k'(x)\,\varphi_i(x)\,dx \int_0^b \dot{\theta}_l(y)\,\ddot{\theta}_j(y)\,dy\}\,a_{kl} = 0 \qquad (2.1.27)$$

i = 1 to m

j = 1 to n

Since Eq. (2.1.27) are a set of homogeneous equations, one solution is the trivial one, $a_{ij} = 0$. Other solutions are possible only when the determinant of the coefficient matrix is zero, and this condition is sufficient to determine the natural frequencies of the free vibration. The numerical computer software was written to solve the eigenvalue problem defined by Eq. (2.1.27). This program forms a matrix M_{pq} which is solved by an eigenvalue solver subroutine, EIGRF. Each M_{pq} is defined by Eq. (2.1.27) for each chosen k, l, i, and j, where m represents a reduced notation for each combination of k and l, and n, for a combination of i and j. The computer software to solve the eigenvalues and eigenvectors is included in Appendix A.

2.2 *Heat Transfer Analysis and Heat Image Simulation*

Heat transfer problems in anisotropic material differs greatly from that in isotropic material. The differential equation for the heat transfer in a general anisotropic material, as given in Ref. 19, is

$$\rho\, c_p \frac{\partial T}{\partial t} = K_{xx} \frac{\partial^2 T}{\partial x^2} + K_{yy} \frac{\partial^2 T}{\partial y^2} + K_{zz} \frac{\partial^2 T}{\partial z^2} + (K_{yz} + K_{zy}) \frac{\partial^2 T}{\partial y \partial z} + (K_{zx} + K_{xz}) \frac{\partial^2 T}{\partial z \partial x} + (K_{xy} + K_{yx}) \frac{\partial^2 T}{\partial x \partial y} + Q \tag{2.2.1}$$

where ρ is the density of the material, c_p is the specific heat of the material, T is the temperature, t is the time, K_{ij} are the thermal conductivities of the material, and Q is the heat generation or heat loss in the material.

The tensor form of the thermal conductivities in the material coordinate system in a unidirectional lamina is

$$K_{kl} = \begin{bmatrix} K_{11} & 0 & 0 \\ 0 & K_{22} & 0 \\ 0 & 0 & K_{33} \end{bmatrix} \tag{2.2.2}$$

In a unidirectional lamina, all fibers lie in parallel planes and the material is transversely isotropic. The only coordinate transformation needing to be consid-

ered, therefore, is in the 1-2 plane, that is, in the plane of fibers. By using the law of coordinate transformation,

$$K'_{ij} = a_{ik}\ a_{jl}\ K_{kl} \tag{2.2.3}$$

where

$$a_{ij} = \begin{bmatrix} \cos\theta & -\sin\theta & 0 \\ \sin\theta & \cos\theta & 0 \\ 0 & 0 & 1 \end{bmatrix} \tag{2.2.4}$$

See Fig. 2 for definition of θ and relationship between the material coordinate system and the global coordinate system.

For a lamina with an angle θ to the global coordinate, the thermal conductivities in the global coordinate system become:

$$\begin{aligned} K_{xx} &= \cos^2\theta\ K_{11} + \sin^2\theta\ K_{22} \\ K_{xy} &= \cos\theta\sin\theta\ K_{11} - \cos\theta\sin\theta\ K_{22} \\ K_{yx} &= K_{xy} \\ K_{yy} &= \sin^2\theta\ K_{11} + \cos^2\theta\ K_{22} \\ K_{zz} &= K_{33} \\ K_{xz} &= K_{zx} = K_{yz} = K_{zy} = 0 \end{aligned} \tag{2.2.5}$$

Therefore, Eq. (2.2.1) can be simplified to

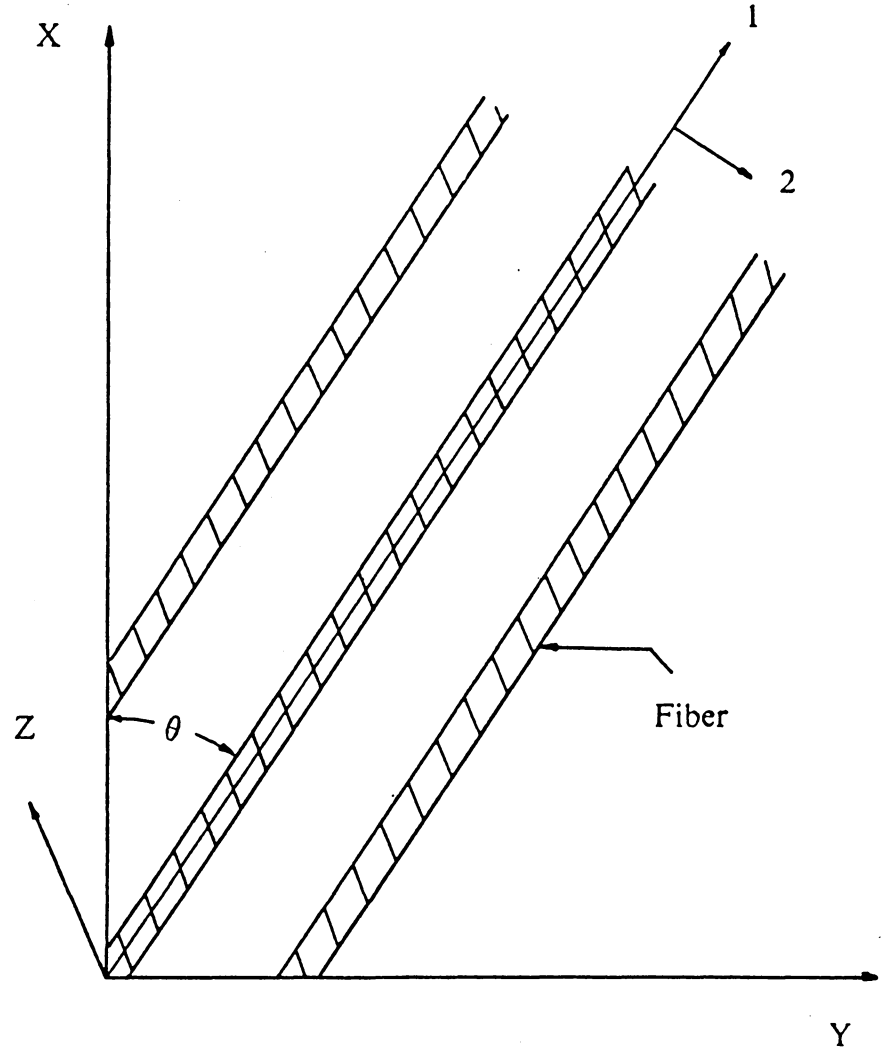

Figure 2. Relationship between material coordinate system and global coordinate system.

$$\rho\, c_p \frac{\partial T}{\partial t} = K_{xx} \frac{\partial^2 T}{\partial x^2} + K_{yy} \frac{\partial^2 T}{\partial y^2} + K_{zz} \frac{\partial^2 T}{\partial z^2} + 2\, K_{xy} \frac{\partial^2 T}{\partial x \partial y} + Q \tag{2.2.6}$$

The finite difference method was chosen to solve this heat transfer problem. Based upon the work done by Jones in Ref. 18, a finite difference heat transfer program was written to calculate the temperature distribution of the heat pattern due to the delamination in the panel during a vibrothermographic test. The detail for the finite difference analysis is presented in Ref. 18. The finite difference program is included in Appendix B. The differences between the finite difference heat transfer program written by the present author and the one in Ref. 18 are as follows:

In Ref. 18, the program was written for an 8-ply symmetric coupon laminate with 10 × 10 nodal points and with damage symmetric to the mid-plane also. The temperature was assumed to be a constant temperature increase at the layer adjacent to the delamination. The program by the present author was written for any layup and damage location and the nodal points can be defined as necessary and required. The heat generation is assumed to be either a constant heat input or proportional to either the displacement field or the strain field for each mode of the local resonant vibration. Which of these three to use is dependent upon the heat generation mechanism. The specimen to be analyzed can be either a coupon or a panel. For a panel specimen, the region to be analyzed

can be a small part of the panel, as long as the boundary of that region is at room temperature.

The problem faced here is how to determine the heat generation, Q. As already noted, constant heat generation or constant temperature increase as assumed by Jones in Ref. 18, did not match the heat pattern observed. For the present study, the heat generation will be chosen proportional to either the displacement field or the strain field. For the local resonance model, the displacement is assumed to be in the form (as Eq. (2.1.5))

$$v\ (x,y) = \sum_{i=1}^{m} \sum_{j=1}^{n} a_{ij}\ \varphi_i\ (x)\ \theta_j\ (y)$$

For a clamped boundary (as Eqs. (2.1.13) and (2.1.14)),

$$\varphi_k\ (x) = [\sin \alpha_k\ a - \sinh \alpha_k\ a]\ [\cosh \alpha_k\ x - \cos \alpha_k\ x] - [\cos \alpha_k\ a - \cosh \alpha_k\ a]\ [\sinh \alpha_k\ x - \sin \alpha_k\ x]$$

$$\theta_l\ (y) = [\sin \beta_l\ b - \sinh \beta_l\ b]\ [\cosh \beta_l\ y - \cos \beta_l\ y] - [\cos \beta_l\ b - \cosh \beta_l\ b]\ [\sinh \beta_l\ y - \sin \beta_l\ y]$$

and for each eigenvalue ω, a set of corresponding eigenvectors, a_{ij}, can be obtained. Hence, the mode shape, v (x,y), can be obtained.

Using the Kirchhoff-Love hypothesis, the strains of a bending plate can be obtained from the displacement as follows

$$\varepsilon_z = \varepsilon_{xz} = \gamma_{yz} = 0 \qquad (2.2.7)$$

$$\varepsilon_x = -z\frac{\partial^2 v}{\partial x^2} = -z\sum_{i=1}^{m}\sum_{j=1}^{n} a_{ij}\frac{\partial^2 \varphi_i(x)}{\partial x^2}\theta_j(y) \tag{2.2.8}$$

$$\varepsilon_y = -z\frac{\partial^2 v}{\partial y^2} = -z\sum_{i=1}^{m}\sum_{j=1}^{n} a_{ij}\varphi_i(x)\frac{\partial^2 \theta_j(y)}{\partial y^2} \tag{2.2.9}$$

$$\gamma_{xy} = -2z\frac{\partial^2 v}{\partial x \partial y} = -2z\sum_{i=1}^{m}\sum_{j=1}^{n} a_{ij}\frac{\partial \varphi_i(x)}{\partial x}\frac{\partial \theta_j(y)}{\partial y} \tag{2.2.10}$$

This is a plane strain condition, so the summation of principal strains can be obtained as

$$\varepsilon_1 + \varepsilon_2 = \varepsilon_x + \varepsilon_y \tag{2.2.11}$$

The heat generation input then can be chosen to be proportional to either the displacement field or the strain field which are defined as above. For the strain field, two additional choices can be made: the heat generation can be proportional to the sum of principal strain field or the shear strain field in the material coordinate. The heat pattern generated by each choice will be compared with the heat pattern observed in a vibrothermographic test to indicate which is more likely.

3. EXPERIMENTAL TECHNIQUE

3.1 Vibrothermographic Inspection

Figure 3 is the schematic of the equipment used to perform a vibrothermographic inspection of a panel specimen. The equipment consists of two parts: thermographic inspection system and ultrasonic shaker system. In this study, an AGA Thermovision 780 infrared camera system is used for the inspection. The AGA Thermovision 780 infrared camera system consists of three pieces of equipment: the camera unit, the control unit and black and white display, and the color display CRT. This system is calibrated to read temperatures linearly in degrees Celsius in the range of 20° − 40° C. Outside of this range, a calibration chart must be used to convert AGA degrees to Celsius degrees. The camera is capable only of differentiating the temperature difference between any points and some reference points within its field of view. That is, the thermal

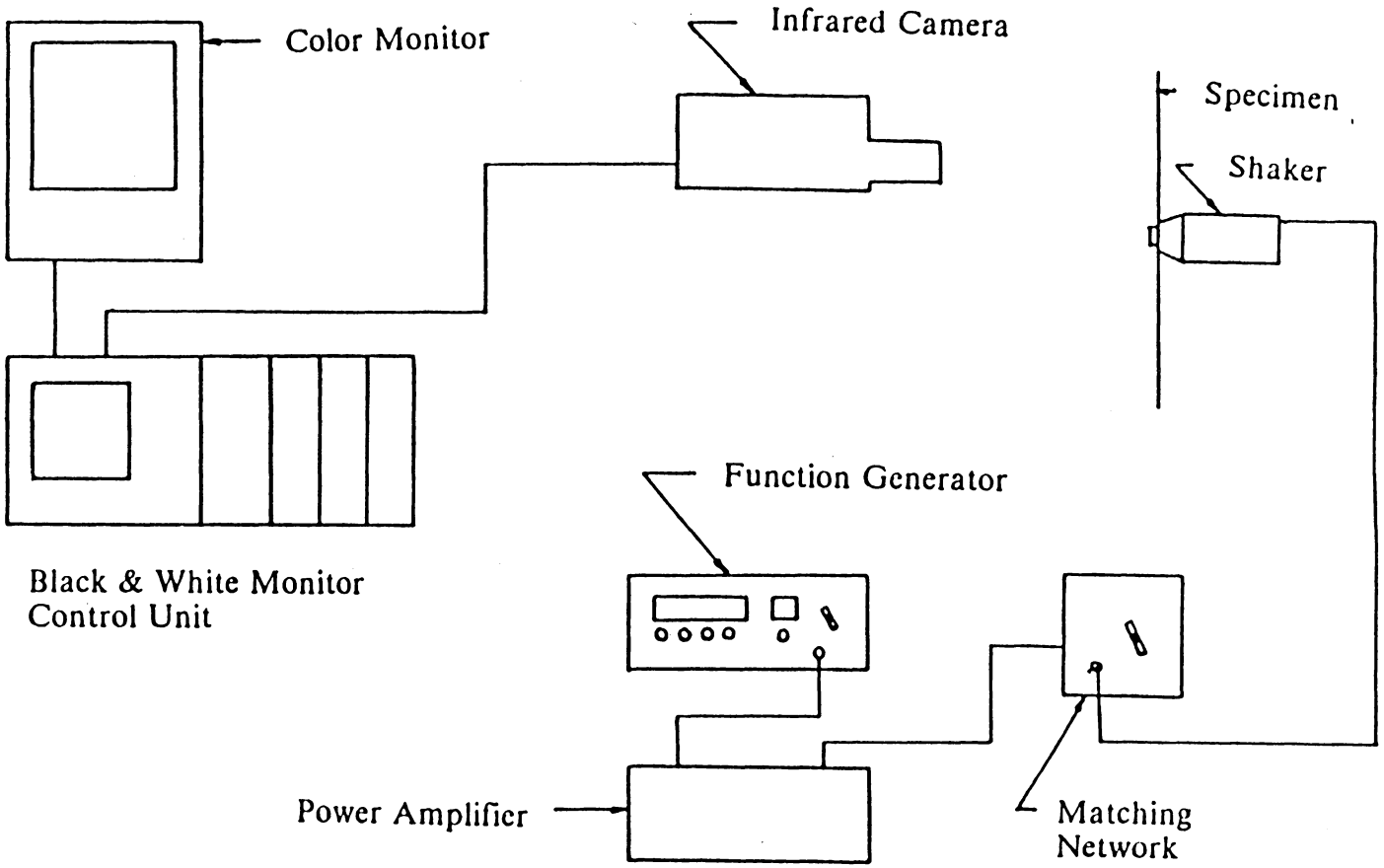

Figure 3. Schematic of vibrothermographic test.

maps of the surface of the specimens interrogated will be as a relative temperature difference to some reference temperature on the surface of the specimen. If the absolute temperature of some point of interest is required, a known temperature reference must be viewed simultaneously with the point of interest. For nondestructive testing technique, the knowledge of the absolute temperature of reference is not necessary, since only the thermal gradients and relative temperature are of interest.

The AGA Thermovision 780 system has ten temperature ranges at steps between 2° and 1000° full range, and for each range, the color monitor has ten colors to represent ten isotherms in this range. Therefore, the smallest resolution of the temperature difference of this system is 0.2°AGA. All specimens were painted with ultra flat black paint to increase the emissivity of the surface to obtain a better and more uniform signal. The AGA Thermovision 780 system also consists of an auxiliary system called Oscar, which can transform an analog heat image signal into a digital signal which can be recorded by a digital tape recorder. Because of malfunctions, this system was not used in the present study. The heat images were recorded by photographing directly from the color display CRT for the present work.

The ultrasonic shaker system also consists of three pieces of equipment: an ultrasonic shaker, a power amplifier, and a function generator. The Wilcoxon Research model F-7 piezoelectric shaker was used to generate the ultrasonic vibration on the specimen, and was driven by a 1800 watts Wilcoxon Research model PA8 high power amplifier through a model N8H matching network. The

signal source for the power amplifier was Hewlett-Packard model 4204A oscillator. This system is specified to have a useful frequency range from 1 Hz to over 100 kHz. However, an observable heat image is not produced if the frequency is lower than 9 kHz. If the frequency is higher than 26 kHz, the system draws excessive power, heating and damaging the shaker. Therefore, in this study, the frequency range used to drive the shaker system was limited between 9 and 25 kHz. For this system and the panel specimen attached to the shaker, there were system resonance frequencies between about 11-13 kHz and 22-25 kHz. When system resonance occurs, it can be observed that hot spots appear other than at the damaged regions and the heating degree of the damaged region increases significantly. Again, the system draws excessive power in this condition, causing the shaker to overheat. Therefore, at these frequencies the amplitude of the function generator must be adjusted down to a lower value, enough to generate a decent heat pattern but low enough to prevent the shaker being damaged.

In the present work, all specimens are panel specimens. A 3/8 inch hole was drilled through the panel and an appropriate length 3/8-24 bolt was used to attach the panel to the shaker. A second method which was stated in Ref. 10, using a vacuum cone, was also tried but was not successful because of the lack of an appropriate vacuum pump. When attaching the panel specimen to the shaker, ultrasonic couplant was always applied to all contact surfaces to ensue the transmission of the mechanical energy from the shaker to the specimen. The ultrasonic couplant used in this study was Ultragel II by Echo Ultra Sound, Inc..

3.2 *Structures and Materials Examined*

In order to understand and verify the local resonance model which was suggested to be the mechanism responsible for the frequency dependent heat generation behavior, and to qualify the heat generation mechanism for vibrothermal heat patterns, several sizes of delaminations in different layups of glass-epoxy panel specimens were examined. For the purpose of application of vibrothermography on real damaged specimens, some impact damaged graphite-epoxy panel specimens were also examined. A description of the types of flaws and layups of the panels which contained the flaws follows.

3.2.1 Fabricated Delaminations

Figure 4 illustrates a method for constructing a simulated delamination in a composite panel, in the present work, an E-glass epoxy panel. A sheet of rectangular mylar tape is folded at the center to form the free surface which simulates the in-plane crack or delamination. The rectangular cellophane tape is also folded at the center with the open end being opposite to the mylar tape. The cellophane tape is slightly larger than the mylar tape and seals around the edges of the mylar tape to prevent the epoxy matrix from flowing into the free surface between the mylar tape during the curing cycle of the prepreg. By the process of including mylar tape during the fabrication of a composite specimen, the ap-

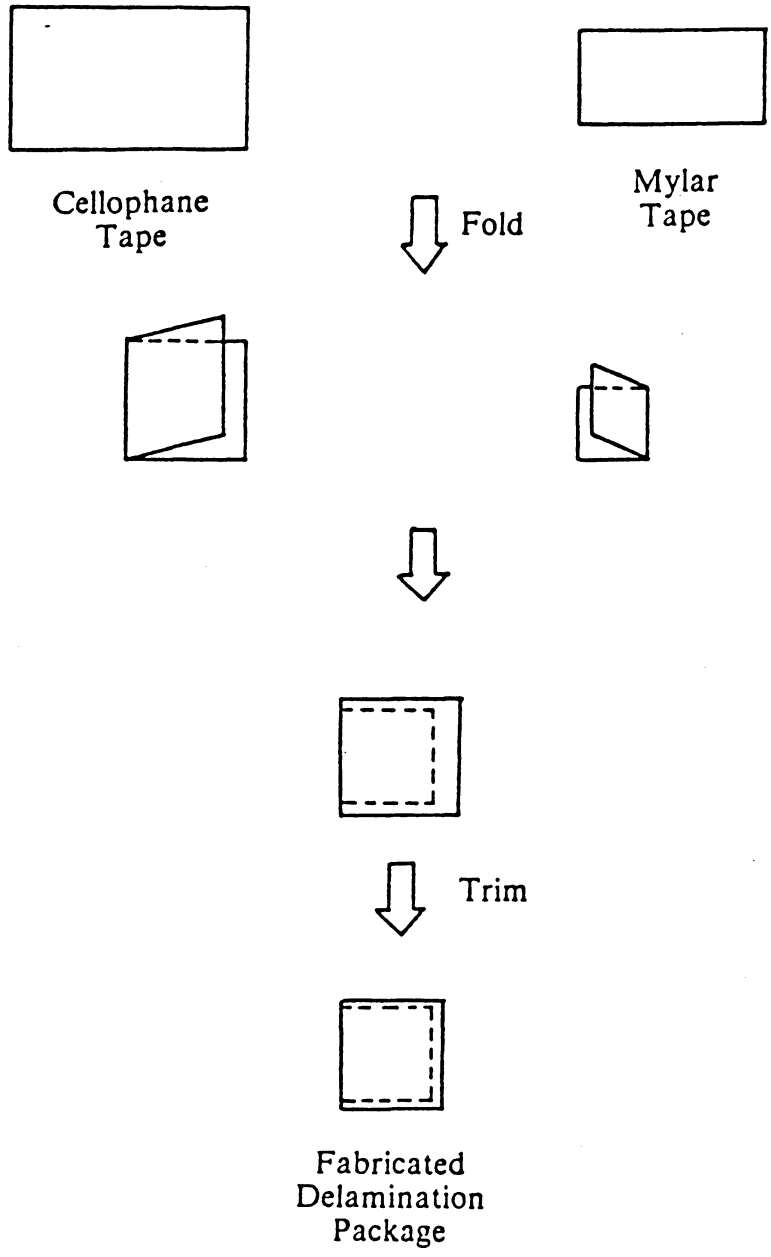

Figure 4. Details of fabrication of a simulated delamination.

proximate geometry and size of the flaw can be controlled. The depth of the simulated delamination in the specimen can also be controlled by placing the flaw package into the desired ply-interface in a laminate.

Four different simulated delaminations were laminated on the mid-plane of a four ply, 0-degree unidirectional, 12 inches square panel of 1002 Scotchply E-glass epoxy. The locations of the simulated delaminations on the panel are as shown in Fig. 5. The choice of the dimensions for the simulated delamination was based upon the local resonance model to yield the lower modes of the predicted natural frequencies in the range of 9-25 kHz. For more verification of the local resonance model, two other panels were also made in the same manner as the above one. One was a $[0_5]$, 12 inches square 1002 Scotchply E-glass epoxy panel with four different sizes of simulated delamination on the 2-3 layer interface of the laminate. The other was a $[0/90/90/0]_s$, 12 inches square 1002 Scotchply E-glass epoxy panel with four different sizes of simulated delamination on the mid-plane of the laminate.

As already noted, the sizes of actual delaminations formed were different from the sizes of the mylar tapes, probably because of the separation of the adhesive tapes surrounding the mylar tapes. To prevent this problem, all the specimens were vibrated by the shaker through the whole working range of frequencies to allow the cellophane tape to have the chance to open. Ultrasonic C-scanning was then performed carefully on each panel to measure the sizes of the simulated delamination. The sizes of the simulated delamination in the above three panel specimens are listed in Tables 1, 2, and 3.

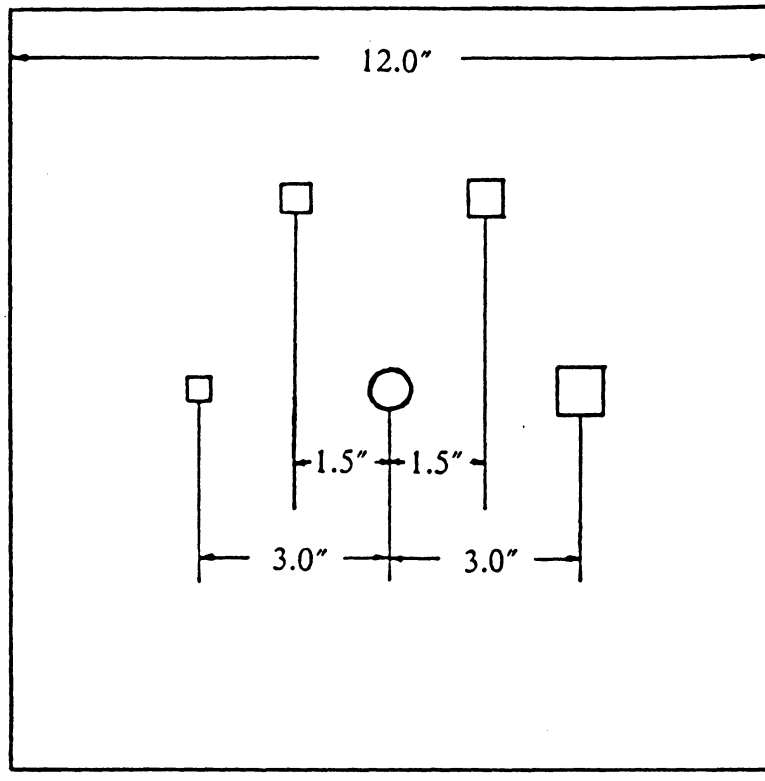

Figure 5. Locations of the simulated delaminations on the panel.

Table 1. Identification and Size of Simulated Delaminations on the Mid-plane of One Foot Square [0_4] Glass-Epoxy Panel

Plate No: 2

Layup and Material: [0_4] Glass-Epoxy

Delamination I.D.	Delamination Size
D-21	0.889 × 0.965 cm (0.350 × 0.380 in.)
D-22	1.118 × 1.041 cm (0.440 × 0.410 in.)
D-23	1.219 × 1.168 cm (0.480 × 0.460 in.)
D-24	1.295 × 1.283 cm (0.510 × 0.505 in.)

Table 2. Identification and Size of Simulated Delaminations on the 2-3 Ply Interface of One Foot Square [0_5] Glass-Epoxy Panel

Plate No: 3

Layup and Material: [0_5] Glass-Epoxy

Delamination I.D.	Delamination Size
D-31	0.940 × 0.902 cm (0.370 × 0.355 in.)
D-32	1.168 × 1.092 cm (0.460 × 0.430 in.)
D-33	1.334 × 1.219 cm (0.525 × 0.480 in.)
D-34	1.410 × 1.245 cm. (0.555 × 0.490 in.)

Table 3. Identification and Size of Simulated Delaminations on the Mid-Plane of One Foot Square $[0/90/90/0]_s$ Glass-Epoxy Panel

Plate No: 4

Layup and Material: [0/90/90/0], Glass-Epoxy

Delamination I.D.	Delamination Size
D-41	1.067 × 1.067 cm (0.420 × 0.420 in.)
D-42	1.219 × 1.156 cm (0.480 × 0.455 in.)
D-43	1.461 × 1.397 cm (0.575 × 0.550 in.)
D-44	1.575 × 1.486 cm (0.620 × 0.585 in.)

3.2.2 Impact Damaged Panels

Russell[20] performed vibrothermographic tests on an impact damaged panel specimen and found that the maximum temperatures at the damage sites were proportional to the impact energy which caused the damage. The result is interesting, but the test was performed on one panel only at two frequencies which caused structure resonance. The test needs to be performed again to verify the result and to determine how frequency affects the heat pattern. Therefore, impact tests on graphite-epoxy panel specimens were performed and vibrothermography was used to investigate the impact damages. These tests constitute an application of vibrothermography on real damaged specimens.

Three 12 inch square panels of cross-ply Narmco 5208 graphite-epoxy were made. The layups were $[0/90]_s$, $[0/90/0/90]_s$, and $[0_2/90_2/0_2/90_2]_s$, respectively. The impact damage zones were created by dropping a spherical steel ball from various heights onto the panel for various impact damage energy. The spherical ball was 2.54 cm (1 inch) in diameter, and 66.7 g in mass. The impact damage zones were located on four different quadrants on each panel, and the heights which the steel ball dropped were 4.343 m (14 ft. 3 in.), 8.065 m (26 ft. 5 $\frac{1}{2}$ in.), 9.874 m (32 ft. 4 $\frac{3}{4}$ in.), and 11.722 m (38 ft. 5 $\frac{1}{2}$ in.), yielding impact energies of 2.84, 5.27, 6.45, and 7.66 joule, respectively.

3.3 *SPATE Thermographic System*

SPATE thermographic system (Stress Pattern Analysis by Thermal Emission) is based upon the measurement of the thermoelastic effect investigated by Lord Kelvin in 1853. Within the elastic range, a body subjected to tensile or compressive stress experiences a reversible conversion between mechanical and thermal forms of energy. If an adiabatic condition is maintained, the reversible temperature change and the corresponding change in the sum of the principal stresses are linearly proportional and the relationship is independent of loading frequency.

The theory (Refs. 21 and 22) given for an isotropic, homogeneous material is as follows:

$$\Delta T = -\frac{\alpha T \Delta\sigma}{\rho c_\sigma} = -K_m T \Delta\sigma \tag{3.3.1}$$

where ΔT is the temperature change (in °Kelvin or °K), α is the thermal coefficient of expansion (K^{-1}), T is the temperature (°K), $\Delta\sigma$ is the change of the sum of the principal stresses, ρ is the density, c_σ is the specific heat at constant stress, and K_m is the thermoelastic constant ($= \alpha/\rho c_\sigma$). Since the stress normal to the free surface is zero,

$$\Delta\sigma = \Delta\sigma_1 + \Delta\sigma_2 = \Delta\sigma_x + \Delta\sigma_y \tag{3.3.2}$$

As T has an absolute unit K, and as K_m changes only insignificantly with the ambient temperature T, temperature control need not be rigorous.

For a small, adiabatic deformation, the equation of state relating stress, deformation, and temperature for anisotropic media was given by Biot[23] as

$$\Delta T = -\frac{T}{\rho\, c_\varepsilon}\alpha_{kl}C_{ijkl}\Delta\varepsilon_{ij} \tag{3.3.3}$$

where c_ε is the specific heat at constant strain, α_{kl} are the components of the thermal expansion tensor, and C_{ijkl} are the components of the elastic stiffness tensor, and $\Delta\varepsilon_{ij}$ are the strain tensor. More details of the thermoelastic micromechanics of an anisotropic material was discussed in Ref. 24.

The SPATE system detects the infrared flux emitted from points on an observable surface as a result of the minute temperature changes in a cyclically stressed structure or component. The Ometron SPATE 8000 equipment consists of an infrared-sensitive camera coupled to a correlator and a computer. The sensitivity of the system can detect a temperature discrimination typically better than 0.001°K. The measurement is taken synchronized with the peak to peak amplitude of the periodic change in the sum of the principal stresses at the measuring point. The points are scanned in a raster-like manner under adjustable computer control and can be identified simultaneously on the surface by means of a visual channel incorporating an eyepiece or a projected light spot with cross wires. Therefore, the image obtained on the screen, which results from adiabatic temperature changes, is point-wise related to the stress field or strain field induced by rapid cyclic loading. For the purpose of obtaining a better

emissivity and hence the infrared flux signal, the surface to be examined was descaled and degreased, and a thin, uniform ultra-flat black paint was then applied on the surface of the specimen.

The output of the SPATE is the thermoelastic emission from the material under cyclic loading. From Eq. (3.3.3), the thermoelastic emission field is related to the normal stress field or normal strain field in the material coordinate. Therefore, this technique was used to inspect the thermoelastic emission field of the mode at each corresponding resonant natural frequency to determine if the delamination region vibrates following the model behavior.

3.4 Supportive Nondestructive Evaluation Techniques

In this study ultrasonic C-scanning and edge replication techniques were used to verify the location and the extent of the damage in the structures being examined. A brief description of these techniques follows.

3.4.1 Ultrasonic C-scanning

Ultrasonic C-scanning is a technique using ultrasonic sound waves to detect the defect in a structure or component. An Automation Industries S80 Reflectoscope was used to provide an ultrasonic C-scan. Water immersion was used to provide coupling of the sound between the transducer and specimen. The

technique involved pulsing the piezoelectric transducer to generate an ultrasonic pulse which traveled through the structure to an aluminum reflection plate and then back through the structure to the transducer which also served as a receiver. The received signal was then compared in amplitude to a preset level. If the received signal amplitude was above this preset level, a high voltage signal was excited to the wire pen on the paper to write on the paper. If the signal travelled through a damage point, the signal was diverged and no signal or a low amplitude signal was received, turning off the pen. All the ultrasonic C-scans in this study are based upon a good ultrasonic transmission zone being grey and a poor region of ultrasonic transmission being white.

3.4.2 Edge Replication

The edge replication technique provides a topographic replica of the specimen edge surface. A piece of cellulose acetate tape is placed on the edge and softened with acetone. The tape is allowed to harden and then is removed from the edge. The impression of the edge surface is then permanently recorded on the tape and the tape can be magnified optically to reveal detail. This technique was used to document the damage of the impact damaged graphite-epoxy panels. The panels were sectioned through the regions of the impact damage and replicas were made of the sectioned edge. A Bell and Howell ABR microfiche reader was used to magnify and print the images of the replicas.

4. RESULTS AND DISCUSSION

The following chapter presents and discusses the results of the experiments on the structure with the techniques stated previously. Experiments were particularly performed to test the validity of the local resonance model and to identify the heat generation mechanism in the delamination region during a vibrothermographic test. However, impact damaged specimens were also inspected constituting an application of vibrothermography on real damaged specimens.

Thermographic patterns of the $[0/90/90/0]_s$ glass-epoxy panel with four simulated delaminations are shown in Figs. 6, 7, and 8, to illustrate how the heat pattern depends on the excitation frequency and how to interpret the information from the thermogram. These figures are heat patterns taken while the panel was being excited by the shaker at frequencies of 17.1, 18.2, and 19.3 kHz, respectively. All the thermograms are products of the AGA Thermovision 780 system. With the 780 system, the reference color bands are at the left of the figure. The

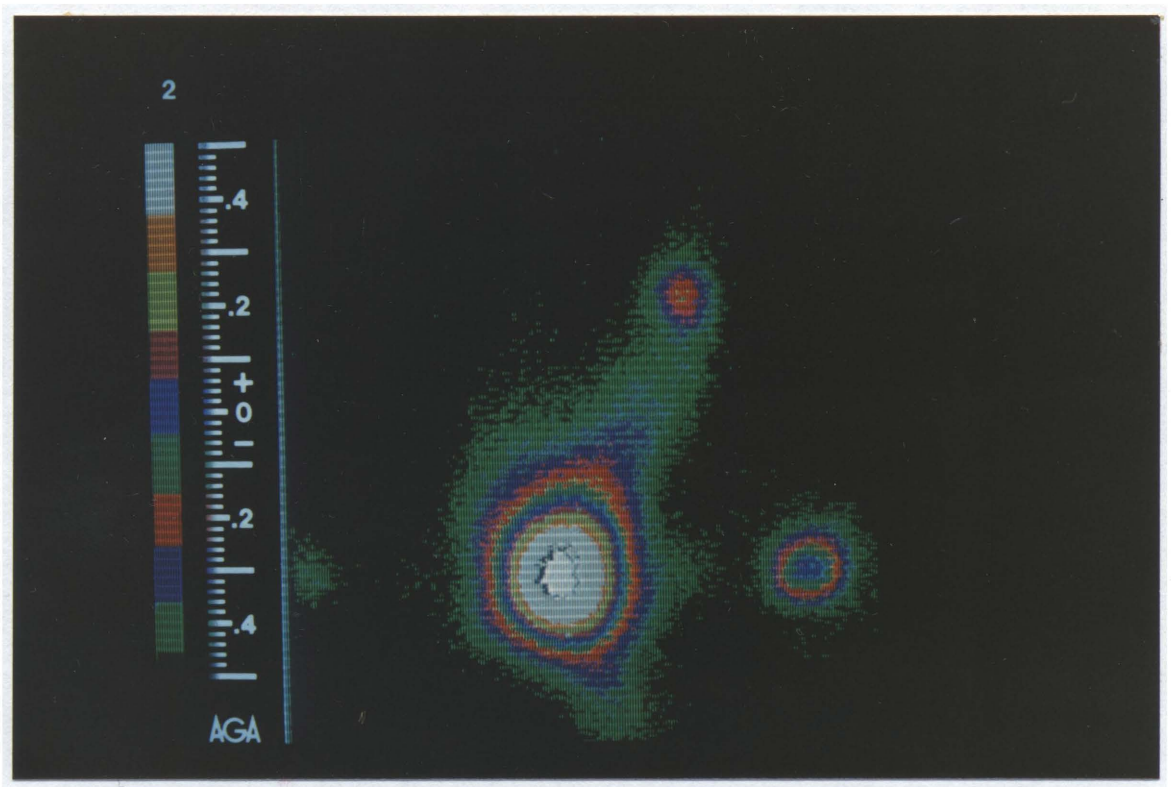

Figure 6. Vibrothermogram of $[0/90/90/0]_s$ glass-epoxy panel at excitation frequencies 17.1 kHz.

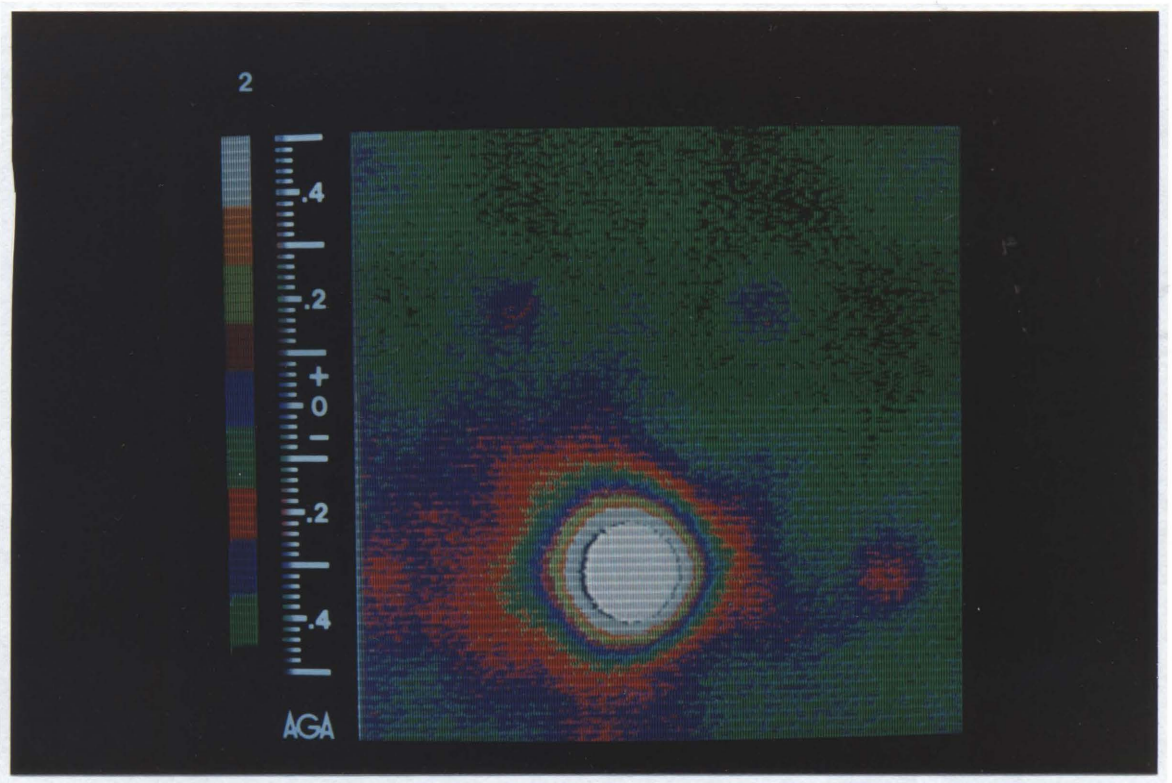

Figure 7. Vibrothermogram of $[0/90/90/0]_s$ glass-epoxy panel at excitation frequencies 18.2 kHz.

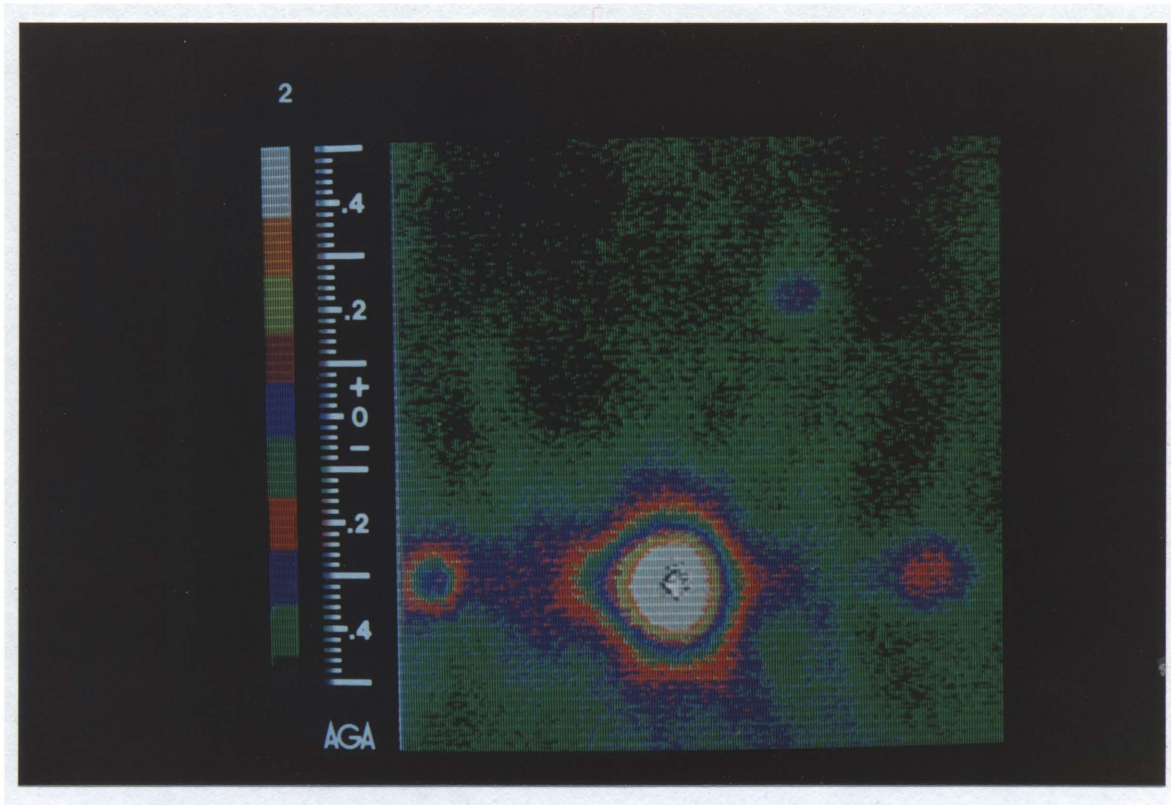

Figure 8. Vibrothermogram of $[0/90/90/0]_s$ glass-epoxy panel at excitation frequencies 19.3 kHz.

ten colors from black to white can be considered to represent ten isotherms from lower to higher temperatures. The scale used is shown at the upper left corner, which is 2°AGA for Figs. 6, 7, and 8. (1°AGA refers to the unit of the temperature as set by the sensor and electronics of the AGA Thermovision system. At room temperature, this is very nearly equivalent to 1°C.) Each color represents a tenth of this scale range. For Figs. 6, 7, and 8, each color represents 0.2°AGA. This is a relative representation of temperature, since no absolute temperature has been defined. If an absolute temperature is needed, a known temperature reference must be viewed by the camera. Also, emissivity and conversion from °AGA to °Celsius must be considered. Tables and charts for conversion of °AGA to °Celsius and correction for emissivity are included in Ref. 25. For using vibrothermography as a nondestructive inspection method, only the relative temperature and thermal gradient are required. Therefore, °AGA was the unit used for all the investigations where only the relative degree of heating was needed.

Figures 6, 7, and 8 were taken from the same panel at three different frequencies, and showed three different heat patterns. The degree of heating for each delamination region was different at each different frequency, and the relative degree of heating between the delaminations was different also. D-42 (which is shown on the upper left in Fig. 7) heated up only at the frequency used in Fig. 7. From these three figures, the frequency dependence phenomenon of the vibrothermograms obtained is quite clear.

4.1 Local Resonance Model

In this section the results of the experiments conducted using simulated delaminations of the type shown in section 3.2 will be presented and discussed. These experiments consisted of tests of the local resonance model for the frequency dependent behavior, and of the thermoelastic emission patterns obtained from SPATE for further verification.

For verifying that the local resonance model is responsible for the frequency dependent behavior during a vibrothermographic test, the delamination region must heat up when the frequency reaches one of the natural frequencies of the delamination plate as stated in section 2.1. Therefore, vibrothermal peak frequencies observed will be compared with the predicted natural frequencies in this section.

As stated in Ref. 10, the error in measuring the size of delamination affected the prediction of the natural frequency significantly. Therefore, the panels containing the delaminations were first vibrated through the whole working frequency range to allow the adhesive tape around the mylar tape to have the chance to open. The separated adhesive tape would be part of the delamination. Then the simulated delamination sizes were measured from carefully performed ultrasonic C-scanning output. The predicted natural frequencies were calculated from the Rayleigh-Ritz approximation program in Appendix A based upon the local resonance model. The material properties of unidirectional 1002 Scotchply, E-glass epoxy for the input of the program were measured in Ref. 26. The

vibrothermal peak frequency was defined as the frequency which produced a local maximum in the frequency domain of the steady state degree of heating of the delamination region relative to the far field temperature of the specimen. This usually was a frequency band bounded by low and high frequencies which caused a cooling from the maximum temperature. These 'drop-off' frequencies were then averaged to yield , for simplicity, a single number as the vibrothermal peak frequency. The degree of heating at the vibrothermal peak frequencies was affected by several factors such as the amplitude of the output signal to the shaker and system resonance. There is no physical meaning that can be given to the comparison of the degree of heating at different vibrothermal peak frequencies under different conditions. Therefore, the degree of heating was not recorded while detecting the vibrothermal peak frequencies.

For the purpose of performing pioneer testing for the validity of the local resonance model, a $[0_4]$, 12 $\times$ 12 in. square, glass-epoxy panel with four different simulated delaminations on the mid-plane was constructed and tested vibrothermographically. Although no delamination should occur naturally in a unidirectional laminate, this layup was chosen for its ease of construction and analytical prediction. The locations of the simulated delaminations were as shown in Fig. 5. Four simulated delaminations produced four sets of data in a single panel. The ultrasonic C-scan of the $[0_4]$ panel is shown in Fig. 9. As can be seen, the delaminations are not perfectly rectangular, and the boundaries of the delaminations are not straight lines. Tables 4 - 7 present the comparison of the experimentally observed vibrothermal peak frequencies and the predicted

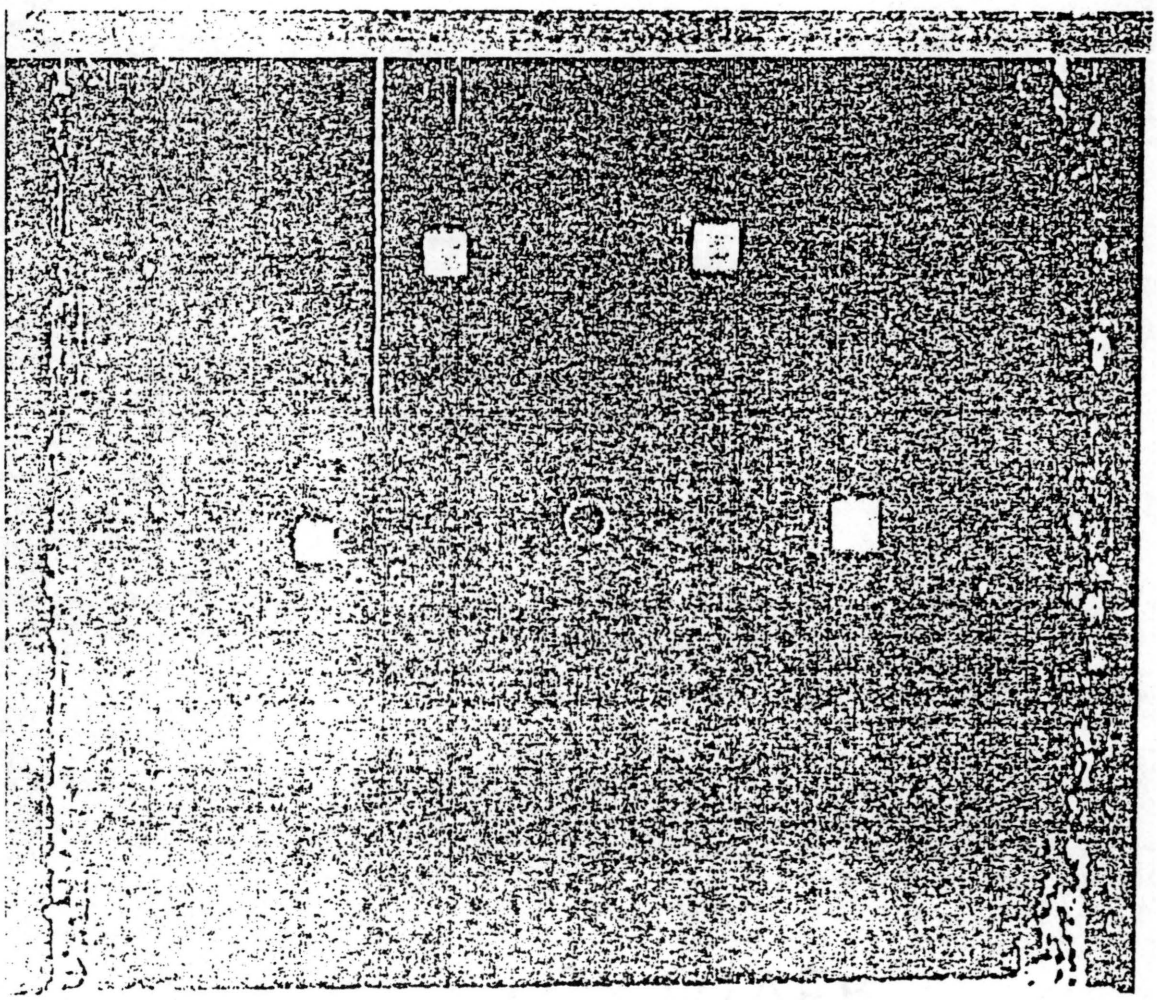

Figure 9. Ultrasonic C-scan of the [0_4] glass-epoxy panel with four simulated delaminations.

Table 4. Comparison of Predicted and Observed Frequencies at Which Local Resonance Occurs at Simulated Delamination D-21 on Mid-Plane of $[0_4]$ Glass-Epoxy Panel

I.D.: D-21

Size: 0.889 × 0.965 cm (0.350 × 0.350 in.)

Excitation Mode No.	Predicted Natural Frequencies (kHz)	Observed Vibrothermal Peak Frequencies (kHz)
1	7.61	N/A
2	11.69	11.80
3	18.86	18.60
4	19.18	19.30
5	21.82	21.80

Table 5. Comparison of Predicted and Observed Frequencies at Which Local Resonance Occurs at Simulated Delamination D-22 on Mid-Plane of $[0_4]$ Glass-Epoxy Panel

I.D.: D-22

Size: 1.118 × 1.041 cm (0.440 × 0.410 in.)

Excitation Mode No.	Predicted Natural Frequencies (kHz)	Observed Vibrothermal Peak Frequencies (kHz)
1	5.22	N/A
2	9.07	N/A
3	12.19	12.30
4	15.04	15.10
5	15.76	15.90
6	20.69	21.40
7	23.07	23.40
8	24.99	25.00

Table 6. Comparison of Predicted and Observed Frequencies at Which Local Resonance Occurs at Simulated Delamination D-23 on Mid-Plane of $[0_4]$ Glass-Epoxy Panel

I.D.: D-23

Size: 1.219 × 1.168 cm (0.480 × 0.460 in.)

Excitation Mode No.	Predicted Natural Frequencies (kHz)	Observed Vibrothermal Peak Frequencies (kHz)
1	4.31	N/A
2	7.32	N/A
3	10.20	10.17
4	12.24	12.30
5	12.60	12.50
6	16.83	16.80
7	19.34	19.30
8	19.93	19.80
9	21.17	21.20
10	23.54	23.40

Table 7. Comparison of Predicted and Observed Frequencies at Which Local Resonance Occurs at Simulated Delamination D-24 on Mid-Plane of $[0_4]$ Glass-Epoxy Panel

I.D.: D-24

Size: 1.295 × 1.283 cm (0.510 × 0.505 in.)

Excitation Mode No.	Predicted Natural Frequencies (kHz)	Observed Vibrothermal Peak Frequencies (kHz)
1	3.75	N/A
2	6.19	N/A
3	8.99	8.93
4	10.55	10.60
5	10.78	10.80
6	14.37	14.48
7	16.61	16.50
8	17.10	17.20
9	18.58	18.20

natural frequencies of the four simulated delaminations in the $[0_4]$ glass-epoxy panel. In spite of the shape of the delaminations not being perfectly rectangular, the agreement of the predicted natural frequencies with the observed vibrothermal peak frequencies for all four simulated delamination is excellent. The maximum difference between those two sets was within 0.3 kHz. These results indicate that the local resonance model is indeed the mechanics model responsible for the frequency dependent behavior during a vibrothermographic test.

If local resonance dominates the vibrothermographic behavior, and there are different plates on each side of the simulated delamination in a panel, the delamination spot should heat up at both sets of the predicted natural frequencies calculated from the plate on each side of the delamination. The hypothesis can be tested by embedding a non-mid-plane delamination in a laminated panel and subjecting the panel to a range of excitation frequencies. Accordingly, a $[0_5]$, 12 × 12 in. square glass-epoxy panel with four different delaminations on the 2-3 layer interface was constructed to investigate the above hypothesis. This resulted in two anisotropic plates of different thickness above and below each delamination (a three-ply-thick plate and a two-ply-thick plate). Figure 10 is an ultrasonic C-scan of the $[0_5]$ panel.

Tables 8 - 11 present the comparison of the experimentally observed results and the predictions of the four simulated delaminations on 2-3 ply interface of the $[0_5]$ glass-epoxy panel. The two rows of numbers under the heading 'Predicted Natural Frequencies' reflect the cases where the thickness of the plate with the size of delamination is either two plies or three plies, respectively. Again, the

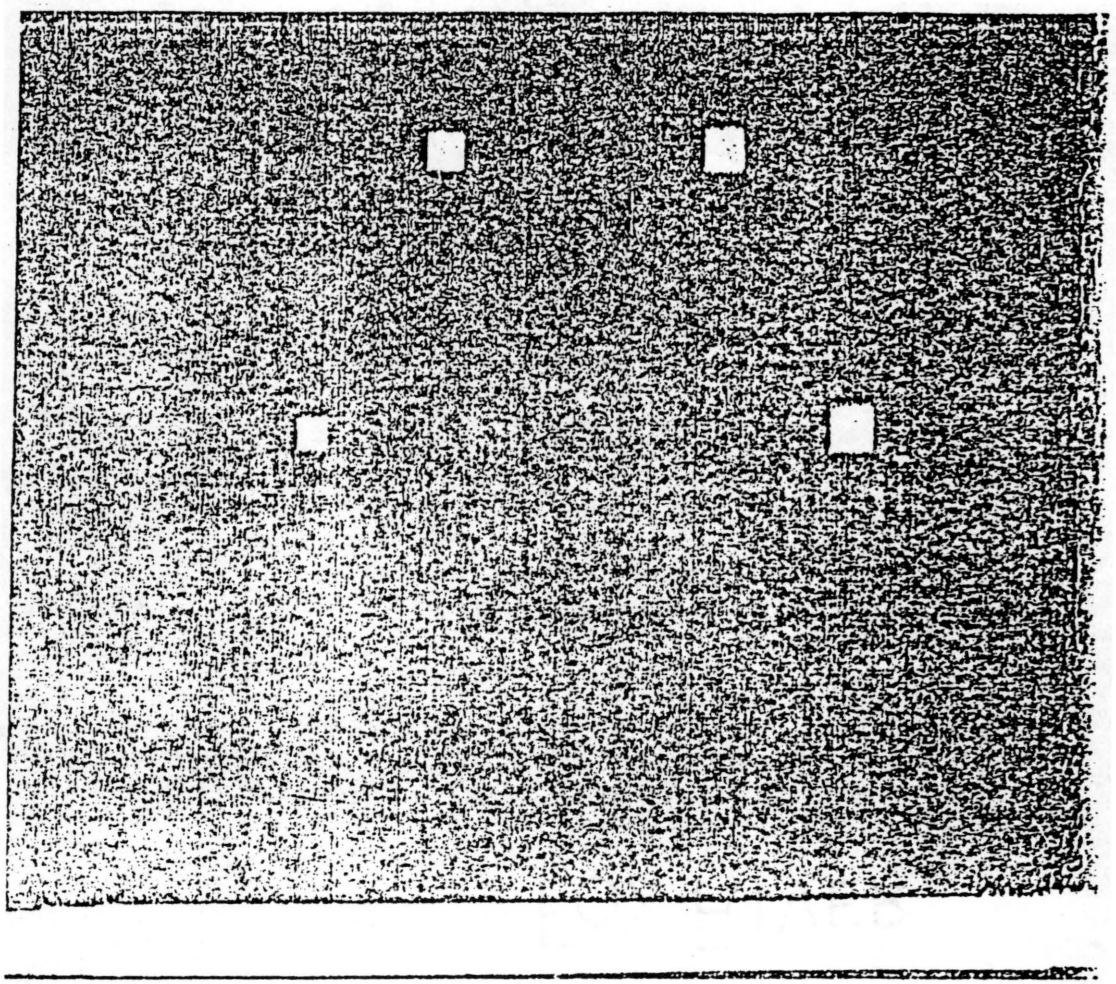

Figure 10. Ultrasonic C-scan of the [0_5] glass-epoxy panel with four simulated delaminations.

Table 8. Comparison of Predicted and Observed Frequencies at Which Local Resonance Occurs at Simulated Delamination D-31 on 2-3 Ply Interface of $[0_5]$ Glass-Epoxy Panel

I.D.: D-31

Size: 0.940 × 0.902 cm (0.370 × 0.355 in.)

Excitation Mode No.		Predicted Natural Frequencies (kHz)		Observed Vibrothermal Peak Frequencies (kHz)
2-ply thickness	3-ply thickness	2-ply thickness	3-ply thickness	
1		7.25		N/A
	1		10.88	10.90
2		12.30		12.30
3		17.16		17.80
	2		18.45	18.30
4		20.86		20.90
5		21.17		21.30
	3		25.74	25.60

Table 9. Comparison of Predicted and Observed Frequencies at Which Local Resonance Occurs at Simulated Delamination D-32 on 2-3 Ply Interface of $[0_5]$ Glass-Epoxy Panel

I.D.: D-32

Size: 1.168 × 1.092 cm (0.460 × 0.430 in.)

Excitation Mode No.		Predicted Natural Frequencies (kHz)		Observed Vibrothermal Peak Frequencies (kHz)
2-ply thickness	3-ply thickness	2-ply thickness	3-ply thickness	
1		4.76		N/A
	1		7.15	N/A
2		8.26		N/A
3		11.15		10.80
	2		12.39	11.95
4		13.73		13.30
5		14.34		14.10
	3		16.72	16.00
6		18.86		18.20
	4		20.60	19.50
7		21.10		21.10
	5		21.50	21.40

Table 10. Comparison of Predicted and Observed Frequencies at Which Local Resonance Occurs at Simulated Delamination D-33 on 2-3 Ply Interface of $[0_5]$ Glass-Epoxy Panel

I.D.: D-33

Size: 1.334 × 1.219 cm (0.525 × 0.480 in.)

Excitation Mode No.		Predicted Natural Frequencies (kHz)		Observed Vibrothermal Peak Frequencies (kHz)
2-ply thickness	3-ply thickness	2-ply thickness	3-ply thickness	
1		3.71		N/A
	1		5.57	N/A
2		6.55		N/A
3		8.59		N/A
	2		9.82	9.70
4		10.70		10.90
5		11.45		11.60
	3		12.89	13.10
6		14.86		14.60
	4		16.05	16.00
7		16.22		16.40
	5		17.17	17.30

Table 11. Comparison of Predicted and Observed Frequencies at Which Local Resonance Occurs at Simulated Delamination D-34 on 2-3 Ply Interface of $[0_5]$ Glass-Epoxy Panel

I.D.: D-34

Size: 1.410 × 1.245 cm (0.555 × 0.490 in.)

Excitation Mode No.		Predicted Natural Frequencies (kHz)		Observed Vibrothermal Peak Frequencies (kHz)
2-ply thickness	3-ply thickness	2-ply thickness	3-ply thickness	
1		3.40		N/A
	1		5.10	N/A
2		6.17		N/A
3		7.73		N/A
	2		9.26	9.30
4		9.82		9.70
5		10.90		10.95
	3		11.61	11.60
6		13.88		13.80
7		14.56		14.50
	4		14.73	15.00
8		16.25		16.10
	5		16.35	16.60
9		17.39		18.00
10		19.63		19.70
	6		20.83	20.70

experimental results correlated with the predictions excellently. The delamination region heated up at both sets of the natural frequencies calculated from two plates above and below the delamination. Therefore, additional verification of the local resonance was obtained.

Since the capability of analyzing a multi-directional, symmetric laminate has been added to the software program of the local resonance model, a vibrothermographic test was performed on a laminated panel. A $[0/90/90/0]_s$, 12 × 12 in. square, glass-epoxy panel with four different simulated delaminations on the mid-plane was constructed and tested vibrothermographically. The ultrasonic C-scan of the $[0/90/90/0]_s$ glass-epoxy panel is shown in Fig. 11. Tables 12 - 15 present the comparison of the predicted and experimentally observed results from the $[0/90/90/0]_s$ panel. As can be seen, the predicted natural frequencies of a laminated panel have a larger separation than those for a unidirectional panel. This is probably due to the difference of the D-matrix, since a unidirectional panel is more anisotropic than a laminated panel is. It was shown, nevertheless, that the correlation between the natural modes of resonance and the observed vibrothermal peak frequencies was quite close. Only two of the differences between the predicted and observed frequencies were greater than 0.5 kHz. Therefore, a further verification of the local resonance model was obtained, and the capability of the software program to calculate the natural frequencies of a laminate was ensured.

From the above observations, the correlation between the observed vibrothermal peak frequencies and the predicted natural frequencies based upon

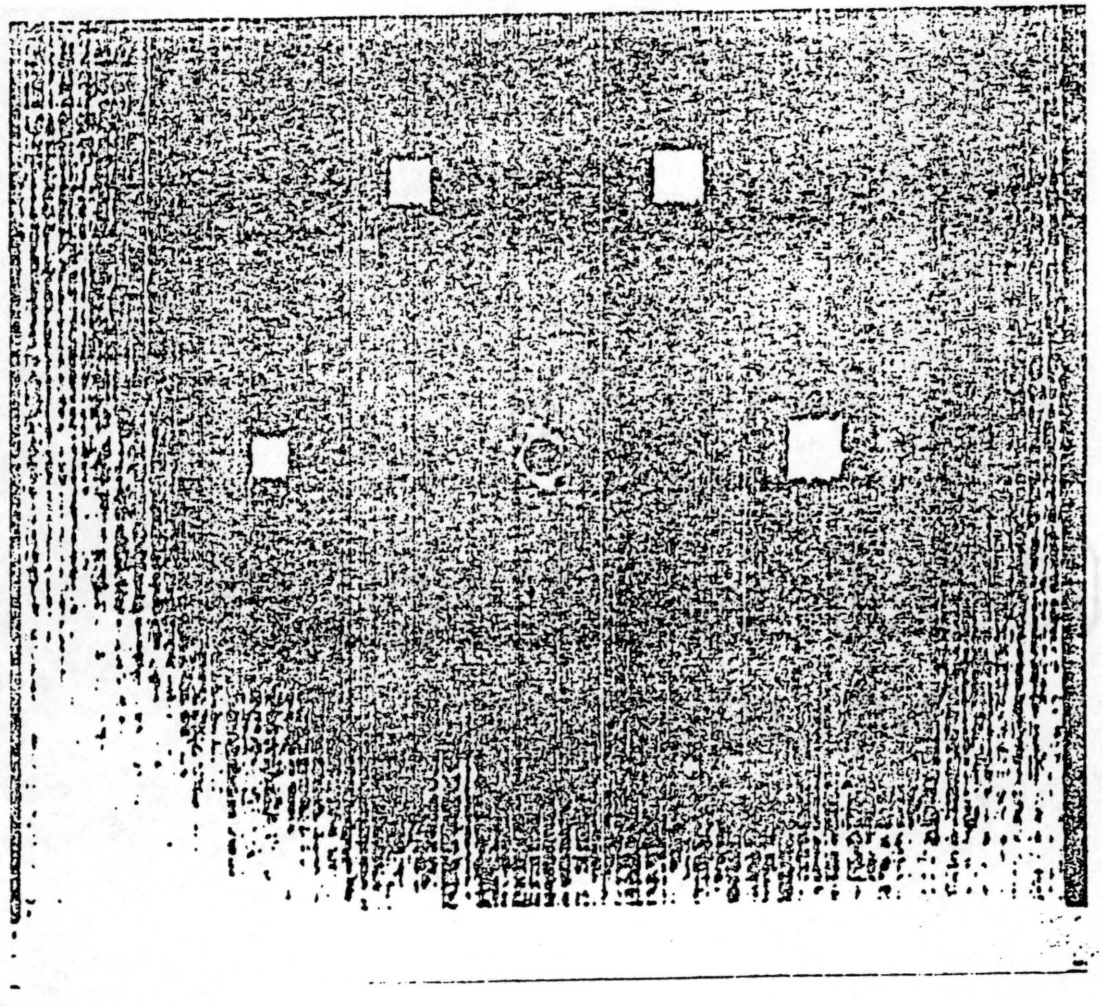

Figure 11. Ultrasonic C-scan of the $[0/90/90/0]_s$ glass-epoxy panel with four simulated delaminations.

Table 12. Comparison of Predicted and Observed Frequencies at Which Local Resonance Occurs at Simulated Delamination D-41 on Mid-Plane of $[0/90/90/0]_s$ Glass-Epoxy Panel

I.D.: D-41

Size: 1.067 × 1.067 cm (0.420 × 0.420 in.)

Excitation Mode No.	Predicted Natural Frequencies (kHz)	Observed Vibrothermal Peak Frequencies (kHz)
1	11.00	10.80
2	19.30	19.30
3	25.57	26.20

Table 13. Comparison of Predicted and Observed Frequencies at Which Local Resonance Occurs at Simulated Delamination D-42 on Mid-Plane of $[0/90/90/0]_s$ Glass-Epoxy Panel

I.D.: D-42

Size: 1.219 × 1.156 cm (0.480 × 0.455 in.)

Excitation Mode No.	Predicted Natural Frequencies (kHz)	Observed Vibrothermal Peak Frequencies (kHz)
1	8.74	N/A
2	16.01	16.10
3	19.77	18.20
4	25.15	24.90

Table 14. Comparison of Predicted and Observed Frequencies at Which Local Resonance Occurs at Simulated Delamination D-43 on Mid-Plane of $[0/90/90/0]_s$ Glass-Epoxy Panel

I.D.: D-43

Size: 1.461 × 1.397 cm (0.575 × 0.550 in.)

Excitation Mode No.	Predicted Natural Frequencies (kHz)	Observed Vibrothermal Peak Frequencies (kHz)
1	6.05	N/A
2	11.00	11.40
3	13.75	13.40
4	17.41	17.10
5	19.48	19.30
6	24.65	24.90

Table 15. Comparison of Predicted and Observed Frequencies at Which Local Resonance Occurs at Simulated Delamination D-44 on Mid-Plane of $[0/90/90/0]_s$ Glass-Epoxy Panel

I.D.: D-44

Size: 1.575 × 1.486 cm (0.620 × 0.585 in.)

Excitation Mode No.	Predicted Natural Frequencies (kHz)	Observed Vibrothermal Peak Frequencies (kHz)
1	5.25	N/A
2	9.66	9.60
3	11.86	11.30
4	15.13	14.70
5	17.17	17.00
6	21.58	21.60
7	22.30	22.50
8	24.91	25.30

the local resonance model was excellent for the simulated delaminations in all three panels with different layups. Therefore, the frequency dependent behavior during a vibrothermographic test results conclusively for these stacking sequences from the fact that when the excitation frequency reaches the natural frequency of the plate, either above or below the delamination, the plate resonates and heat is dissipated through some mechanism responsive to the increased stresses and/or strains. Hence, the plate should vibrate following its own particular mode behavior at the corresponding natural frequency. While calculating natural frequencies (the eigenvalues) by the Rayleigh-Ritz approximation software program, a set of eigenvectors can be obtained along with each eigenvalue. From the characteristics of the eigenvector, the mode for each natural frequency can be identified. Also, the mode shape (the displacement field) and the strain field can be obtained in the manner stated in section 2.2.

Figure 12 shows the predicted thermoelastic emission field for mode (1,2). The thermoelastic emission field was generated by calculating the thermoelastic emission using Eq. (3.3.3), for 11 × 11 nodes in the delamination region with the strain of mode (1,2), and then using SAS/GRAPH on the IBM mainframe computer to plot thermoelastic emission contours. Each contour line represents points having the same thermoelastic emission. The legends below the plot are the relative thermoelastic emission value for each contour. The coefficients of thermal expansion of glass-epoxy were obtained from Ref. 27. A high thermoelastic emission region corresponds to a region having relative high stresses in the material coordinate system.

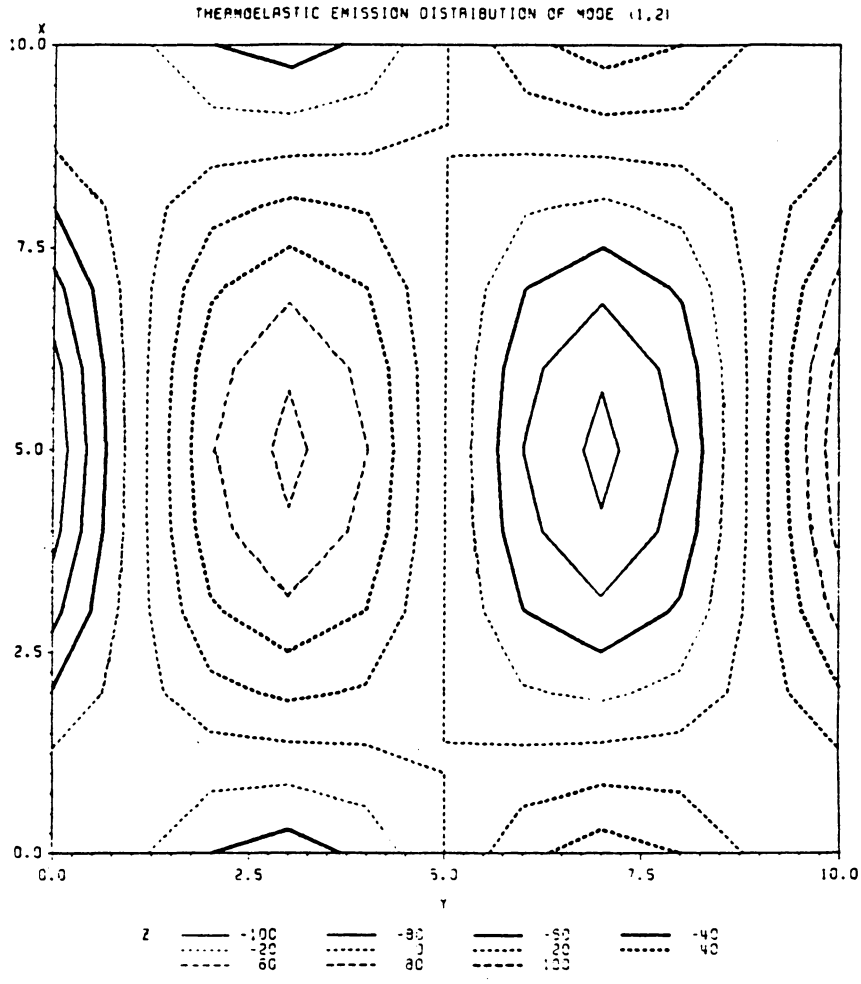

Figure 12. Predicted thermoelastic emission field for mode (1,2).

In Fig. 12, there are two sets of ellipses, representing a high stress region on the left and a low stress region on the right, which shows the behavior of mode 2 in the horizontal direction. For each set of ellipses, a maximum or minimum at the center is seen, which corresponds to the mode 1 behavior in the vertical direction. Figure 13 was the observed thermoelastic emission pattern obtained from the SPATE camera showing the stress field of mode (1,2) of D-44 of $[0/90/90/0]_s$ glass-epoxy panel at 9.6 kHz excitation frequency. The color band on the right of the figure represents the relative thermoelastic emission for each color. The unit was uncalibrated. That is, the patterns shown give correct relative values of the thermoelastic pattern, but not calibrated absolute values. Since a thin, uniform ultra-flat black paint was applied on the surface of the panel to obtain better emissivity, the boundary of the simulated delamination could not be identified by sight. The yellow cross marks in Fig. 13 delineate the approximate positions of the delamination edges. The light blue region on the left of the figure indicates a higher stress region just as the left set of ellipses in Fig. 12. Also, at the right of Fig. 13, the light purple color region represents lower stresses corresponding to the right set of ellipses in Fig. 12. Figure 13 also shows the mode one behavior in the lower stress zone (on the right), but not quite in the higher stress zone. Although the observed stress pattern did not exactly fit the predicted stress pattern, it did show the model behavior of the mode (1,2). It should be noted here that the high and low stress regions are just relative. If the phase is altered 180°, the high or low stress regions could be reversed.

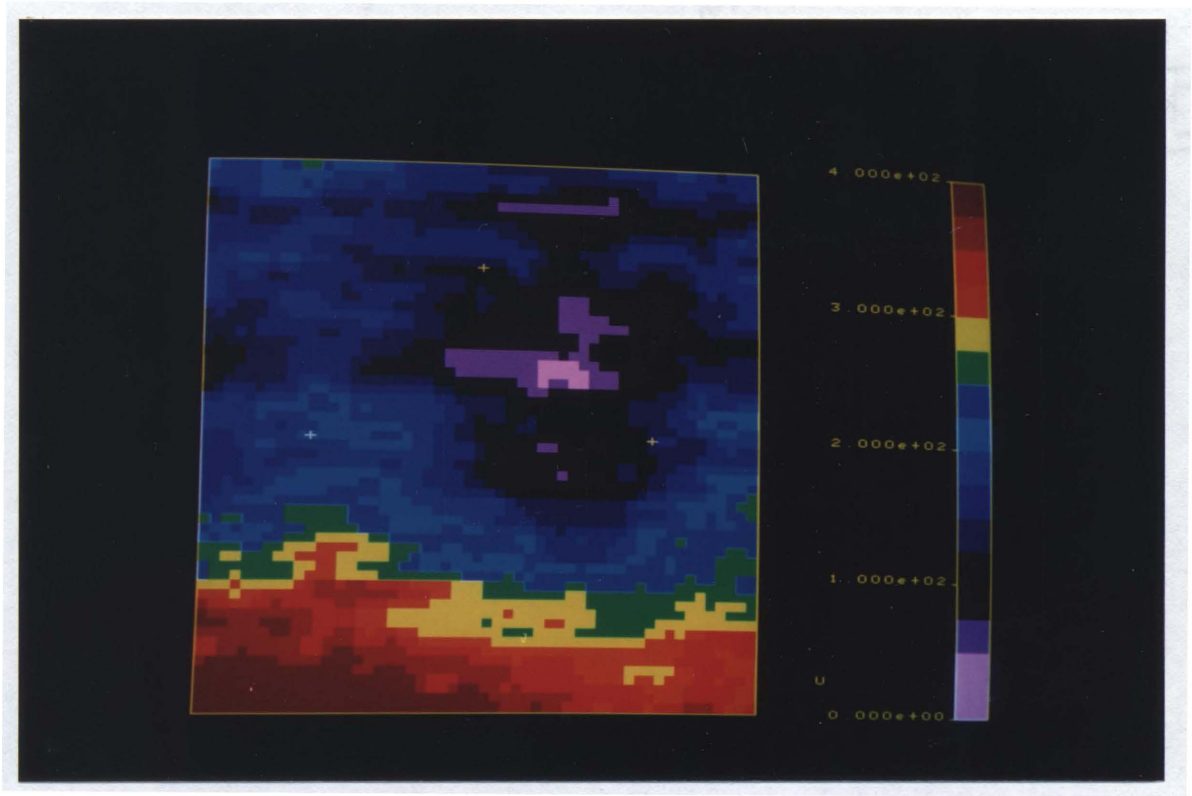

Figure 13. Thermoelastic emission field for mode (1,2) of D-44 at 9.6 kHz excitation frequency.

The predicted thermoelastic emission pattern of mode (2,2) is shown in Fig. 14. The pattern is diagonally symmetric, i.e., for a lower stress quadrant, the adjacent quadrants would be higher stress regions and vise versa. Figure 15 was the observed thermoelastic emission pattern of mode (2,2) of the same delamination as in Fig. 13, at the excitation frequency of 14.7 kHz. The red region in the third quadrant in Fig. 15 shows the highest stress region. The adjacent quadrants, the second and the fourth, show two lower stress regions. Contrary to the predicted pattern, the first quadrant shows an even lower stress region than the second and fourth quadrants. Even with this anomaly, mode 2 behavior is nevertheless displayed qualitatively in both the horizontal and vertical directions.

The predicted thermoelastic emission pattern of mode (1,3) is shown in Fig. 16. Three sets of ellipses represent three peaks of mode 3 in the horizontal direction, two maxima and one minimum. For each set of ellipses, the center shows either a maximum or minimum which is the mode 1 behavior in the vertical direction. Figure 17 was the observed thermoelastic emission pattern at the excitation frequency of 17.1 kHz which was predicted to be mode (1,3). The dark blue zone in the center represents the lower stress zone as in Fig. 16. The two higher stress zones beside the dark blue zone, which are yellow and red, represent the two maximum peak stress zones for mode 3. In the vertical direction, Fig. 16 also shows the mode 1 behavior.

For all of the above 3 modes, the observed thermoelastic emission patterns did not quite fit the predictions exactly. There are several possible reasons for the discrepancy. The predictions were generated for the free vibration condition, but

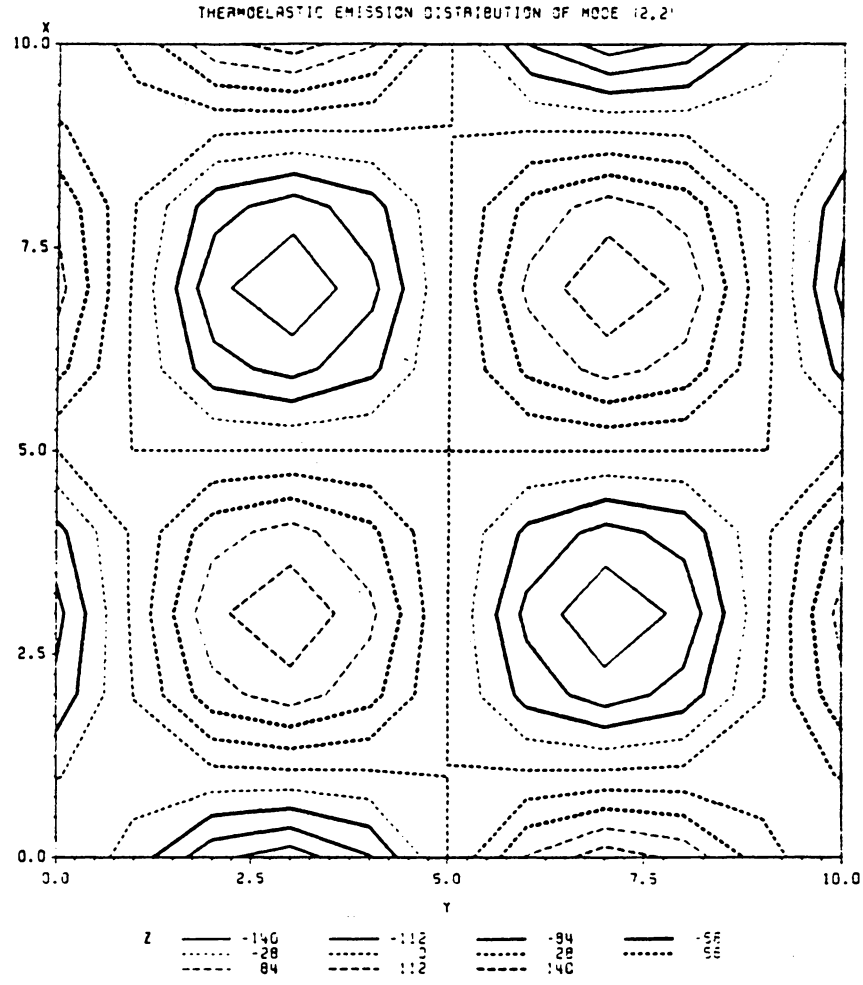

Figure 14. Predicted thermoelastic emission field for mode (2,2).

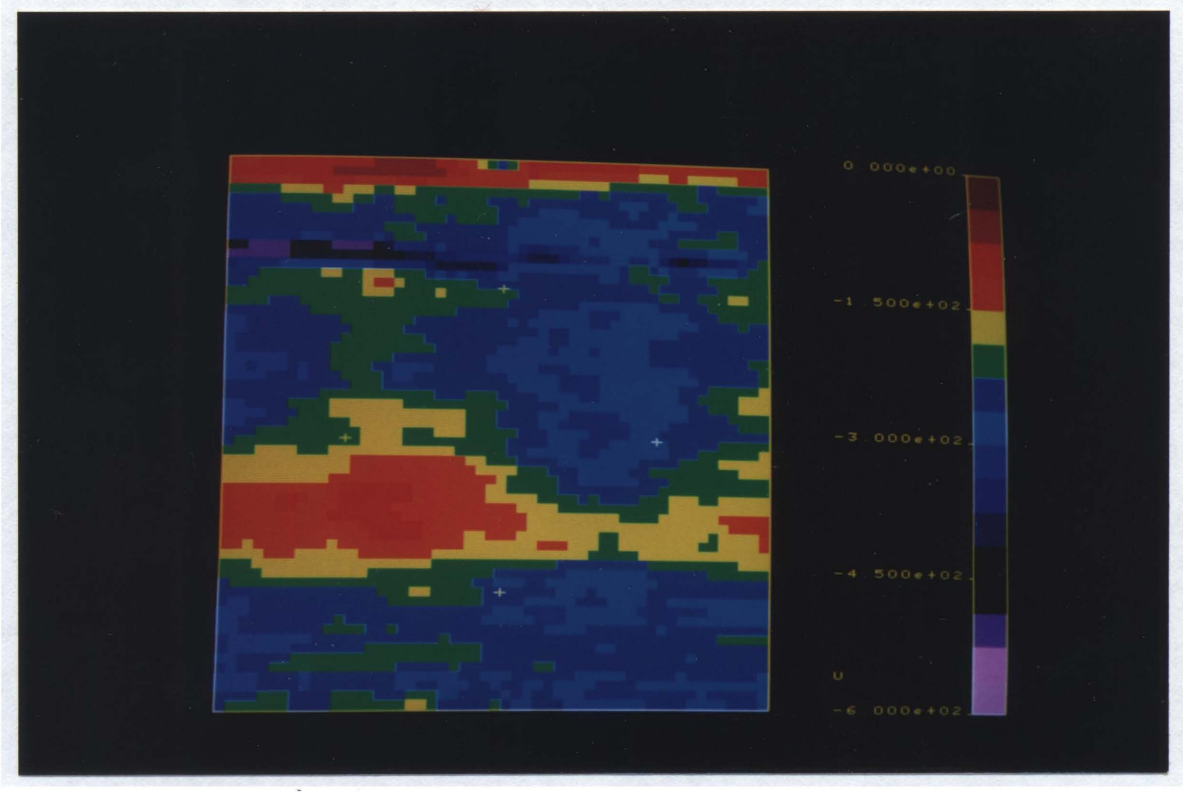

Figure 15. Thermoelastic emission field for mode (2,2) of D-44 at 14.7 kHz excitation frequency.

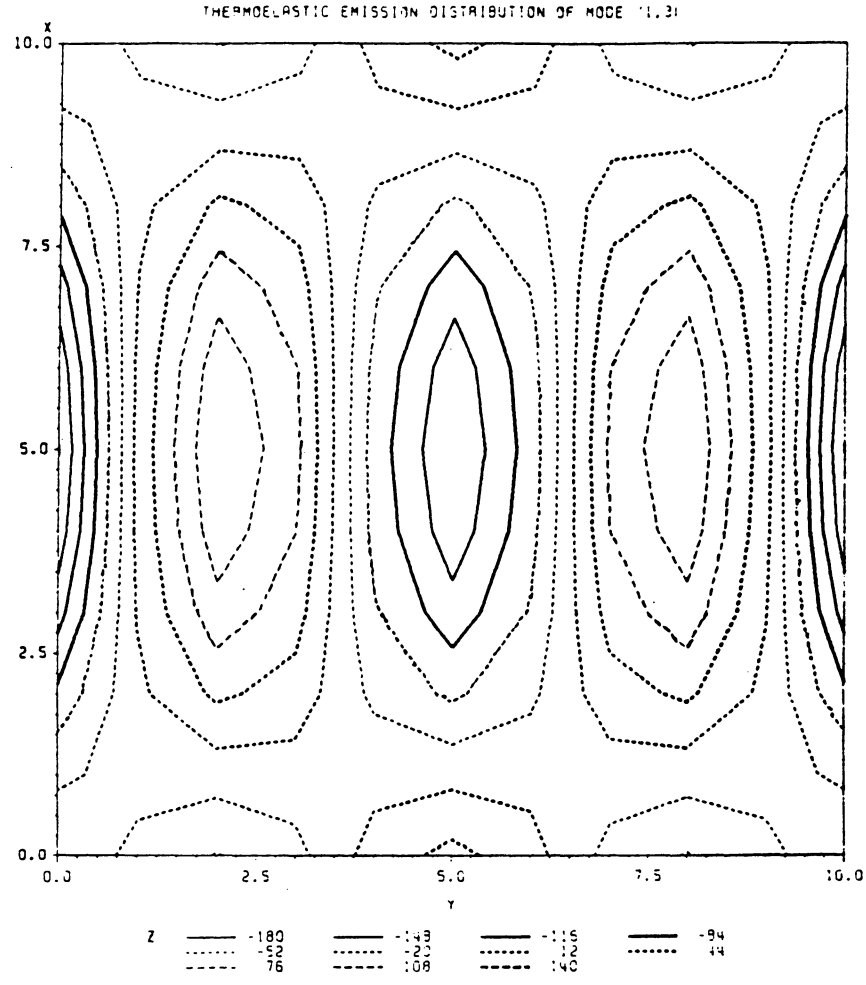

Figure 16. Predicted thermoelastic emission field for mode (1,3).

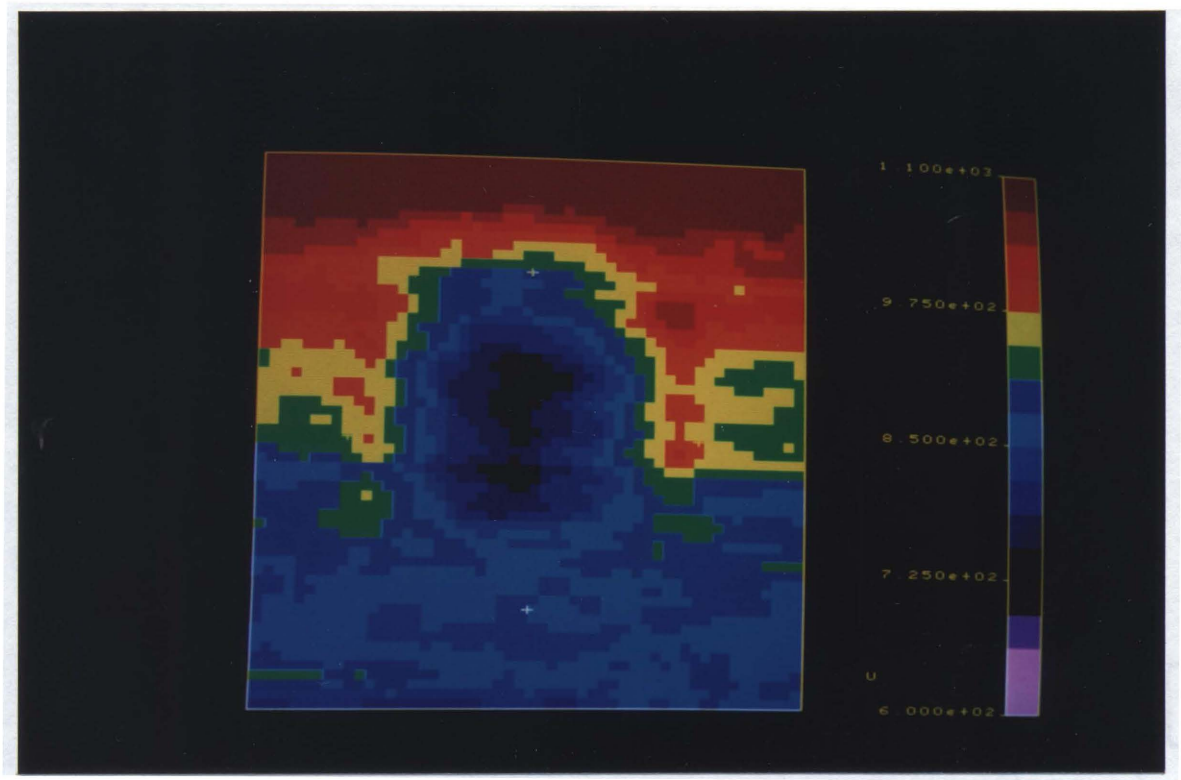

Figure 17. Thermoelastic emission field for mode (1,3) of D-44 at 17.1 kHz excitation frequency.

the actual condition for the delamination plate was forced vibration. The boundary condition was assumed to be clamped, but the boundary vibrated along with the whole panel. As can be seen in the ultrasonic C-scan shown in Fig. 11, the shape of the delamination plate may not have been truly rectangular. Also, the excitation frequency might be off the exact natural frequency slightly, resulting in some change of the mode shape. However, the observations did show qualitatively the model behavior at the corresponding natural frequency. This is additional evidence for the local resonance model.

4.2 Heat Generation Mechanism and Heat Image Simulation

As stated in section 1.2, likely heat generation mechanisms during vibrothermographic testing are heat dissipation of nonconservative deformation due to local high stresses, or heat dissipation due to clapping or rubbing of the defect surfaces. Which of these mechanisms is actually responsible has never been ascertained, and it was believed that the latter one is the main mechanism responsible for the heat generation.

It was already verified that local resonance dominates the vibrothermographic behavior, and if there are different plates on each side of the simulated delamination in a panel, the delamination spot heats up at both sets of the predicted natural frequencies calculated from those plates on two sides of

the delamination. In order to qualify the heat generation mechanism during vibrothermographic testing, the following hypothesis was tested. If the heat generation is due to delamination surface interactions (clapping or rubbing), then, since the delaminated surface is closer to the laminate surface on the side of the thinner plate, the degree of heating of this side should always appear greater than the other side at a resonance frequency of either plate, or at least the temperatures of both sides would be the same. On the other hand, if heating is caused by a nonconservative deformation dependent upon local stresses, the side of the laminate containing the plate which is under a natural resonance should heat up more than the side which is not resonating at a particular applied frequency. The hypothesis was tested by careful measurement of the heat patterns and the degree of heating generated on both surfaces of the same $[0_5]$ glass-epoxy panel excited at each resonance frequency.

The surface temperature distribution of both sides of the laminate was calculated by the finite difference heat transfer program for the $[0_5]$ glass-epoxy panel with the heat generation occurring on the delamination surface located on the 2-3 ply interface. The output showed that the expected difference of the maximum temperatures at the laminate surface on the two sides of the laminate was about 0.02°C if the maximum temperature was about 1.0°C greater than the far field temperature. This difference can not be discriminated by the AGA 780 system. Tables 16 - 19 present the comparison of the degree of heating on both sides of the $[0_5]$ glass-epoxy panel. The output level was the relative voltage output amplitude from the function generator. Since the temperature difference was

Table 16. Comparison of The Degrees of Heating on Two Sides of [0_5] Glass-Epoxy Panel with Simulated Delamination D-31 on 2-3 Ply Interface at Frequencies Which Local Resonance Occurred

I.D.: D-31

Size: 0.940 × 0.902 cm (0.370 × 0.355 in.)

Predicted Natural Frequencies (kHz)		Observed Vibrothermal Peak Frequencies (kHz)	Steady State Temperature (°AGA)		Ouput Level
2-ply thickness	3-ply thickness		2-ply thickness	3-ply thickness	
7.25		N/A	N/A	N/A	N/A
	10.88	10.90	1.4	1.6	2.6
12.30		12.30	1.0	0.8	3.0
17.16		17.80	1.0-1.2	1.0	3.0
	18.45	18.30	0.4-0.6	0.6	3.0
20.86		20.90	0.4	0.2	3.0
21.17		21.30	0.6	0.4	3.0
	25.74	25.60	1.4-1.6	1.6-1.8	1.2

Table 17. Comparison of The Degrees of Heating on Two Sides of [0_5] Glass-Epoxy Panel with Simulated Delamination D-32 on 2-3 Ply Interface at Frequencies Which Local Resonance Occurred

I.D.: D-32

Size: 1.168 × 1.092 cm (0.460 × 0.430 in.)

Predicted Natural Frequencies (kHz)		Observed Vibrothermal Peak Frequencies (kHz)	Steady State Temperature (°AGA)		Ouput Level
2-ply thickness	3-ply thickness		2-ply thickness	3-ply thickness	
4.76		N/A	N/A	N/A	N/A
	7.15	N/A	N/A	N/A	N/A
8.26		N/A	N/A	N/A	N/A
11.15		10.80	0.8	0.6	3.0
	12.39	11.95	1.0	1.2	3.0
13.73		13.30	0.8	0.6	3.0
14.34		14.10	0.6	0.4	3.0
	16.72	16.00	0.8	0.8	3.0
18.86		18.20	0.6	0.4	3.0
	20.60	19.50	0.4	0.4-0.6	3.0
21.10		21.10	0.4-0.6	0.2	3.0
	21.50	21.40	0.6	0.6-0.8	3.0

Table 18. Comparison of The Degrees of Heating on Two Sides of [0_5] Glass-Epoxy Panel with Simulated Delamination D-33 on 2-3 Ply Interface at Frequencies Which Local Resonance Occurred

I.D.: D-33

Size: 1.334 × 1.219 cm (0.525 × 0.480 in.)

Predicted Natural Frequencies (kHz)		Observed Vibrothermal Peak Frequencies (kHz)	Steady State Temperature (°AGA)		Ouput Level
2-ply thickness	3-ply thickness		2-ply thickness	3-ply thickness	
3.71		N/A	N/A	N/A	N/A
	5.57	N/A	N/A	N/A	N/A
6.55		N/A	N/A	N/A	N/A
8.59		N/A	N/A	N/A	N/A
	9.82	9.70	0.2-0.4	0.6	4.0
10.70		10.90	0.6-0.8	0.6	2.0
11.45		11.60	2.0	1.2	1.4
	12.89	13.10	1.2	1.4	3.0
14.86		14.60	1.2	1.0	3.0
	16.05	16.00	1.4	1.6	2.6
16.22		16.40	1.8-2.0	1.4-1.6	3.0
	17.17	17.30	0.8	0.8-1.0	3.0

Table 19. Comparison of The Degrees of Heating on Two Sides of [0_5] Glass-Epoxy Panel with Simulated Delamination D-34 on 2-3 Ply Interface at Frequencies Which Local Resonance Occurred

I.D.: D-34

Size: 1.410 × 1.245 cm (0.555 × 0.490 in.)

Predicted Natural Frequencies (kHz)		Observed Vibrothermal Peak Frequencies (kHz)	Steady State Temperature (°AGA)		Ouput Level
2-ply thickness	3-ply thickness		2-ply thickness	3-ply thickness	
3.40		N/A	N/A	N/A	N/A
	5.10	N/A	N/A	N/A	N/A
6.17		N/A	N/A	N/A	N/A
7.73		N/A	N/A	N/A	N/A
	9.26	9.30	0.4-0.6	0.6	4.0
9.82		9.70	1.2	1.0	4.0
10.90		10.95	1.6	1.2	2.4
	11.61	11.60	1.4-1.6	1.6	1.2
13.88		13.80	1.4-1.6	1.4	1.4
14.56		14.50	1.0-1.2	1.0-1.2	2.6
	14.73	15.00	1.2-1.4	1.4-1.6	1.6
16.25		16.10	0.8-1.0	0.8	2.2
	16.35	16.60	1.2	1.2-1.4	2.6
17.39		18.00	1.2-1.4	1.0	3.0
19.63		19.70	0.6-0.8	0.6	3.0
	20.83	20.70	0.4-0.6	0.6	3.0

normally small, the output level was adjusted to yield the maximum temperature relative to the far field temperature within the 2°AGA range. The degree of heating on both sides of the laminate was measured at the same output level and with the same distance between panel and camera. The experimental results show that the temperature on the side of the plate which was under a resonant condition was always greater than or at least equal to the temperature of the other side which was not resonating at the particular applied frequency.

The above experimental observation indicates that the main heat generation mechanism under local resonance condition is not clapping or rubbing of the delamination surface. Therefore, the majority of heat generated is probably caused by nonconservative deformation related to higher stresses and/or strains due to local resonance. This is a reasonable conclusion and can be used to explain some observations during vibrothermographic testing. When system resonance occurs during vibrothermographic testing, there are hot spots generated at locations where there is no detected damage. Therefore, these hot spots are caused by local high stresses due to the system resonance. This indicates that heat dissipation due to a nonconservative deformation related to local high stresses is enough to generate heat patterns which are detectable. Jones[18] performed an experiment on a panel with holes drilled partially through the thickness to simulate damages. It was found that the heat patterns generated on the region of the partially drilled holes were also frequency dependent during a vibrothermographic test. There are no contact surfaces for this type of damage, and hence the surface interaction can not be the source of heat dissipation. This

can be explained as follows. When the frequency reaches one of the natural frequencies of the plate with the size of the hole and the thickness of the panel at the hole, heat is dissipated by nonconservative deformation related to local high stresses and/or strains caused by local resonant vibration. Although the actual heat generation mechanism has not been identified as yet, it has been narrowed down to being stress and/or strain related.

From the above observations and discussion, the likely heat generation mechanism during a vibrothermographic test seems to be related to higher stresses and/or strains due to local resonant vibration. To test strain dependency, the heat generation input for the finite difference heat transfer program was chosen to be proportional to the strain field, either the sum of the principal strain field, or the shear strain field in material coordinates. For the panel specimen as used in this study, the boundary was chosen far enough from the delamination region to believe that the boundary temperature was the far field temperature. The delamination was assumed to be square and was divided into 6×6 nodes. For each node in the delamination, the strain on the node was averaged by integrating the strain from the midpoint between the previous node to the midpoint between the next node in both x and y directions, and dividing by the area integrated over. The heat generation was input to the nodal points of each layer in the delamination region. The thermal properties of unidirectional glass-epoxy was obtained from Ref. 28. The temperature distribution generated from the heat transfer program was then plotted as isothermal contours using SAS/GRAPH on IBM mainframe computer.

Figure 18 represents the observed heat pattern of D-44 of $[0/90/90/0]_s$ glass-epoxy panel generated at the excitation frequency of 11.3 kHz. This was mode (2,1). Figures 19 and 20 represent the predicted heat patterns of mode (2,1) generated from the finite difference heat transfer program, with the heat generation proportional to the sum of the principal strain field or the shear strain field in material coordinates, respectively. As can be seen, the isothermal contours at the center of the vibrothermogram in Fig. 18 elongated in the x-direction (which was vertical), and the outer isotherms elongated slightly in y-direction (which was horizontal). Compared with Figs. 19 and 20, the heat pattern of mode (2,1) was affected by the combination of the sum of the principal strain field and the shear strain field. Figure 21 was the vibrothermogram of mode (1,3) of D-44 generated at an excitation frequency of 17.1 kHz. Figures 22 and 23 represent the predicted heat patterns of mode (1,3). Comparison between Figs. 21, 22, and 23, shows the same result as mode (2,1). Figure 24 was the heat pattern of D-44 generated at an excitation frequency of 22.5 kHz which was mode (3,1). Comparison between the observed heat pattern of mode (3,1) and the predicted heat patterns which are shown in Figs. 25 and 26, shows a difference from the previous two modes. The heat pattern was affected by the shear strain field dominantly in the latter case.

From the above comparisons and observations of other modes not presented here, it seems that the heat pattern is affected by the combination of the sum of the principal strain field and the shear strain field for the lower modes of resonant vibration, and is dominated by the shear strain field for the higher

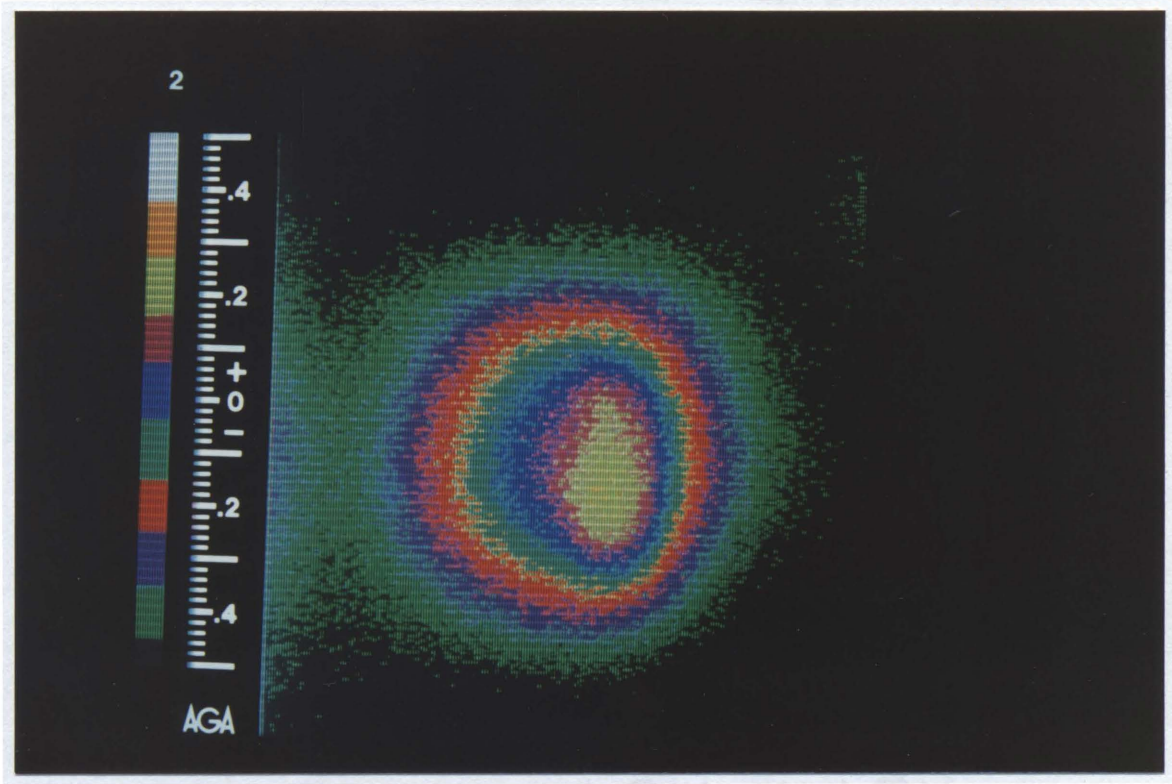

Figure 18. Vibrothermogram of mode (2,1) of D-44 at 11.3 kHz excitation frequency.

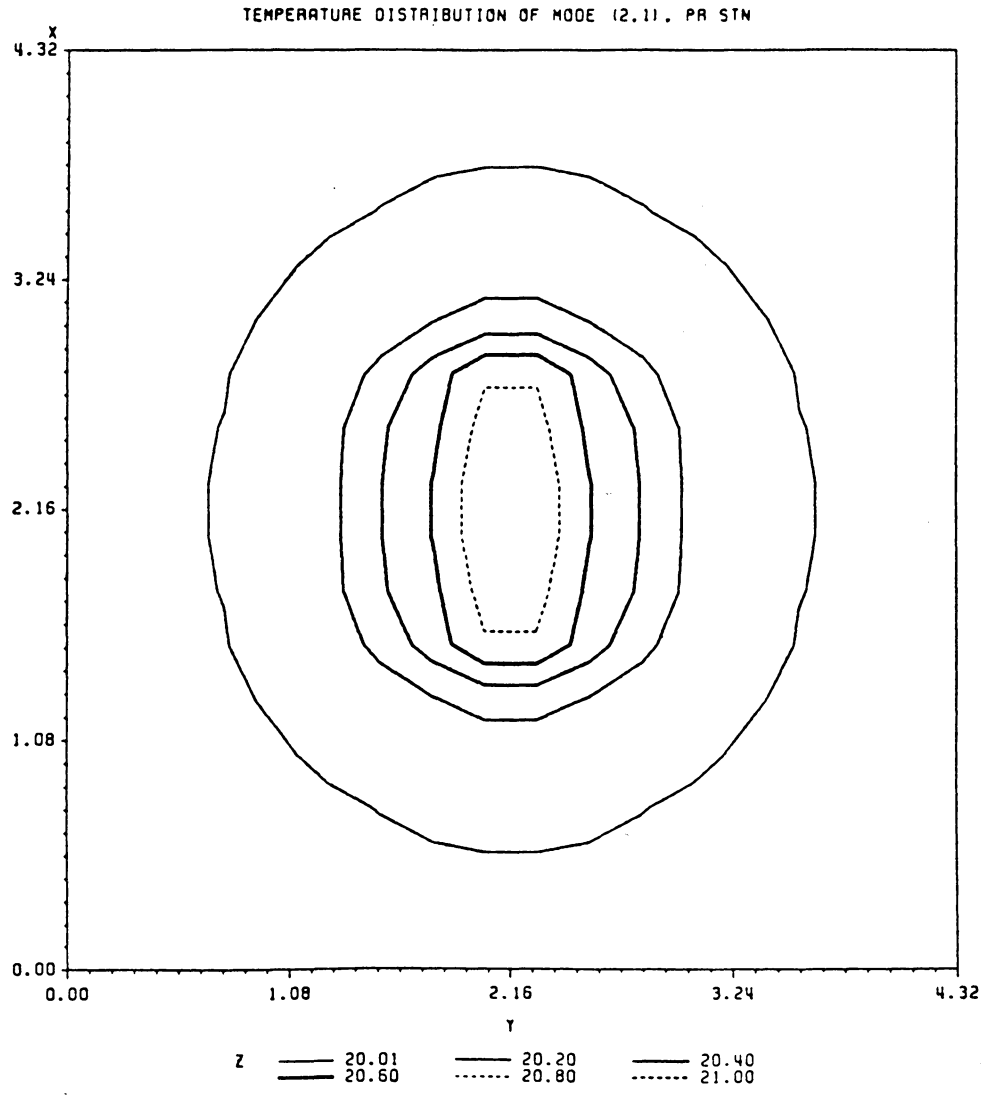

Figure 19. Predicted heat pattern of mode (2,1) with heat generation proportional to the principal strain field.

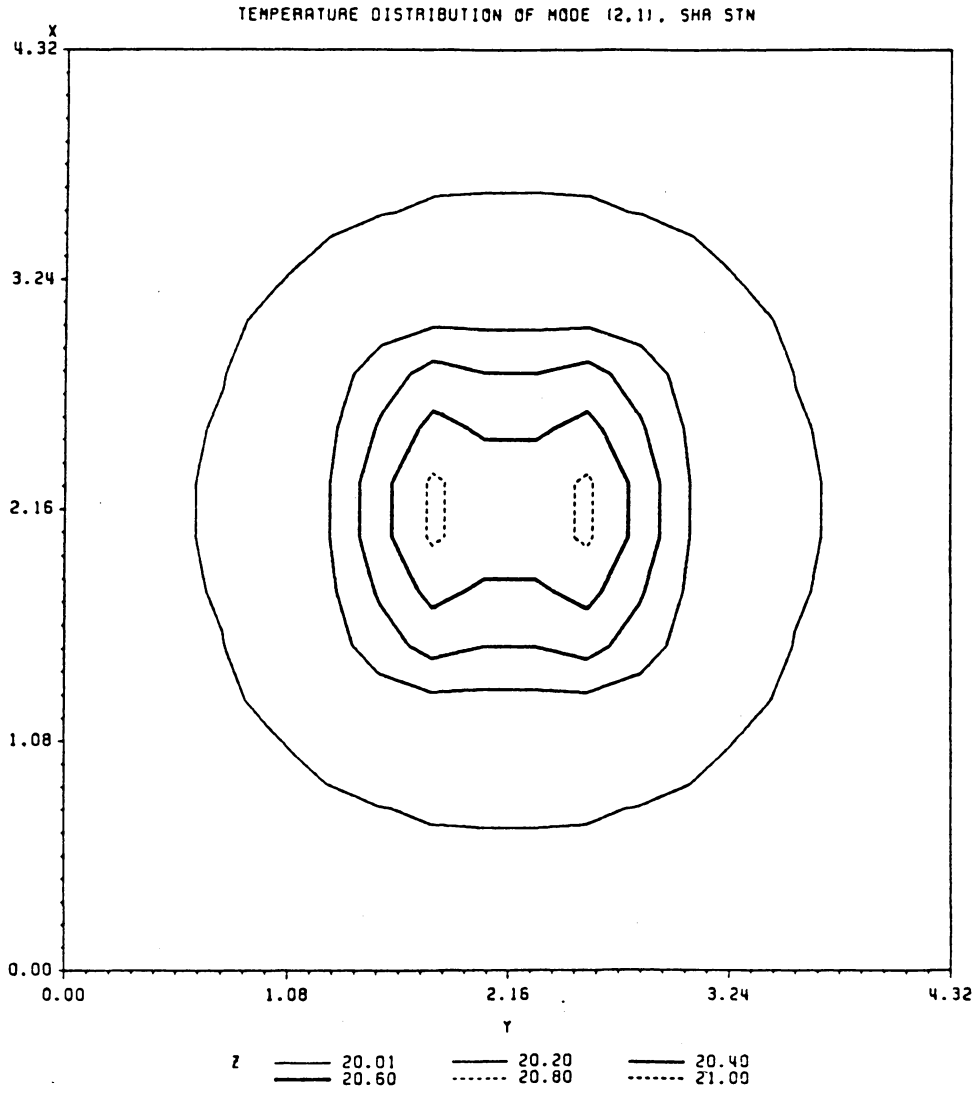

Figure 20. Predicted heat pattern of mode (2,1) with heat generation proportional to the shear strain field.

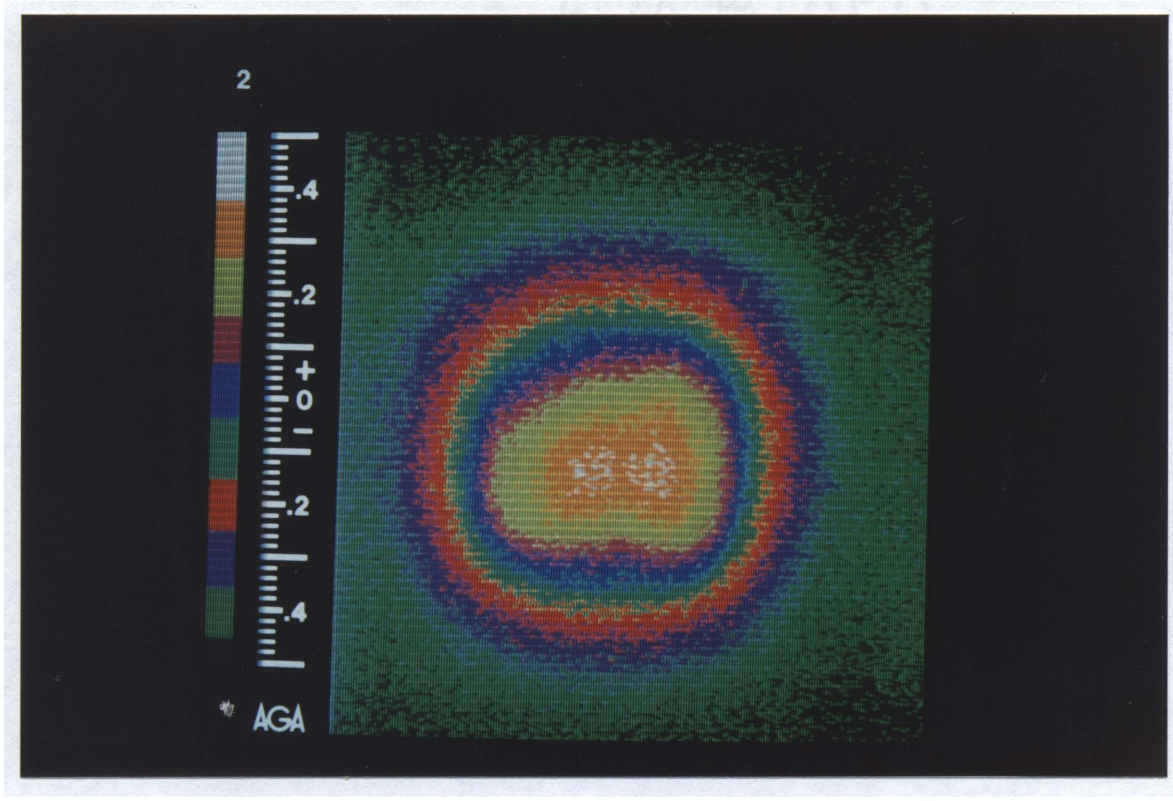

Figure 21. Vibrothermogram of mode (1,3) of D-44 at 17.1 kHz excitation frequency.

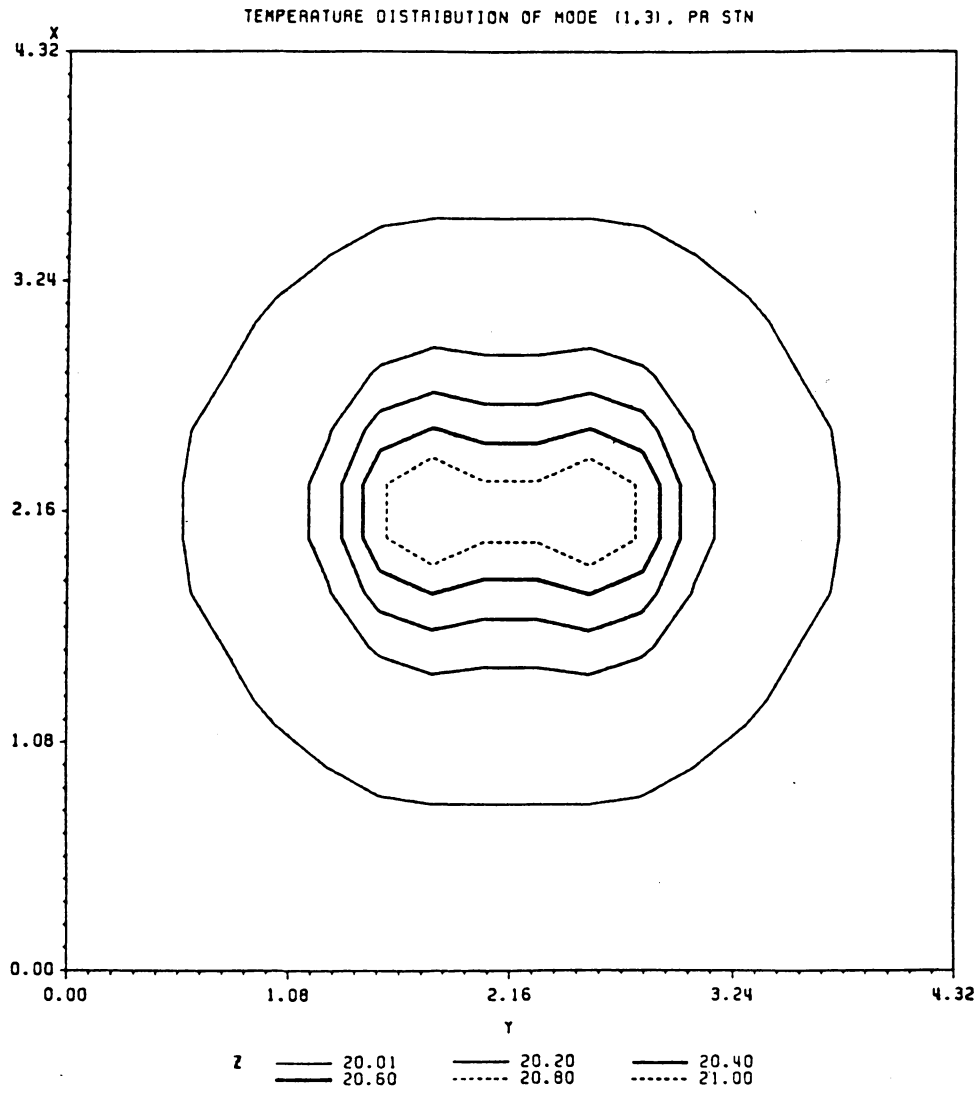

Figure 22. Predicted heat pattern of mode (1,3) with heat generation proportional to the principal strain field.

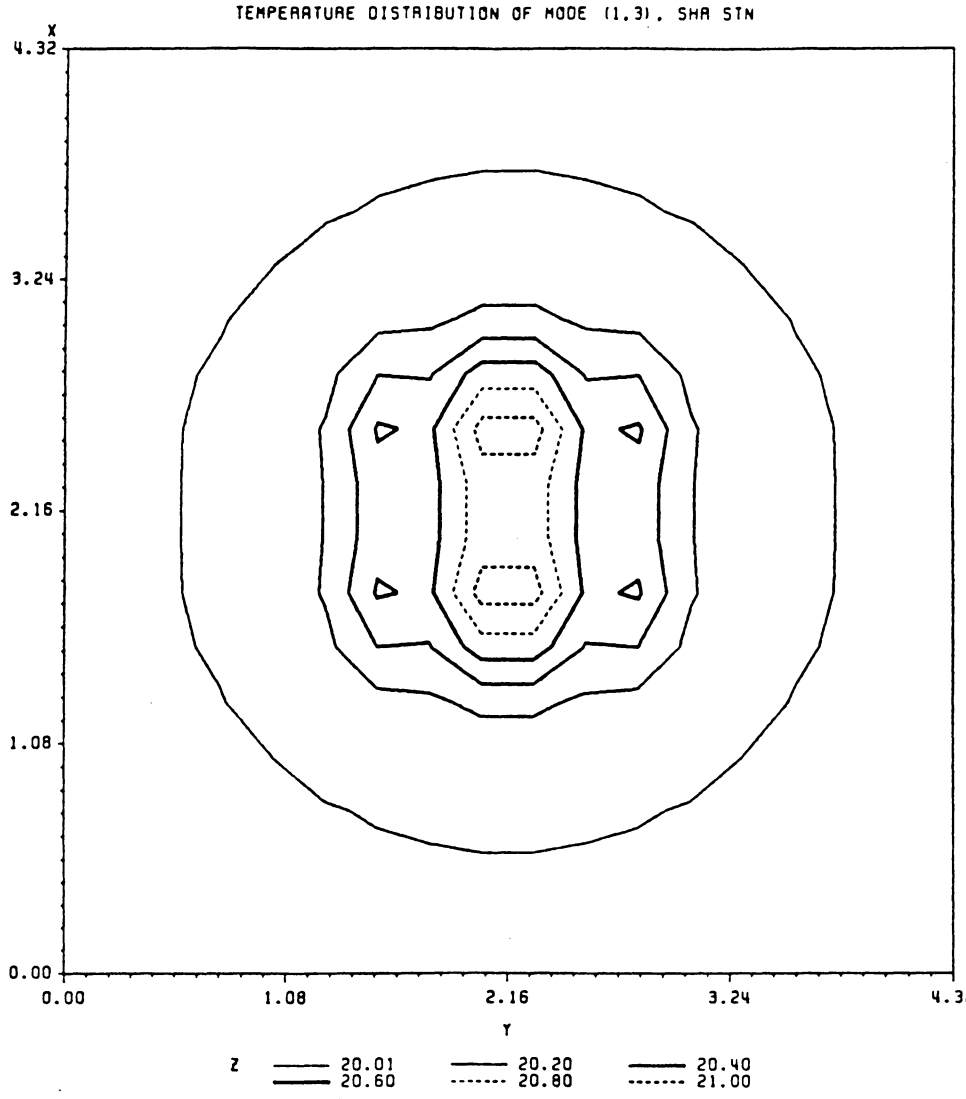

Figure 23. Predicted heat pattern of mode (1,3) with heat generation proportional to the shear strain field.

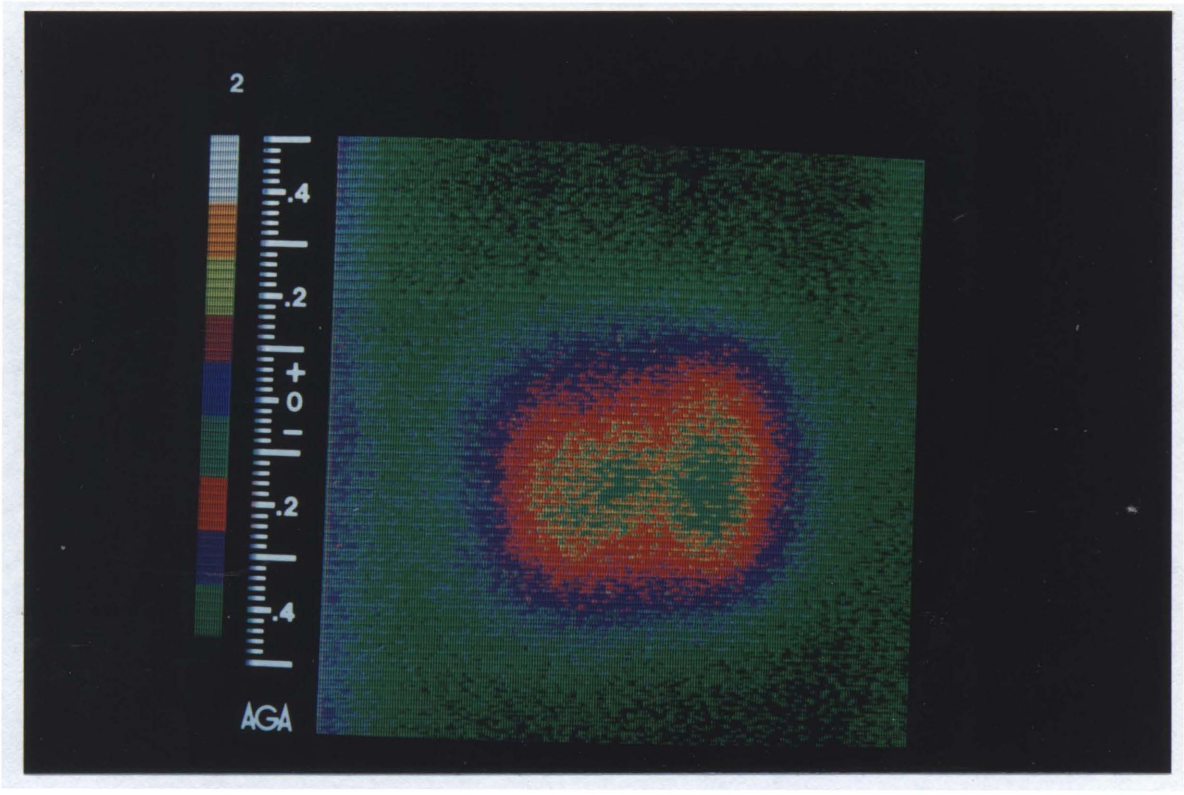

Figure 24. Vibrothermogram of mode (3,1) of D-44 at 22.5 kHz excitation frequency.

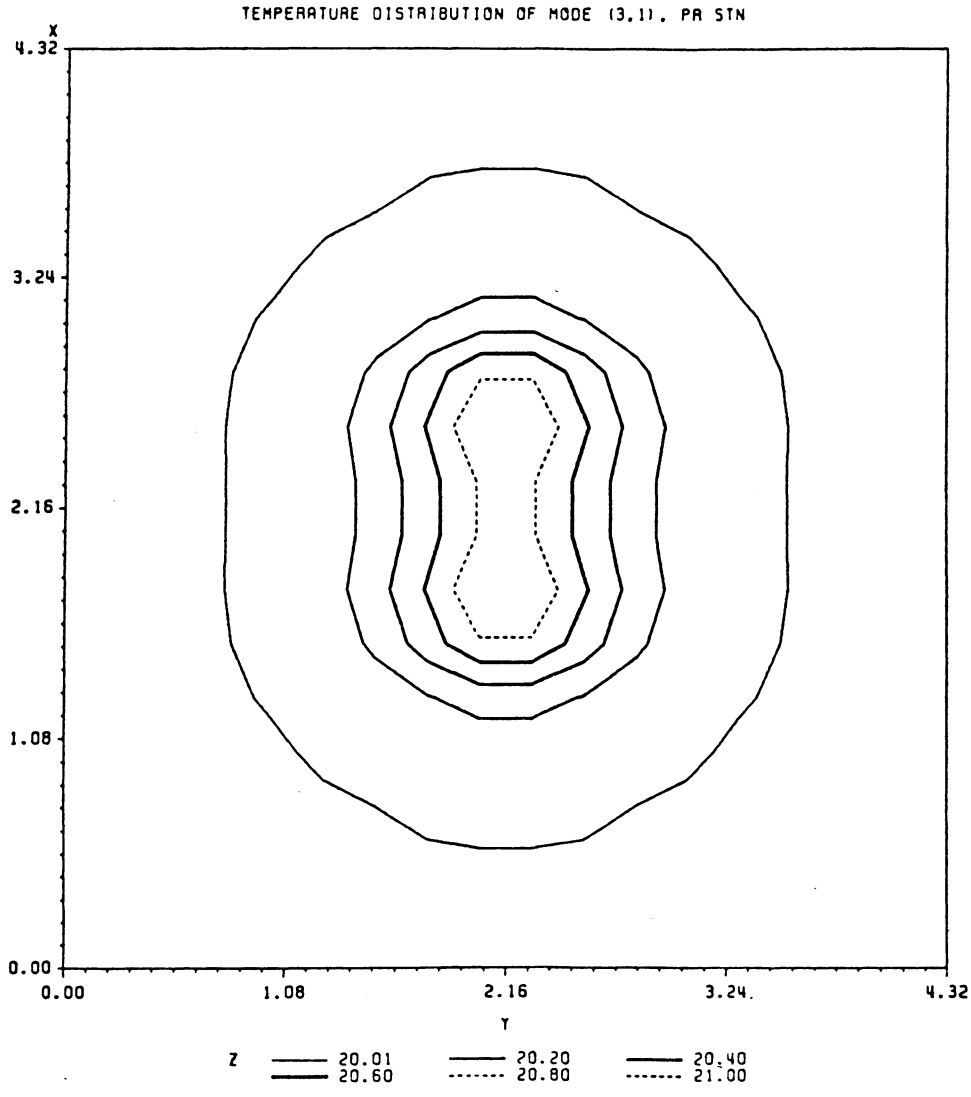

Figure 25. Predicted heat pattern of mode (3,1) with heat generation proportional to the principal strain field.

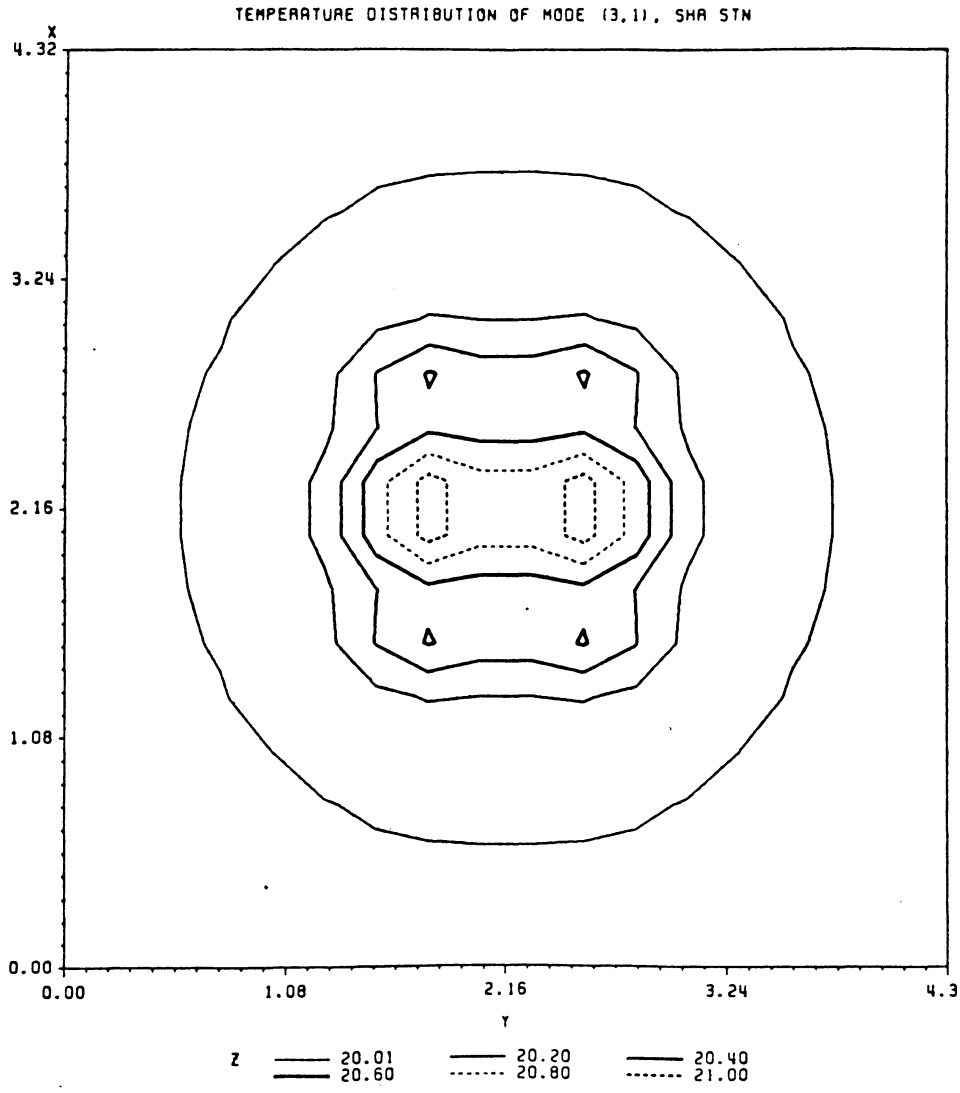

Figure 26. Predicted heat pattern of mode (3,1) with heat generation proportional to the shear strain field.

modes of resonant vibration. The reason for this phenomenon is not known yet. More research on this phenomenon has to be performed.

4.3 Impact Damaged Cross-Ply Graphite-Epoxy Panels

For constituting an application of vibrothermography on a real damaged specimen, three 12 in. square graphite-epoxy panels with layups of $[0/90]_s$, $[0/90/0/90]_s$, and $[0_2/90_2/0_2/90_2]_s$ respectively, were constructed and impact damaged. The impact damage zones were created by dropping a spherical steel ball from various heights onto the panel for various energies. However, the lowest impact energy, 2.84 joule, failed to produce damage detectable by either ultrasonic C-scan or vibrothermographic inspection in all three panels.

Figure 27 is an ultrasonic C-scan of the entire $[0/90]_s$, 12 in. square, graphite-epoxy panel with the poor ultrasonic transmission indicated in white. The regions marked with "2", "3", and "4" are the results of the impact damage zones with energies of 5.27, 6.45, and 7.66 joule, respectively. This 4-ply graphite-epoxy panel can not withstand these impacts, and some pop-out caused by the delamination and fiber fracture can be seen on both surface plies. The damage sizes were much larger than those in the other two panels. Figures 28 - 30 show the impact caused delaminations between the 0° and 90° ply and the fiber fracture, by edge replicas magnified 51 times (A) and maps of damage (B), of sections through the impact regions with energies of 5.27, 6.45, and 7.66 joule,

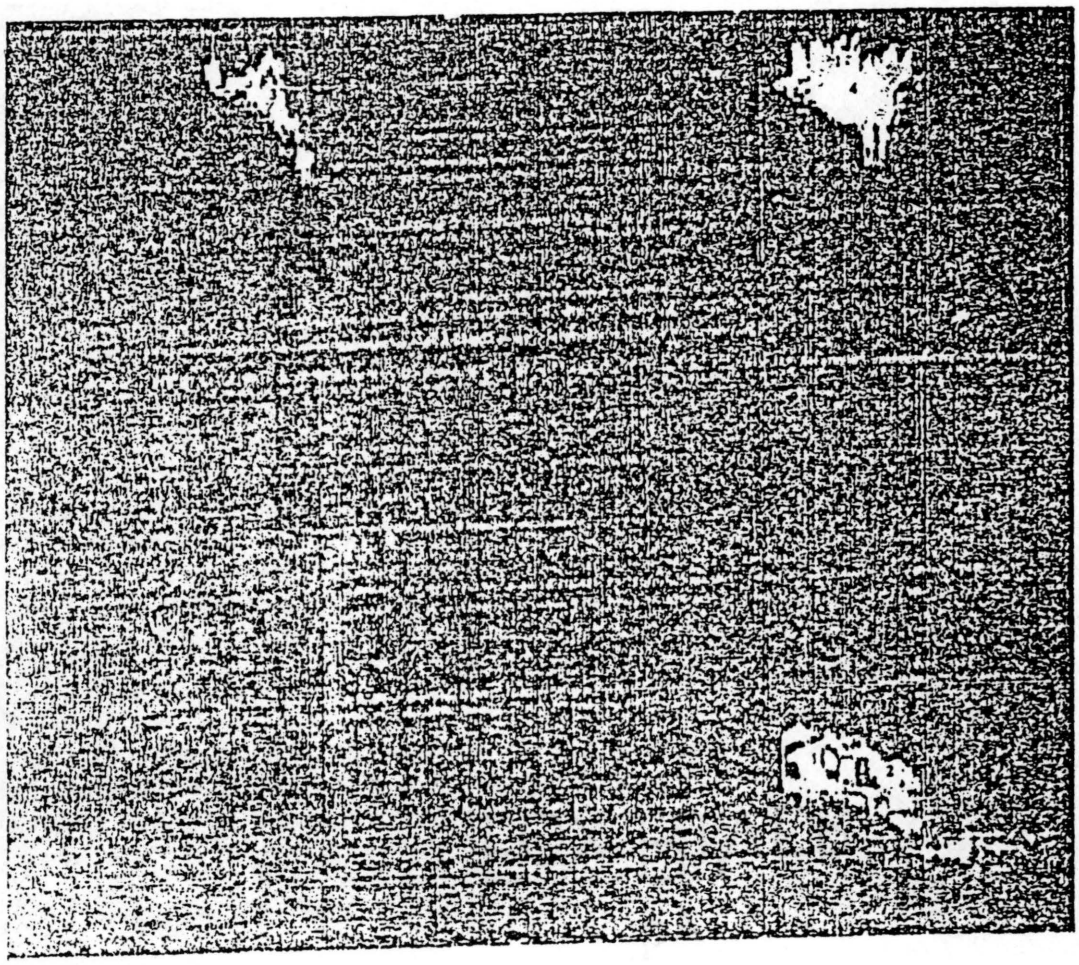

Figure 27. Ultrasonic C-scan of entire $[0/90]_s$ graphite-epoxy panel: Damage regions with impact energies of 5.27, 6.45, and 7.66 joule are mark with ″2″, ″3″, and ″4″, respectively.

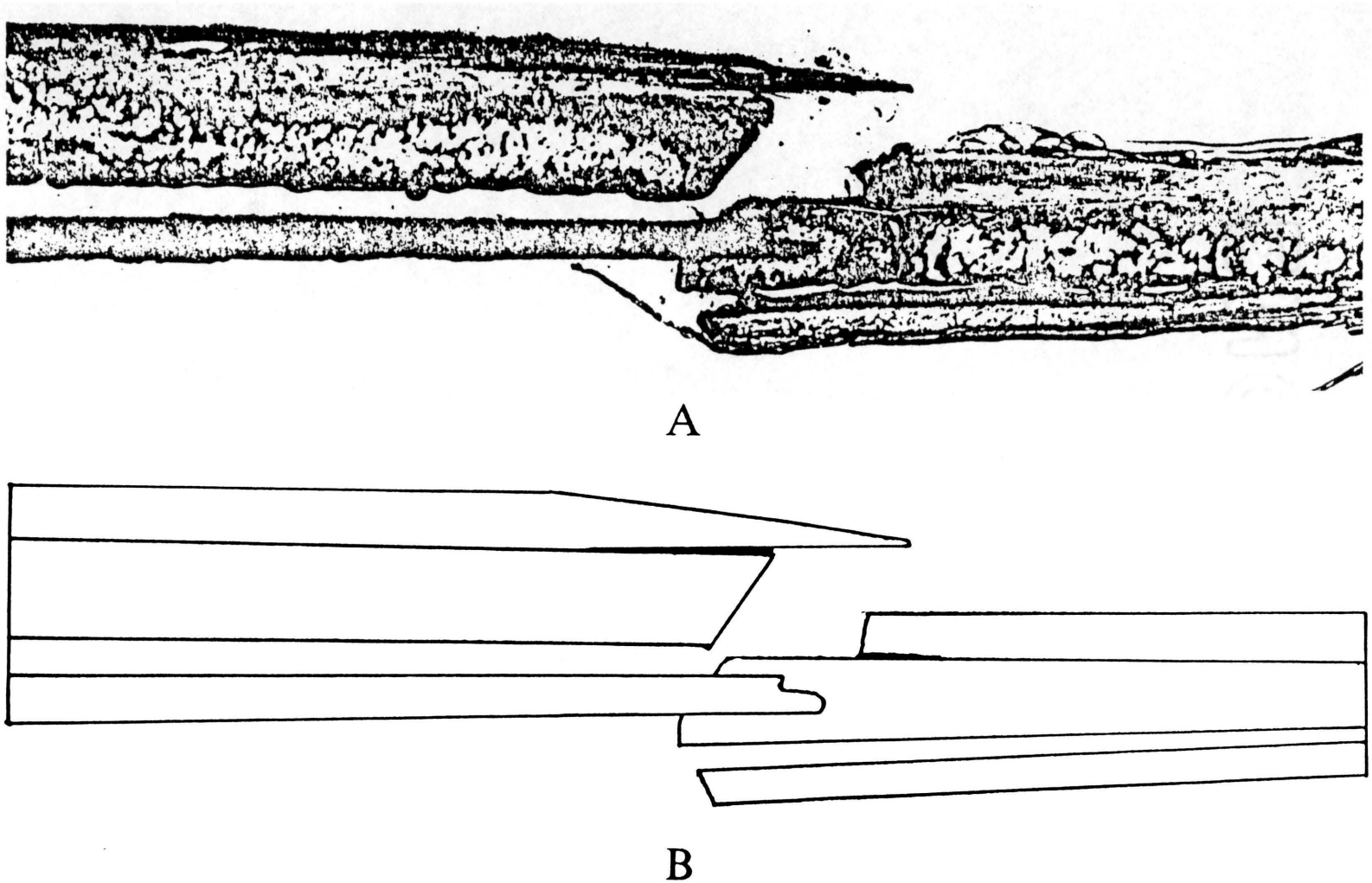

Figure 28. Edge replica (A) and a map of damage (B) of section through damage region with impact energy of 5.27 joule of 4-ply panel (top side impacted).

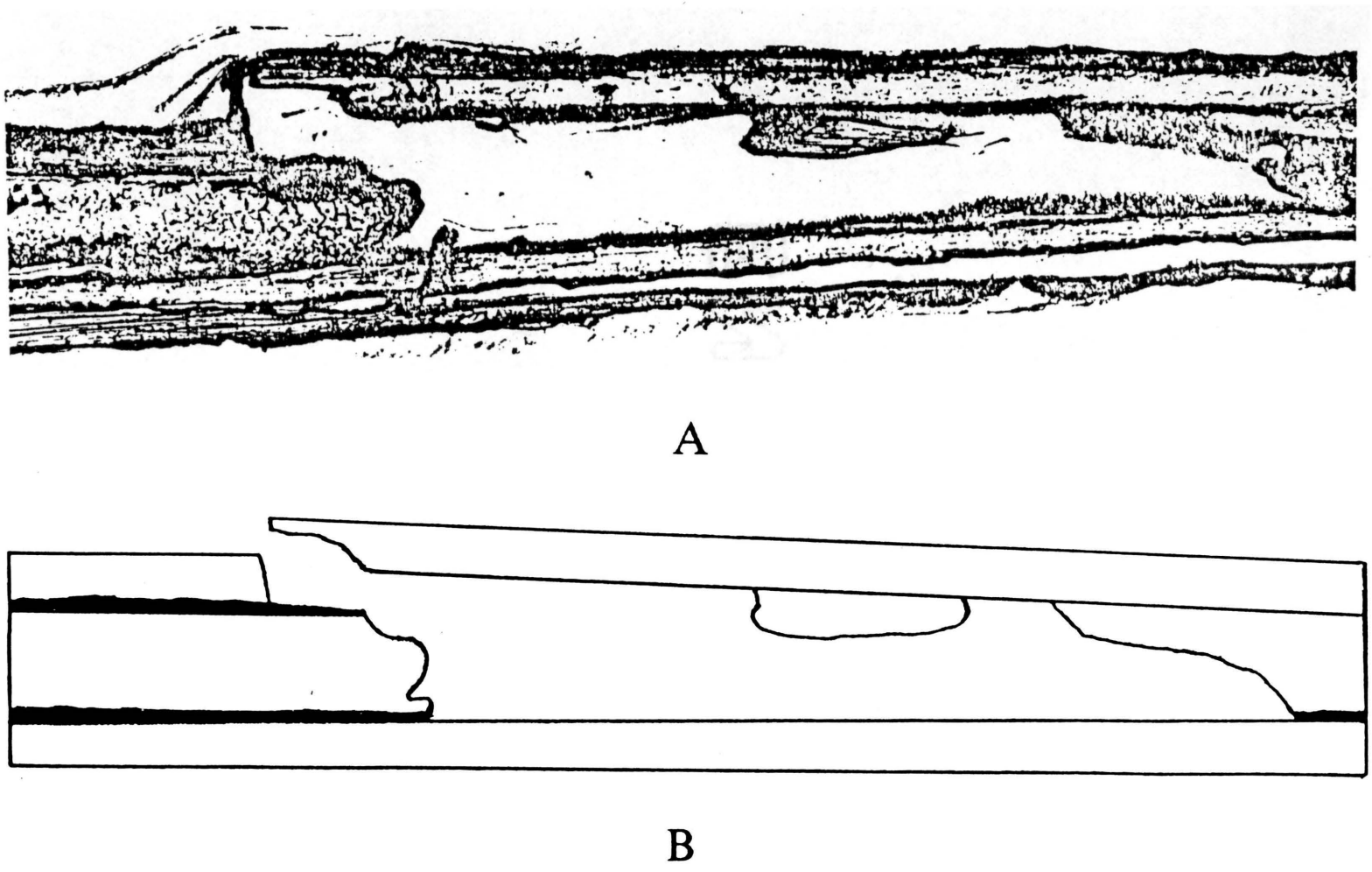

Figure 29. Edge replica (A) and a map of damage (B) of section through damage region with impact energy of 6.45 joule of 4-ply panel (top side impacted).

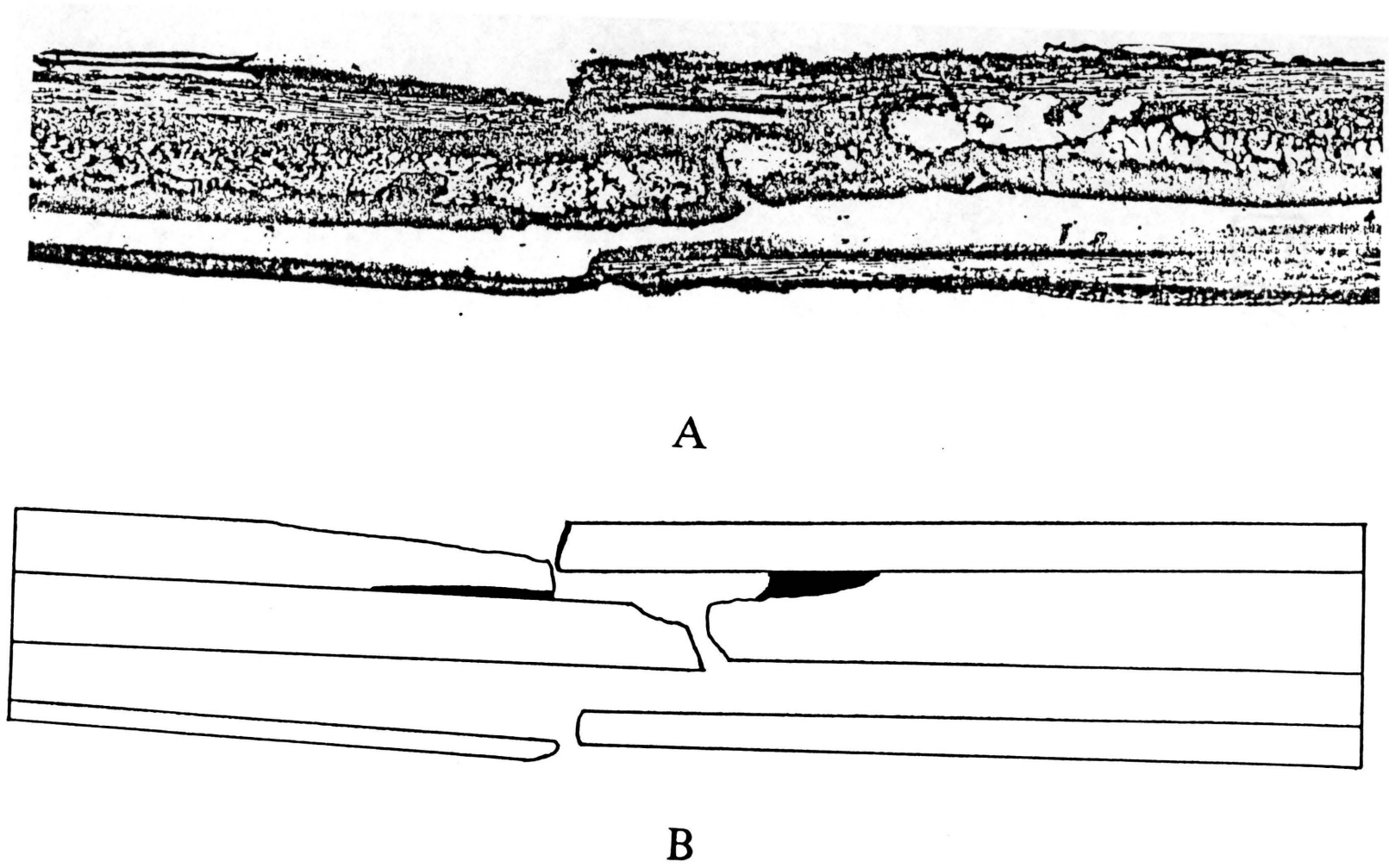

Figure 30. Edge replica (A) and a map of damage (B) of section through damage region with impact energy of 7.66 joule of 4-ply panel (top side impacted).

respectively. In these edge replicas, the side of the panel impacted is on the top. As expected, the damage is more severe on the side opposite the impact.

Vibrothermographic tests were performed on the impacted damaged panels through the frequency range of 9.0 - 22.0 kHz with the increment of 0.1 kHz, and the degree of heating of the damaged regions was measured. The plots of the degree of heating versus the frequency, at the damage regions with those three levels of impact energies, are shown in Figs. 31 - 33. The results indicated that the degree of heating is strongly dependent upon the exciting frequency. Those vibrothermal peak frequencies should be related to the natural frequencies of the delaminated plate on the damage zones. In general, the more severe the damage is, the greater the degree of heating obtained at the vibrothermal peak frequencies. At some particular applied frequency, the degree of heating of the less severe damage region can be greater than the more heavily damaged regions. As can be seen in Figs. 31 - 33, the degree of heating maintained a detectable level even at the frequency which is away from a vibrothermal peak frequency. This basic heat generation is suspected to be caused by the friction of the pop-out surface and is independent of the frequency. Compared to the degree of heating at vibrothermal peak frequencies, this type of heat generation is much lower than the heat generation due to local resonance.

The ultrasonic C-scan of the entire $[0/90/0/90]_s$, 12 in. square, graphite-epoxy panel with the damage regions marked with "2", "3", and "4", which are caused by those three level impact energies, respectively, is shown in Fig. 34. As can be seen, the damage sizes are much smaller than those in the 4 ply panel, and

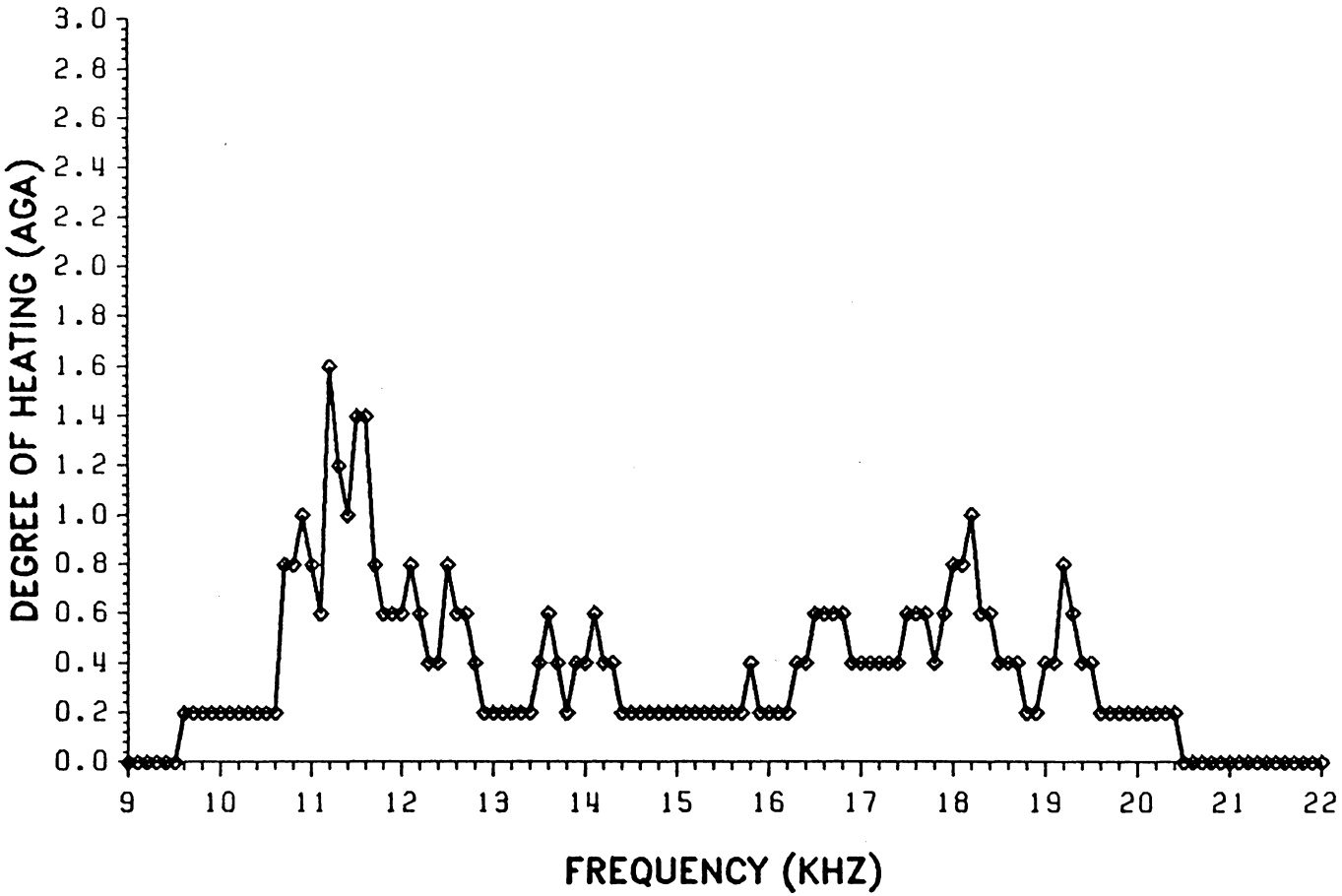

Figure 31. Degree of heating in the frequency range of 9.0 - 22.0 kHz on damage region with impact energy of 5.27 joule of 4-ply panel.

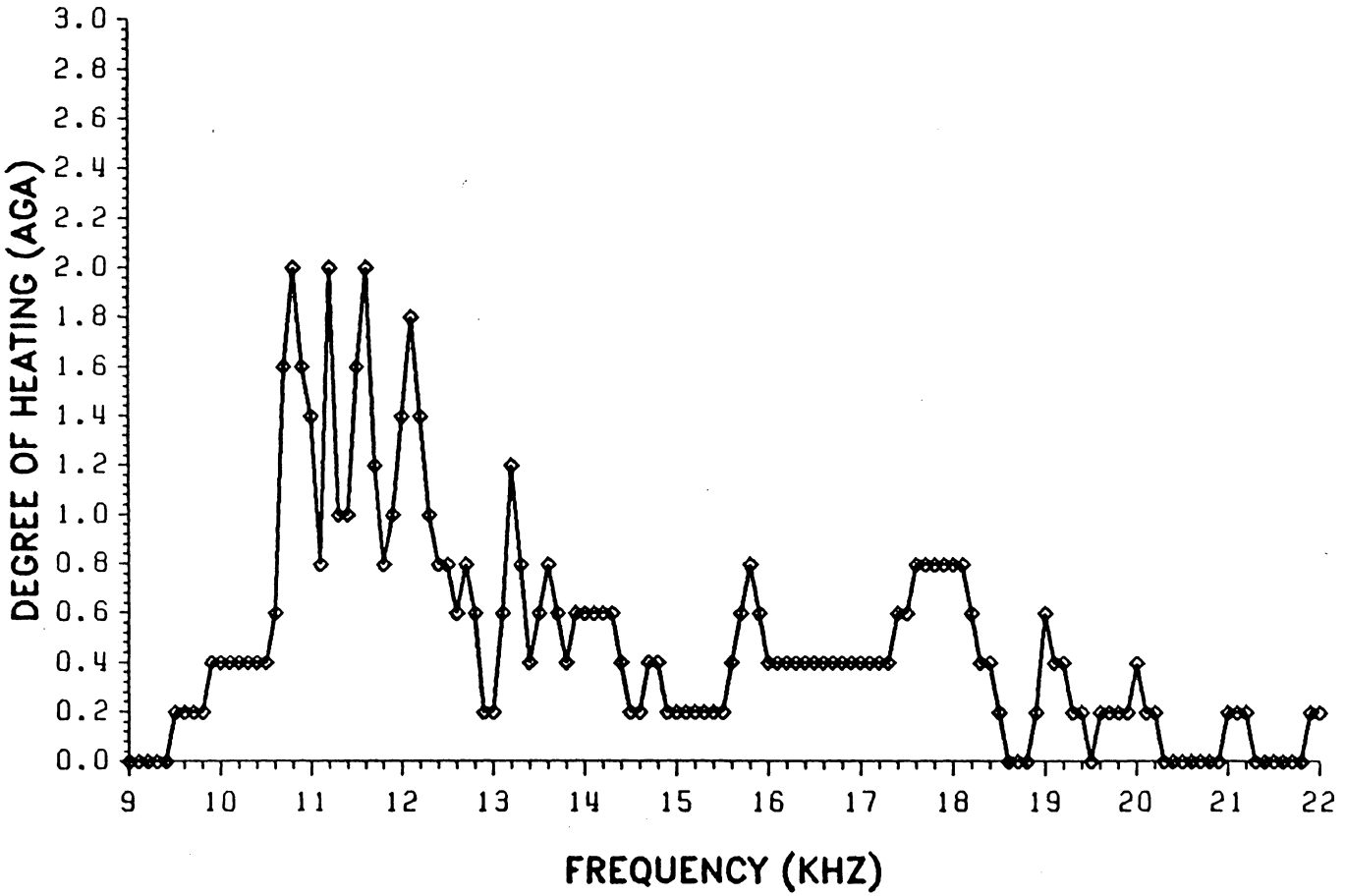

Figure 32. Degree of heating in the frequency range of 9.0 - 22.0 kHz on damage region with impact energy of 6.45 joule of 4-ply panel.

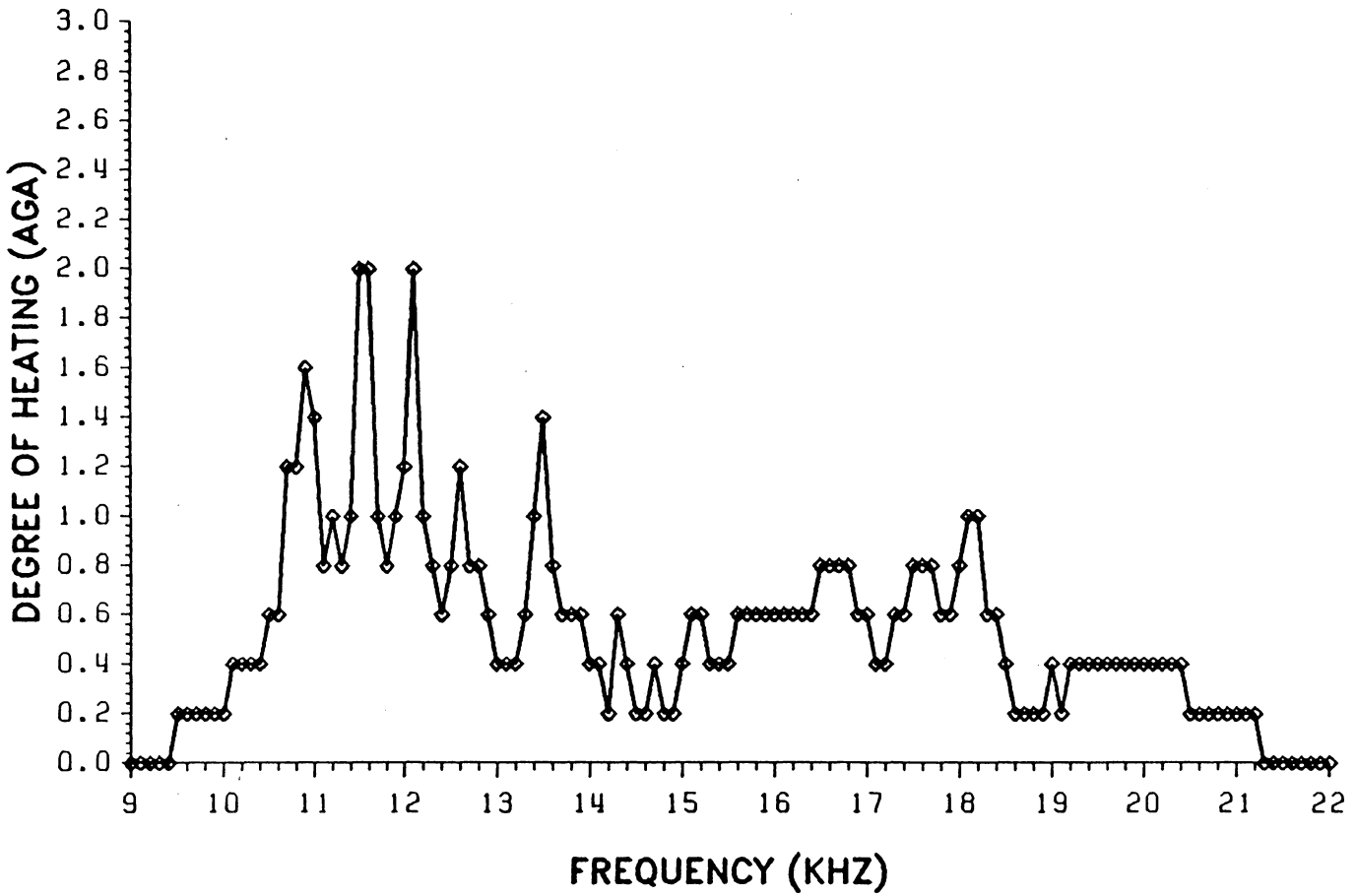

Figure 33. Degree of heating in the frequency range of 9.0 - 22.0 kHz on damage region with impact energy of 7.66 joule of 4-ply panel.

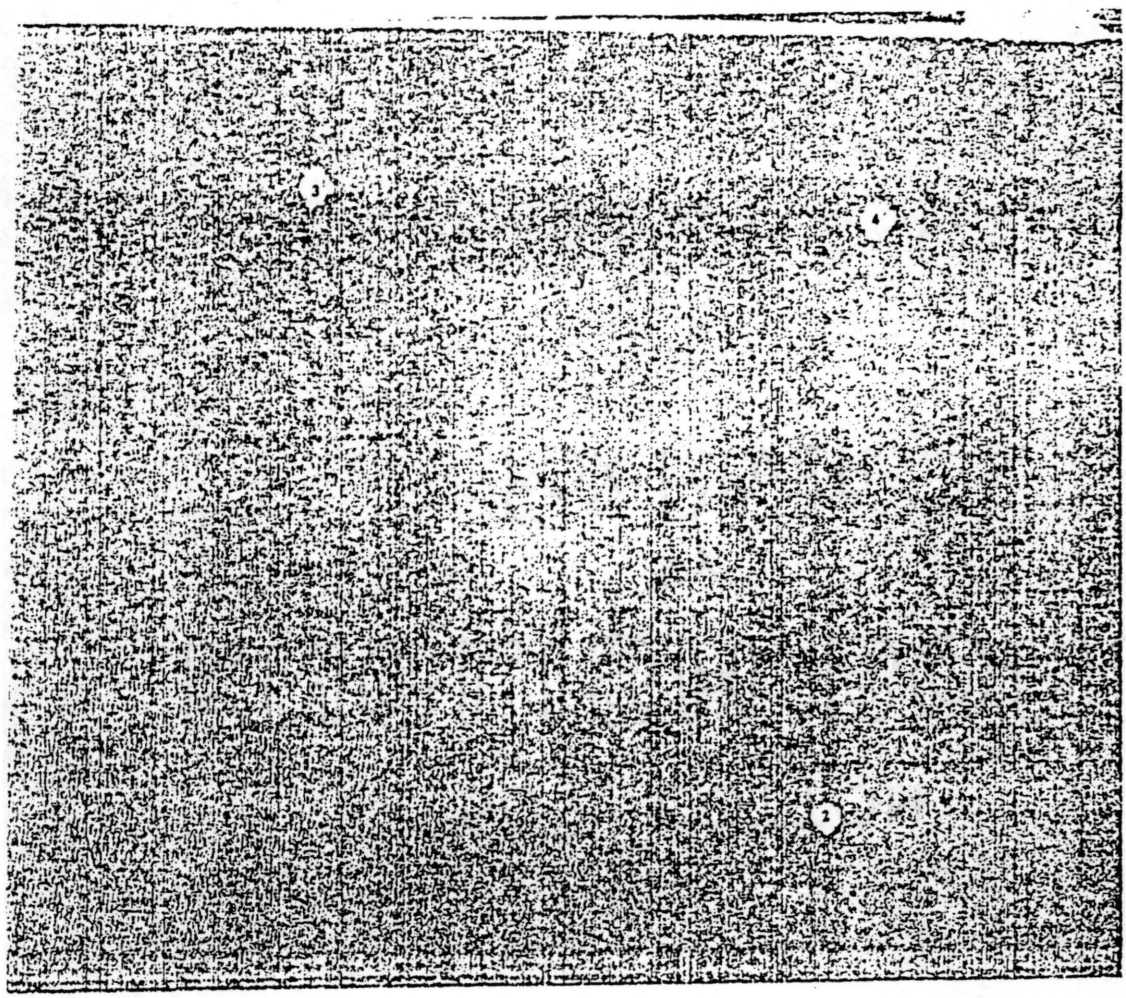

Figure 34. Ultrasonic C-scan of entire $[0/90/0/90]_s$ graphite-epoxy panel: Damage regions with impact energies of 5.27, 6.45, and 7.66 joule are mark with "2", "3", and "4", respectively.

there is no visible damage on the surface. Sections through the damage regions caused by impact are shown as edge replicas in Figs. 35 - 37. In all of these figures the top of the panel is the side impacted and the magnification factor was 51.

It was shown in the edge replicas that the damage caused by the impact energy of 6.45 joule (″3″) is even more severe (with more delaminations) than the damage caused by the impact energy of 7.66 joule (″4″). It is also shown in the vibrothermographic test. Figures 38 - 40 show the plots of the degree of heating vs. the frequency at the damage regions. The results show that region ″3″ has more vibrothermal peak frequencies than region ″4″ has.

Figure 41 is the ultrasonic C-scan of the entire $[0_2/90_2/0_2/90_2]_s$, 12 in. square, graphite-epoxy panel. In Fig. 41, the damage regions caused by the impact energy 5.27, 6.45, and 7.66 joule, are marked with an ″2″, ″3″, and ″4″, respectively. Figures 42 - 44 are the edge replicas (A) and the map of the damage (B) of sections through the impact damage zones ″2″, ″3″, and ″4″, respectively. The impact sides in all figures are on the top and the magnification factor was 23. Only in Fig. 44 can some transverse cracking in the 90° ply be seen. Comparing the damage sizes in the 16-ply laminate to the damage sizes in the 8-ply laminate, one sees that doubling the thickness of each ply may cause more damage for the same impact energy. These results were the same as reported in Ref. 10.

Figures 45 - 47 are plots of degree of heating observed excited through the frequency range of 9.0 - 22.0 kHz for those three damage regions. The output

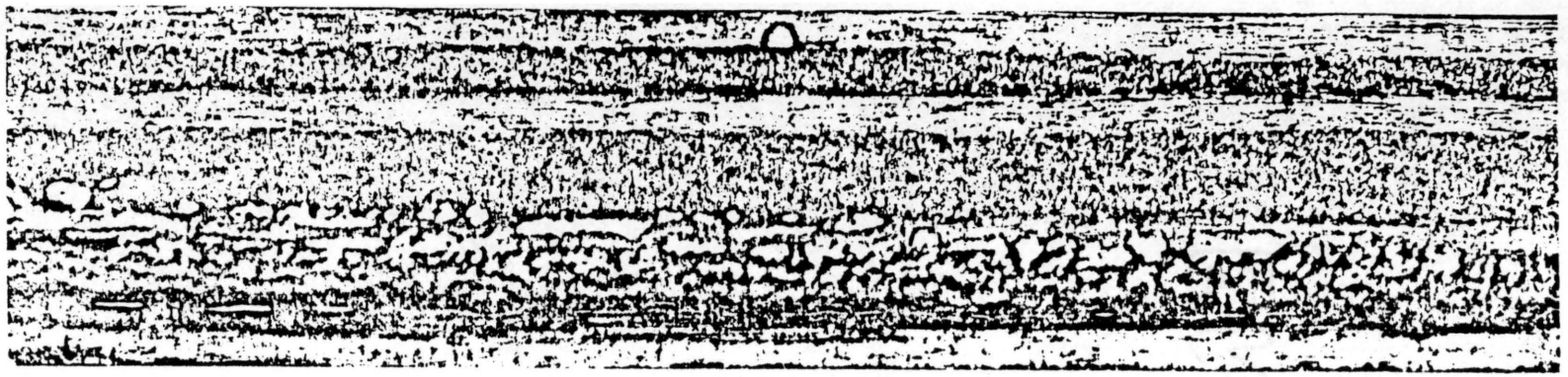

A

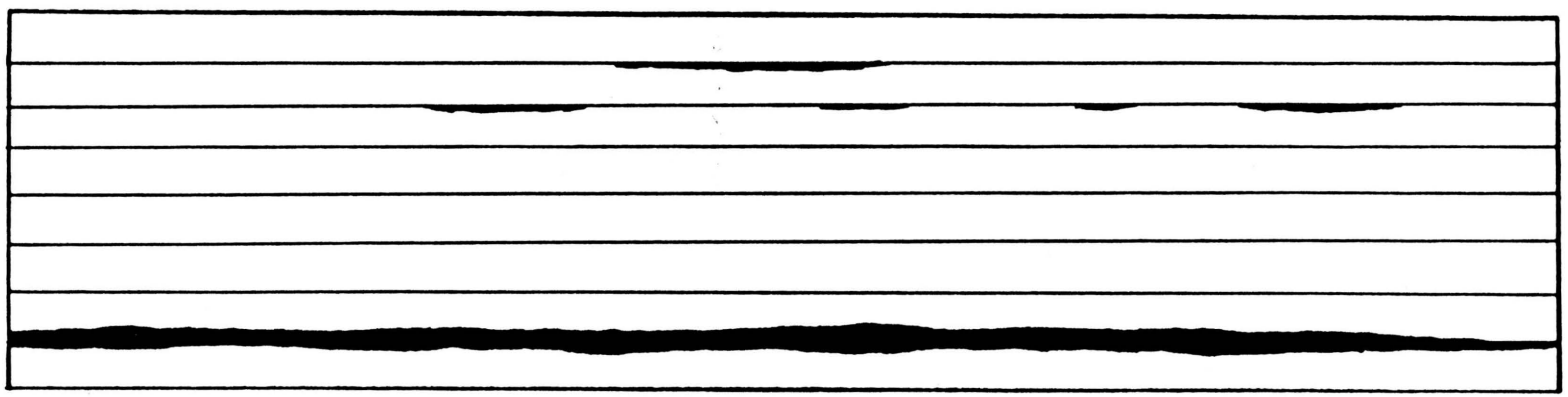

B

Figure 35. Edge replica (A) and a map of damage (B) of section through damage region with impact energy of 5.27 joule of 8-ply panel (top side impacted).

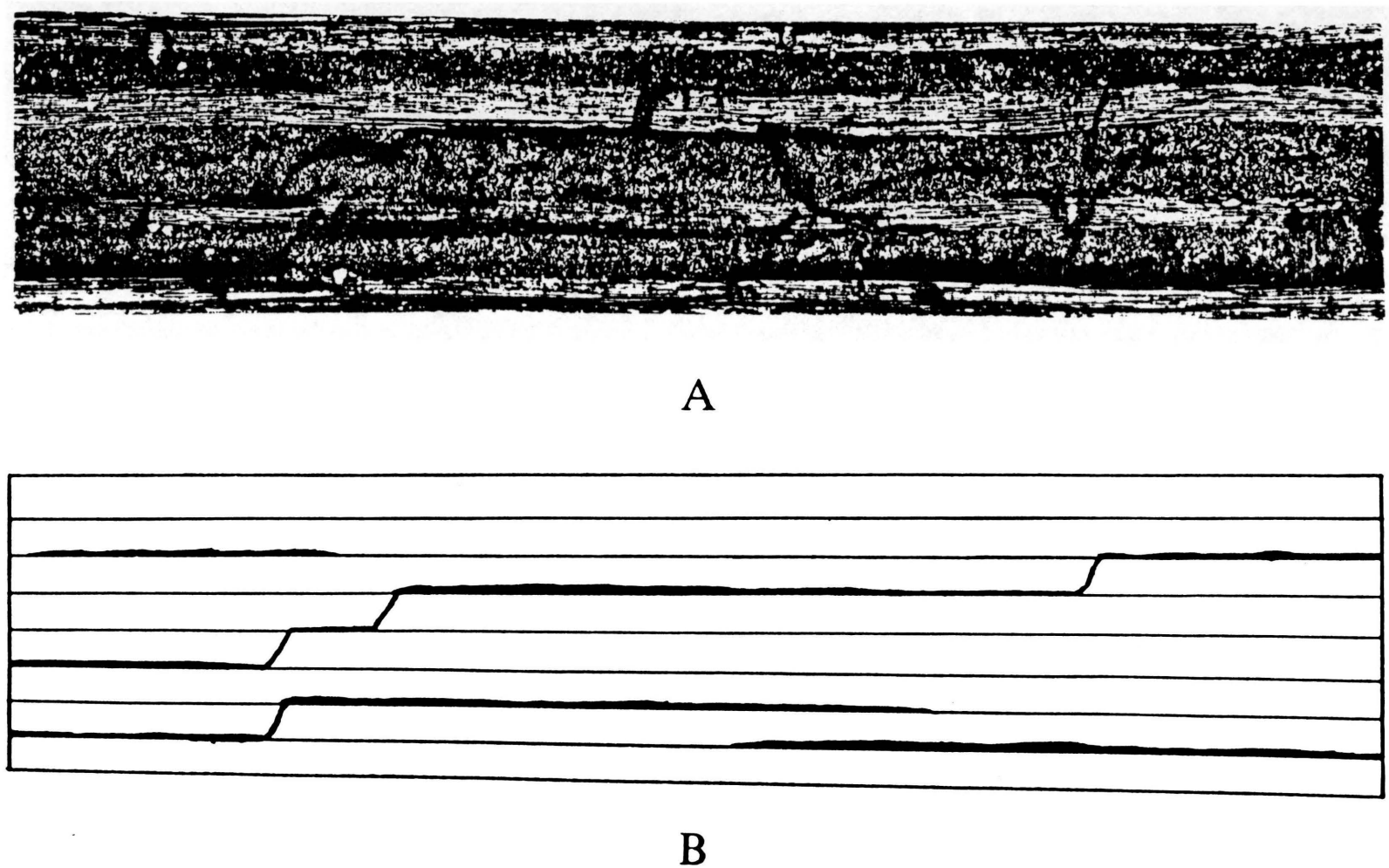

Figure 36. Edge replica (A) and a map of damage (B) of section through damage region with impact energy of 6.45 joule of 8-ply panel (top side impacted).

A

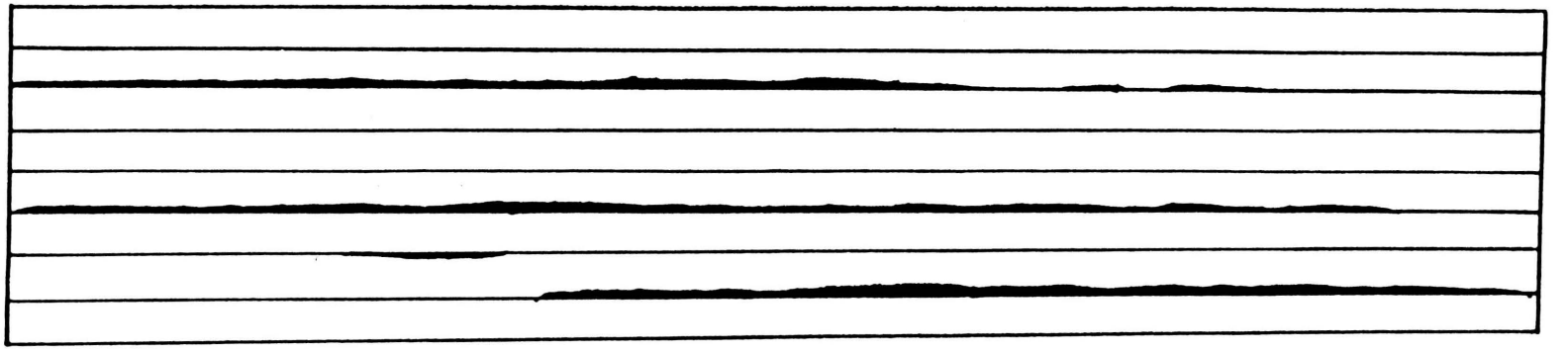

B

Figure 37. Edge replica (A) and a map of damage (B) of section through damage region with impact energy of 7.66 joule of 8-ply panel (top side impacted).

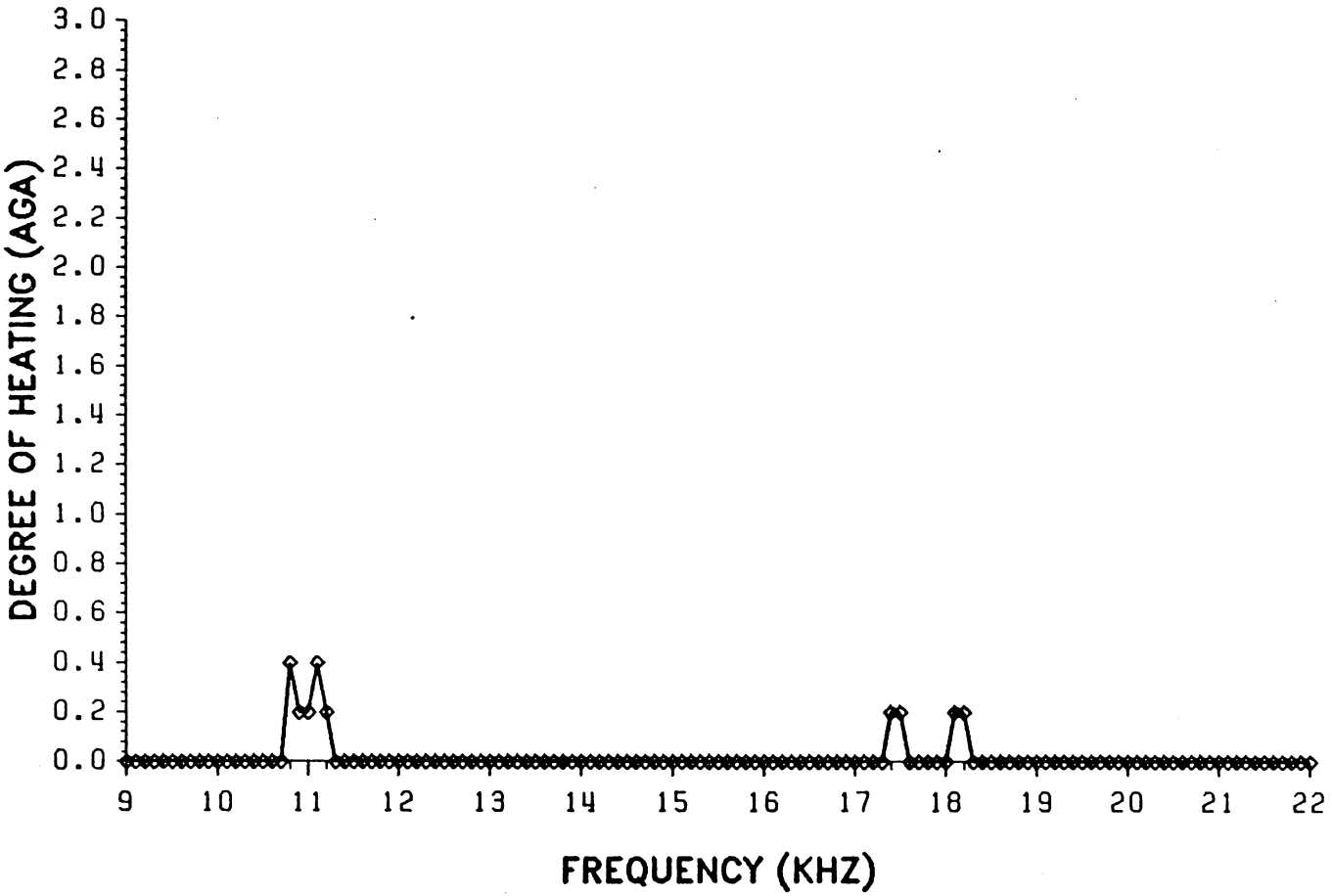

Figure 38. Degree of heating in the frequency range of 9.0 - 22.0 kHz on damage region with impact energy of 5.27 joule of 8-ply panel.

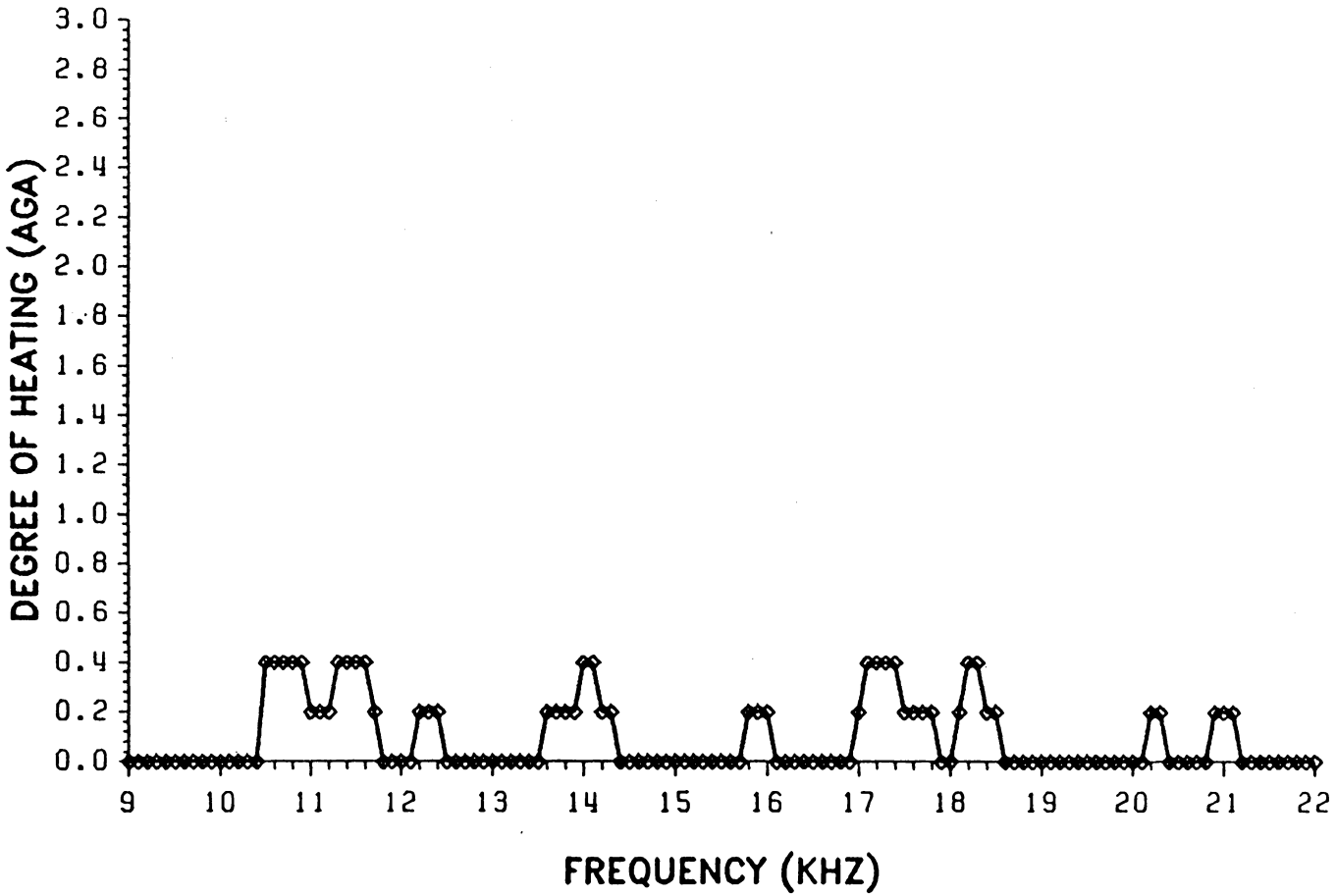

Figure 39. Degree of heating in the frequency range of 9.0 - 22.0 kHz on damage region with impact energy of 6.45 joule of 8-ply panel.

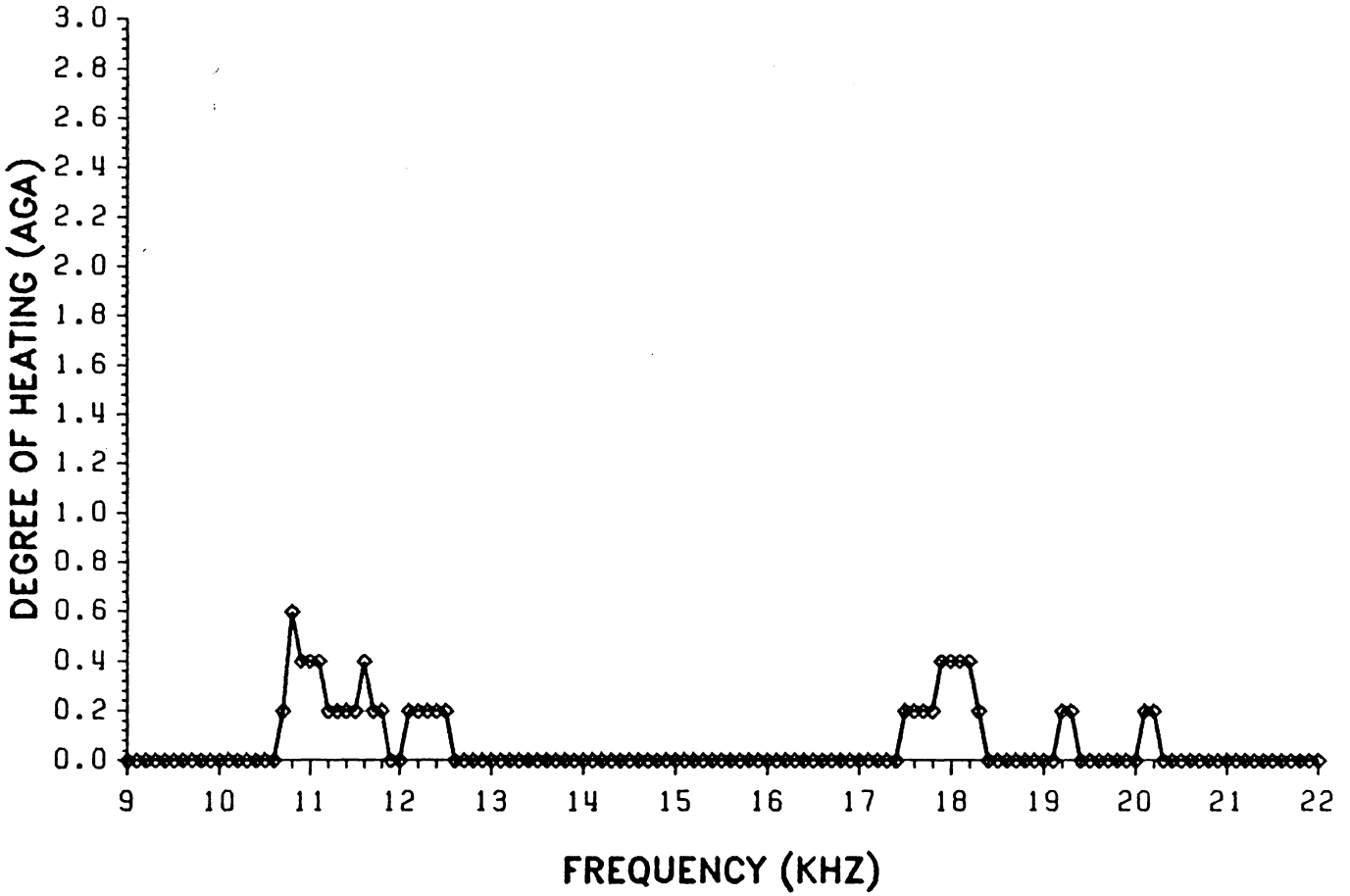

Figure 40. Degree of heating in the frequency range of 9.0 - 22.0 kHz on damage region with impact energy of 7.66 joule of 8-ply panel.

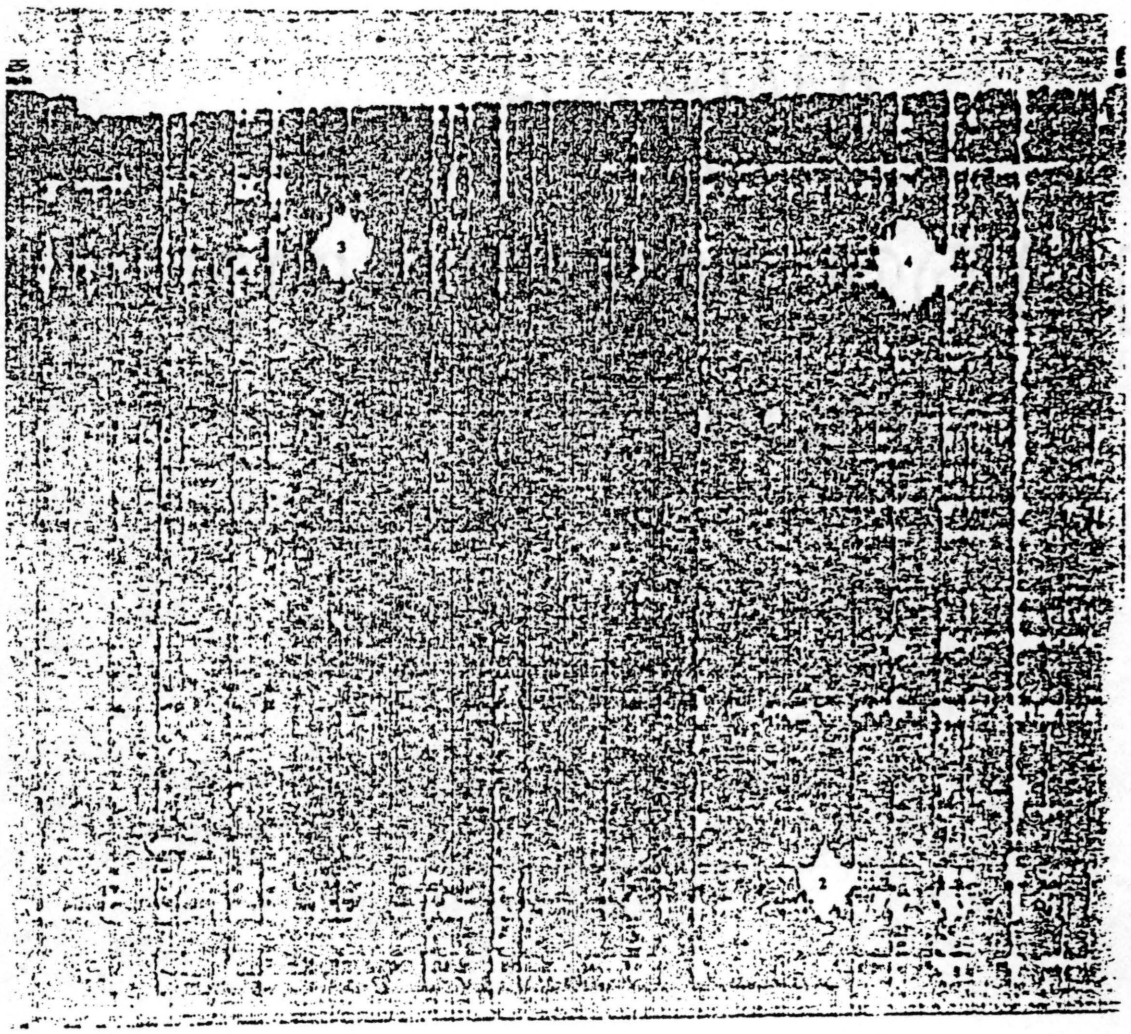

Figure 41. Ultrasonic C-scan of entire $[0_2/90_2/0_2/90_2]_s$ graphite-epoxy panel: Damage regions with impact energies of 5.27, 6.45, and 7.66 joule are mark with "2", "3", and "4", respectively.

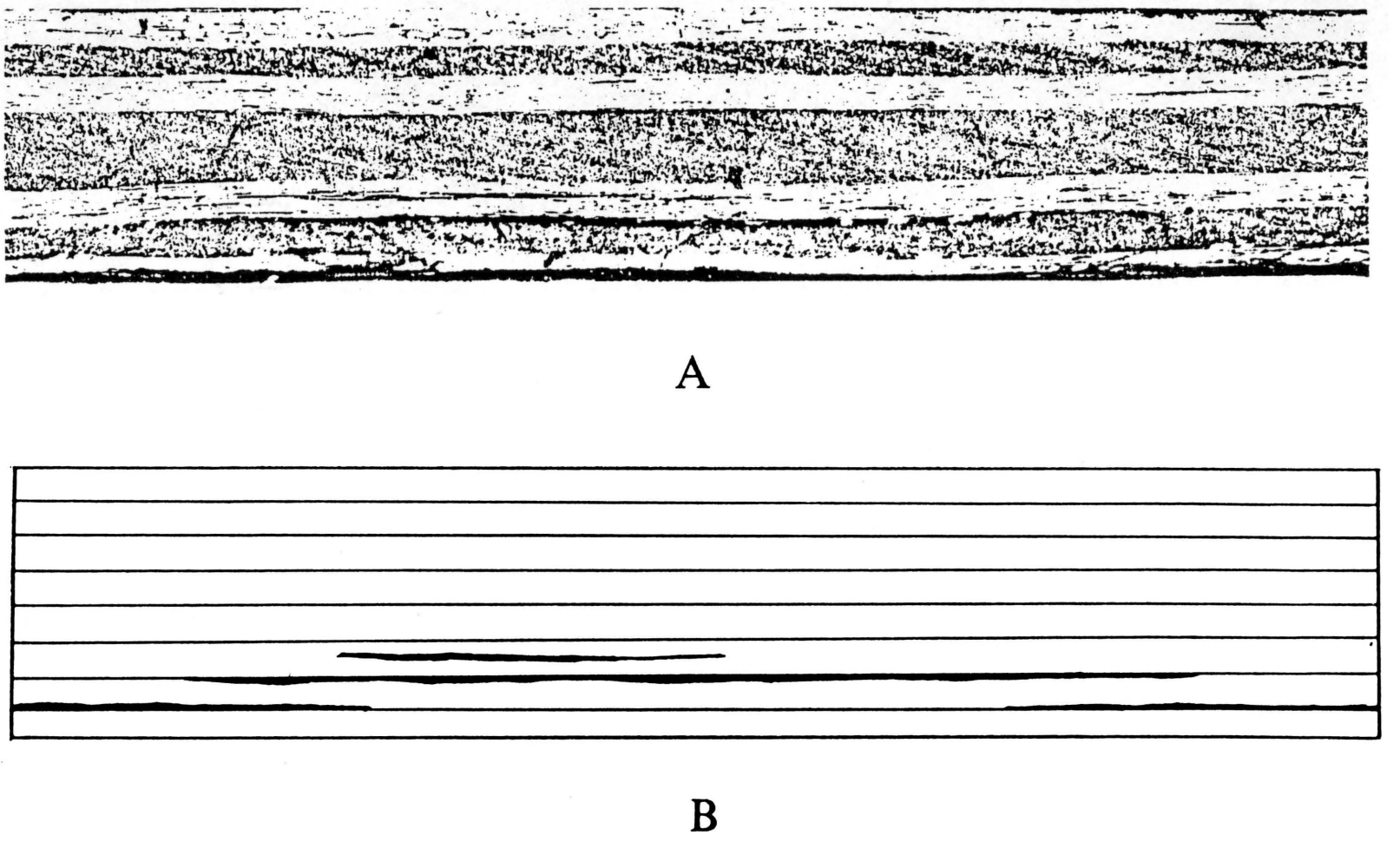

Figure 42. Edge replica (A) and a map of damage (B) of section through damage region with impact energy of 5.27 joule of 16-ply panel (top side impacted).

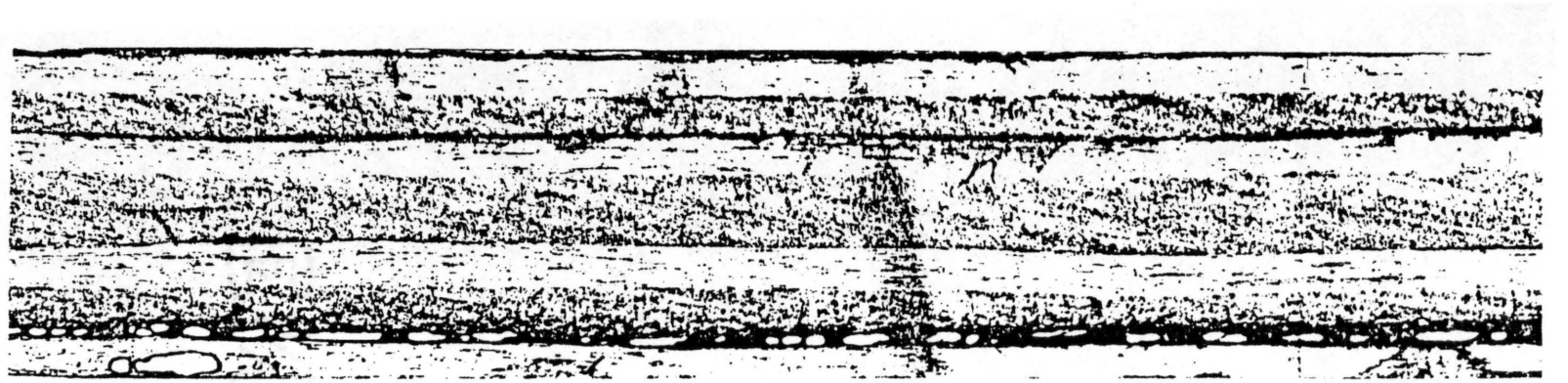

A

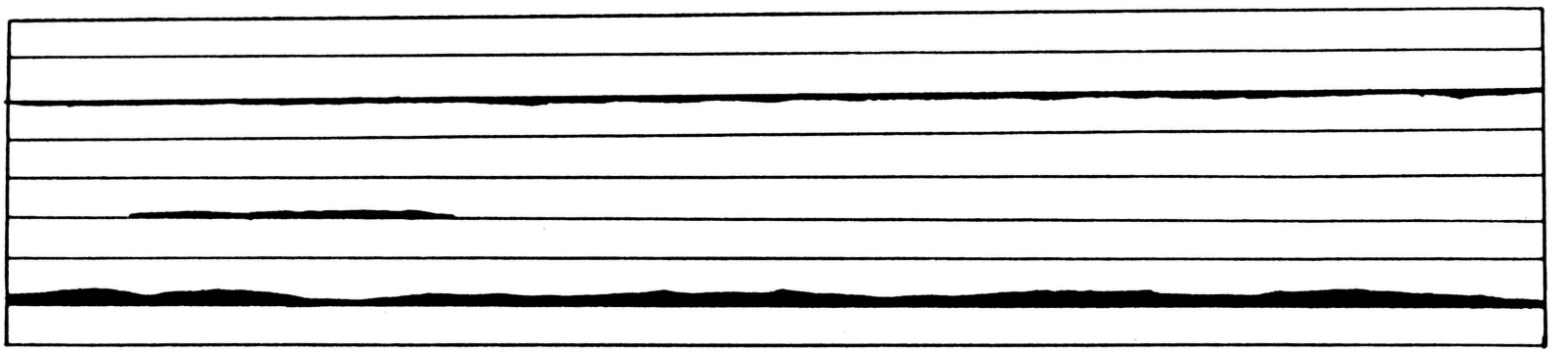

B

Figure 43. Edge replica (A) and a map of damage (B) of section through damage region with impact energy of 6.45 joule of 16-ply panel (top side impacted).

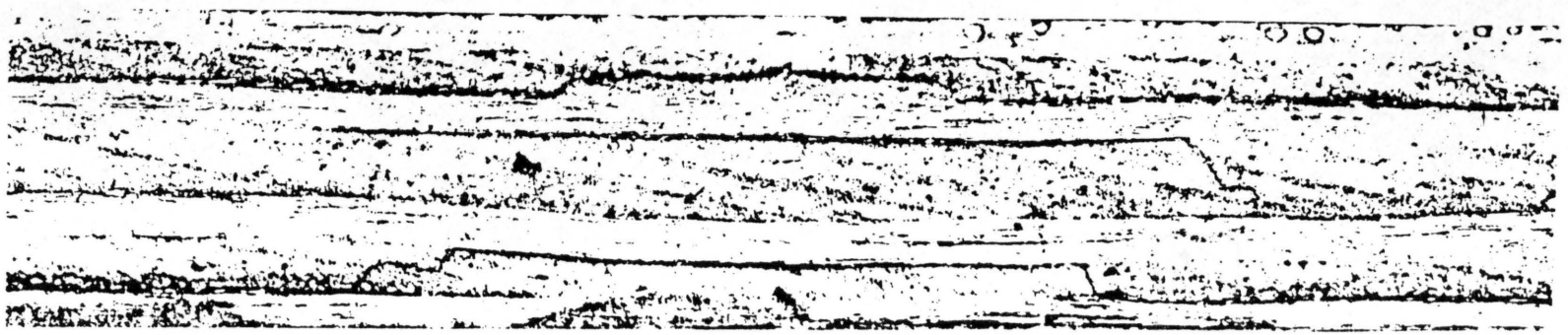

A

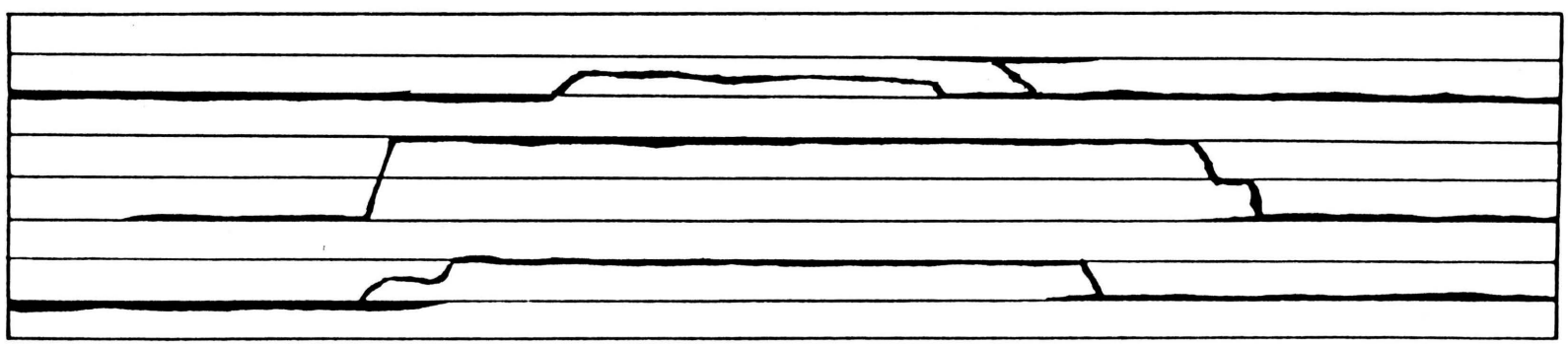

B

Figure 44. Edge replica (A) and a map of damage (B) of section through damage region with impact energy of 7.66 joule of 16-ply panel (top side impacted).

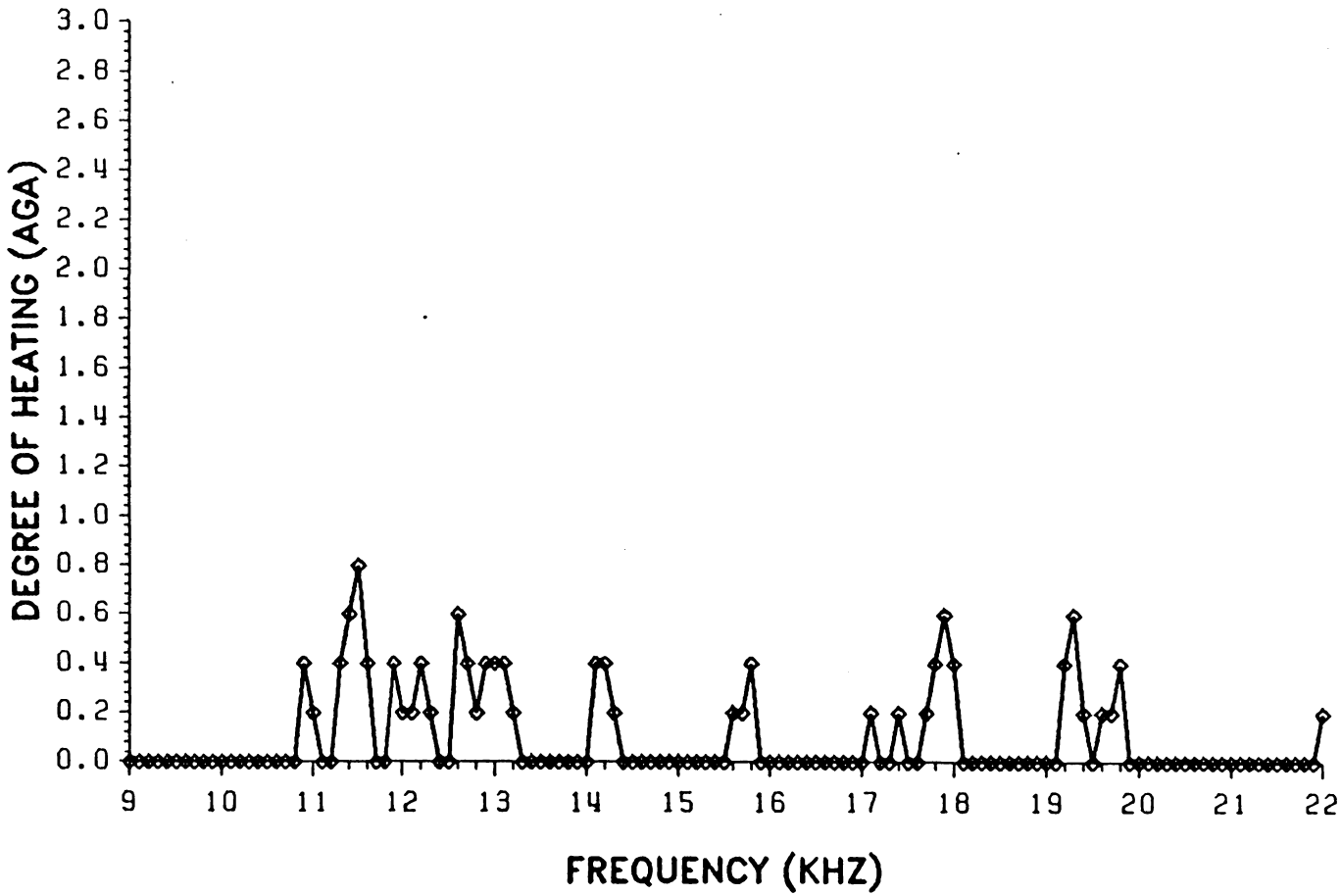

Figure 45. Degree of heating in the frequency range of 9.0 - 22.0 kHz on damage region with impact energy of 5.27 joule of 16-ply panel.

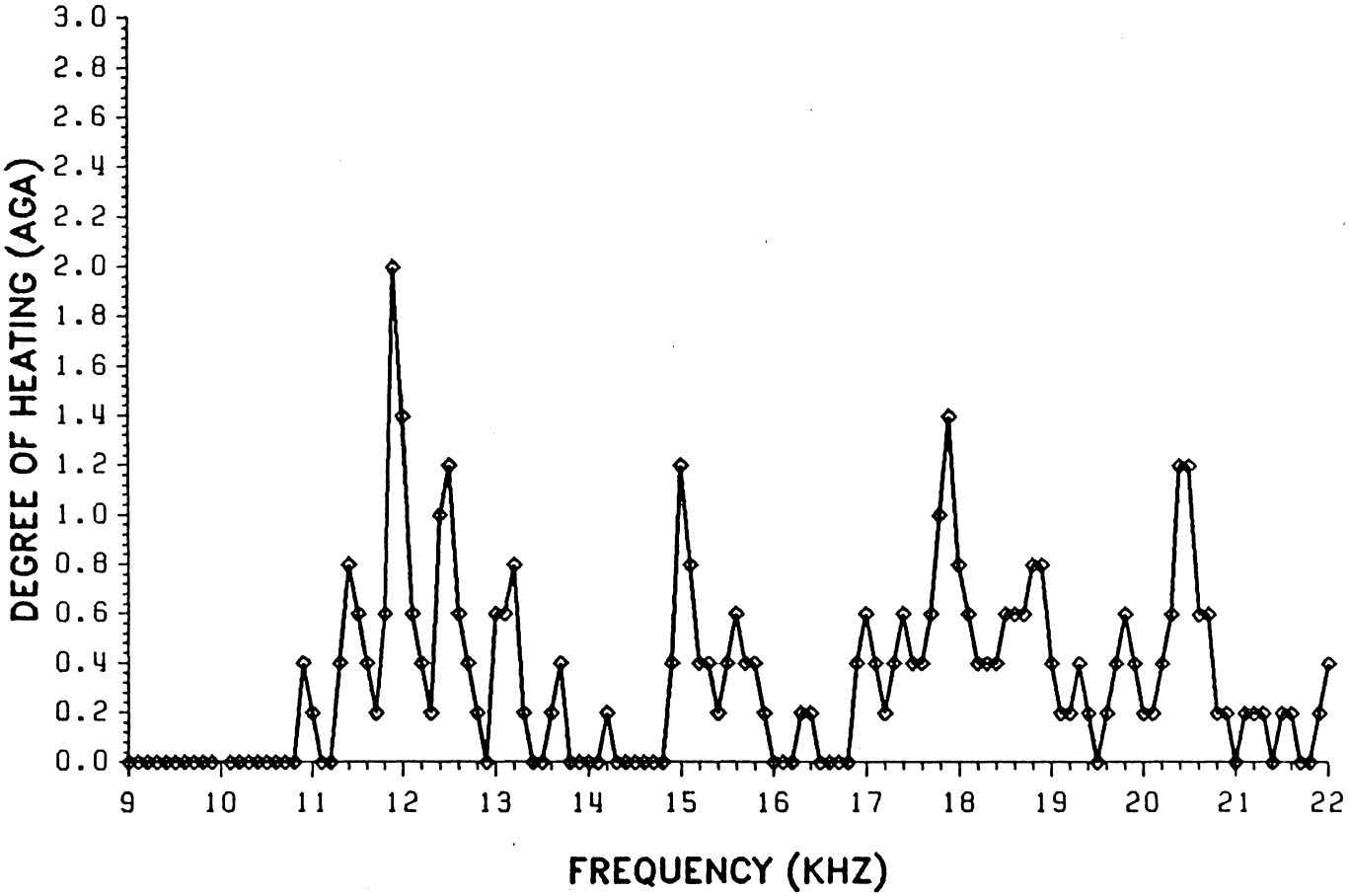

Figure 46. Degree of heating in the frequency range of 9.0 - 22.0 kHz on damage region with impact energy of 6.45 joule of 16-ply panel.

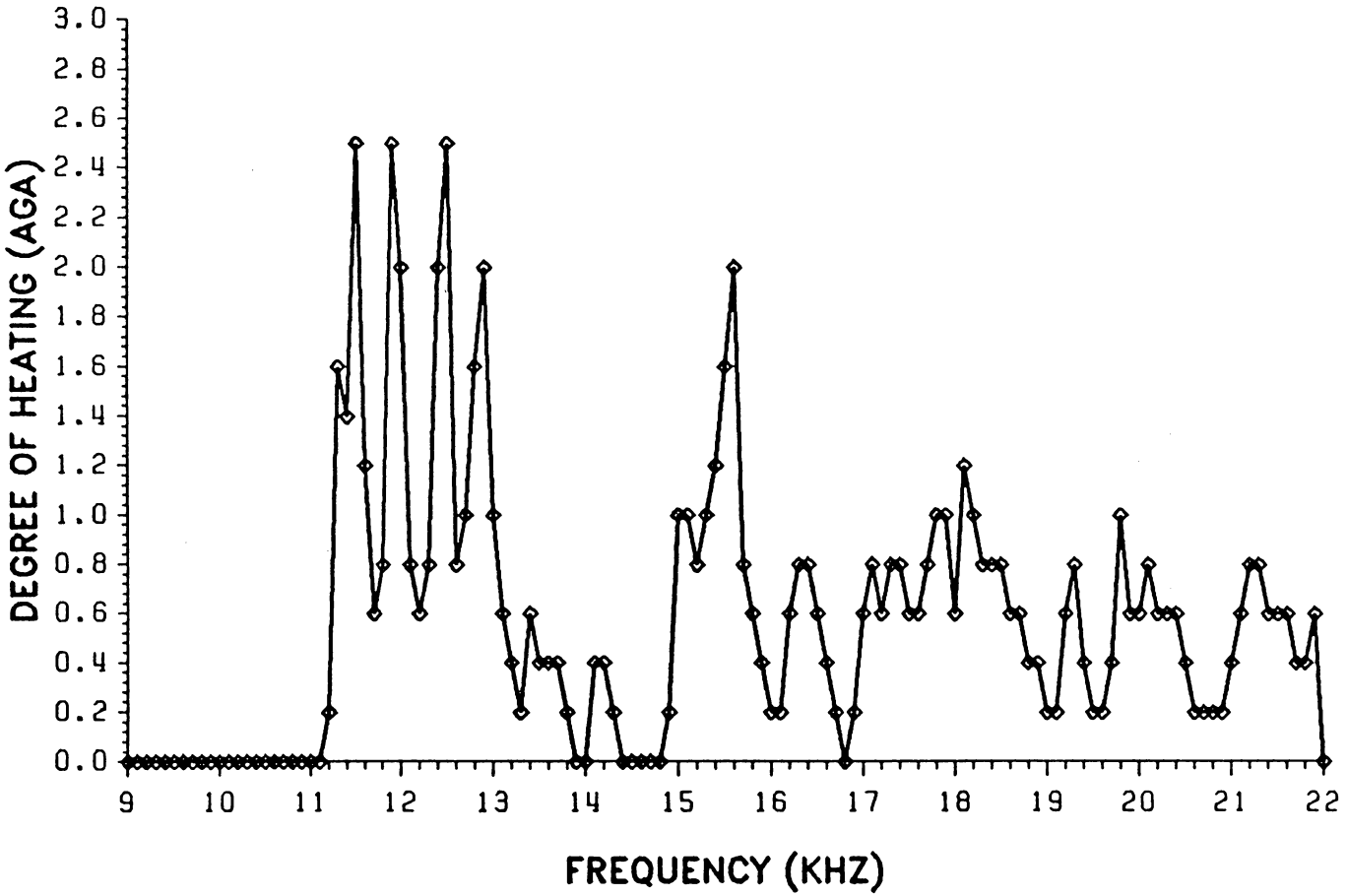

Figure 47. Degree of heating in the frequency range of 9.0 - 22.0 kHz on damage region with impact energy of 7.66 joule of 16-ply panel.

voltage of the function generator used for this panel was 2/3 of the one used for the previous two panels. The results also show that, in general, with more severe damage, the degree of heating at the vibrothermal peak frequencies is greater and/or the number of the vibrothermal peak frequencies is greater.

From the above observations, the proportionality between the degree of heating at particular applied frequency and the impact energy which caused the damage obtained by Russell[20] was not found, since the degree of heating is strongly dependent upon the exciting frequency. But from comparison of two plots of degree of heating versus frequency, e.g. Figs. 46 and 47, the severity of the damage can be qualified. It was also found that the majority of heat generation is due to the local resonance of the delamination plate. In Ref. 10, Russell found that by changing the size of the laminate, some vibrothermal peak frequencies observed would be changed. It was concluded that the structure resonance dominates this behavior. It is suspected that the vibrothermal peak frequency which he inspected was the natural frequency which happened to coincide with the system resonance frequency. Because of lack of sufficient energy input, only the natural frequency which coincides with the system resonance frequency can generate enough heat to be observed. By changing the size of the laminate panel, the system resonance frequency changed. Hence, the other natural frequency which had not been observed fell in the new system resonance frequency range, and generated an observable heat image. Therefore, it is believed that local resonance also dominates the frequency dependent heat generation behavior of impact damaged panel during vibrothermographic testing.

4.4 *Physical Significance of Results*

A very significant damage type in a composite laminate is delamination occurring between layers. Delamination greatly reduces the stiffness of the composite laminate, and it produces a free surface in the laminate acting as a stress concentrator.

Vibrothermography can locate delamination type damage in a laminate very easily in a short time. Also, the thermographic methods are field techniques and hence can interrogate areas of a structural component or even larger structures. Therefore, vibrothermography can be a complementary method for other nondestructive testing methods such as ultrasonic C-scanning.

The results obtained in this study lead to additional understanding of the vibrothermographic technique, the frequency dependent heat generation behavior and the heat generation mechanism during vibrothermographic testing. It has been found that the frequency dependent heat generation behavior during vibrothermographic testing is due to local resonance of the small plate, either above or below the delamination, and the heat generation mechanism is stress and/or strain related. Further research based upon the results obtained might achieve the desired goal of determining the size of the delamination and depth of the delamination into the laminate directly from analyzing the heat image obtained from a vibrothermographic test.

5. CONCLUSIONS

5.1 List of Conclusions

The concise statements of conclusions are listed as follows:

1. Local resonance is indeed the mechanics model that is responsible for the frequency dependent heat generation behavior during vibrothermographic testing of symmetric laminates.
2. The majority of the heat generation during vibrothermographic testing results from a dissipation mechanism caused by higher stresses and/or strains in the region of delaminations due to local resonance.
3. The heat generation was affected by the combination of the principal strains and shear strain for the lower modes of resonant vibration, and was dominated by the shear strain for the higher modes of resonant vibration.

4. For the two plots of the degree of heating versus exciting frequency, by comparing either the area under the curve or the number of the vibrothermal frequencies, the severity of the damage can be qualitatively identified.

The supporting materials for the conclusions are stated in the following two sections.

5.2 Frequency Dependent Behavior during Vibrothermographic Testing

A local resonance model was proposed to describe the frequency dependent heat generation behavior for a delamination in a composite laminate panel during vibrothermographic testing. The local resonance model postulates that when the excitation frequency reaches the natural frequency of the plate either above or below the delamination, the "local" plate resonates and heat is dissipated through some thermal/mechanical mechanism. The model was used as a basis for writing software for calculating the natural frequencies of a mid-plane symmetric, anisotropic plate having the size of delamination.

Three 12 inches square, glass-epoxy panels with layups of $[0_4]$, $[0_5]$, $[0/90/90/0]_s$, respectively, were constructed to test this model. During fabrication, four different simulated delaminations were laminated on the mid-plane of $[0_4]$ and $[0/90/90/0]_s$ panels, and on the 2-3 ply interface of the $[0_5]$ panel.

The vibrothermographic testing results obtained from each of the three panels show excellent correlation between the observed vibrothermal peak frequencies and the predicted natural frequencies calculated from the software program based upon the local resonance model. The observations using SPATE show qualitatively that the delamination vibration follows the model behavior at the corresponding natural frequency. All the above results show conclusively that the local resonance model is indeed the mechanics model that is responsible for the frequency dependent heat generation behavior for these stacking sequences.

There is also an argument to exclude the structural resonance from being the responsible mechanism. If the frequency dependent behavior is due to structural resonance, the geometrically symmetric position in the 12 inch square panel should have the same vibration state. Hence, the size of the delamination should not affect the vibrothermal peak frequency. But, the experimental results show that the observed sets of vibrothermal peak frequencies for two different sizes of delamination at geometrically symmetric positions on the panel were greatly different. However, the system resonance sometimes affects the vibrothermographic observation. If the input energy from the shaker system is not sufficient, only the natural frequency that coincides with the system resonance frequency can generate enough heat to be observed. This might be what happened in Russell's observations (in Ref. 10) for smaller delaminations created by impact. In this study, the vibrothermal peak frequencies away from the system resonance frequency were well observed for those impact damaged panels. Therefore, it is concluded that if the energy input from the shaker system is high enough, the system reso-

nance will not affect the vibrothermal peak frequencies of a delamination but only the degree of heating at the vibrothermal peak frequencies.

5.3 Heat Generation Mechanism

Two likely heat generation mechanisms during vibrothermographic testing were proposed, heat dissipation of nonconservative deformation due to local high stresses, or heat dissipation due to clapping or rubbing of the delamination surfaces. Which of these mechanisms is responsible has not yet been ascertained, but it has been believed and reported in the literature, that the latter one is the main mechanism responsible for the heat generation.

A careful measurement of the degree of heating of both sides of $[0_5]$ glass-epoxy panel with delaminations on the 2-3 ply interface was made to qualify the heat generation mechanism. The experimental observations show that there is preferential heating of the side of the laminate corresponding to the side of the plate which is being excited by application of a frequency corresponding to a natural mode for that thickness plate. This indicates that the majority of heat generation during vibrothermographic testing results from higher stresses and/or strains due to local resonance. Comparison between the predicated heat patterns generated from a finite difference heat transfer program and observed heat patterns were made. This showed that the heat generation was affected by the combination of the principal strains and shear strain for lower modes of resonant

vibration, and was dominated by the shear strain for the higher modes of resonant vibration.

Russell[20] performed vibrothermographic tests on an impact damaged panel specimen, and found that the degree of heating at the damage sites at a particular applied frequency were proportional to the impact energy which caused the damage. From the results here, the proportionality was not found. The degree of heating was strongly dependent upon the exciting frequency, since the major damage was delamination. But for the two plots of degree of heating versus exciting frequency, by comparing either the area under the curve or the number of the vibrothermal peak frequencies, the severity of the damage can be qualitatively identified. It was also found that clapping or rubbing of the pop-out surface ply can generate a small amount of heat observable, and that is independent of frequency. But the majority of heat generation is due to the local resonance of the delaminationed plates.

5.4 Suggested Research

This study concludes that the frequency dependent heat generation is due to the local resonance of the delamination plate for the stacking sequences used. Since the model for calculation of the natural frequencies of the delamination plate is limited to mid-plane symmetric, anisotropic plates, the delaminations were imbedded between two layers with same direction so that a laminate could

be constructed without warping it. This is not the place where an actual delamination normally occurs. Therefore, the model should be advanced to be able to calculate the natural frequencies of any anisotropic plate. Then, the delamination can be imbedded between any interface to have the delamination between two layers of different orientation, and more tests can be performed to prove the generality of local resonance model.

In this study, the predicted heat patterns used to be compared with the observed heat patterns were generated using the strain distribution of free vibration, which was not the actual boundary condition. Using the finite element method to predict the vibratory motion of the panel at the frequency at which the local resonance of the delaminationed plate occurs, would be useful in predicting the heat pattern. With the predicted boundary condition for the delamination plate, the forced vibration strain field of delamination plate at resonance condition can be obtained. The comparison between the observed heat pattern and the predicted heat pattern with the heat generation proportional to the forced vibration strain field might be more meaningful.

REFERENCES

1. Reifsnider, K. L. and Henneke, E. G. II, "Thermography Applied to Reinforced Plastics," *Developments in Reinforced Plastics - 4*, G. Pritchard, Ed., Elsevier Applied Science Publishers, London, 1984, pp. 89-130.

2. Wilson, D. W. and Charles, J. a., "Thermographic Detection of Adhesive-bond and Interlaminar Flaw in Composite," *Experimental Mechanics*, July 1981, pp. 276-280.

3. McLaughlin, P. V., McAssey, E. V., and Deitrich, R. C., "Nondestructive Examination of Fibre Composite Structures by Thermal Field Techniques," *NDT International*, Apr. 1980, pp. 55-62.

4. McAssey, E. V., McLaughlin, P. V., and Koert, D. N., and Deitrich, R. C., "Thermographic NDT of Composites Using Externally Applied Thermal Fields," *35th Annual Technical Conference*, 1980, Reinforced Plastics/Composites Institute, The Society of the Plastics Industry, Inc., Sec. 26-A, pp. 1-8.

5. Pye, C. J. and Adams, R. D., "Heat Emission from Damaged Composite Materials and Its Use in Nondestructive Testing," *J. Phys. D.: Appl. Phys.*, 14, 1981, pp. 927-941.

6. Pye, C. J. and Adams, R. D., "Detection of Damage in Fibre Reinforced Plastics Using Thermal Fields Generated During Resonant Vibration," *NDT International*, June 1981, pp. 111-118.

7. Duke, J. C. Jr. and Russell, S. S., "The Investigation of Imperfections in Sheet Molding Compound," *Mater. Eval.*, Vol. 40, No. 5, Apr. 1982, pp. 566-571.

8. Henneke, E. G. II and Russell, S. S., "Impact Damage Detection and Evaluation By Active and Passive Thermography and Stereo X-Ray Radiography in Advanced Composite Panels," *14th Symposium on Nondestructive Evaluation*, San Antonio, TX, U. S. A., Apr. 1983.

9. Russell, S. S. and Henneke, E. G. II, "Dynamic Effects During Vibrothermographic NDE of Composites," *NDT International*, Vol. 17, No. 1, Feb. 1984, pp. 19-25.

10. Russell, S. S., "An Investigation of the Excitation Frequency Dependent Behavior of Fiber-Reinforced Epoxy Composites during Vibrothermographic Inspection," Ph.D. Dissertation, Virginia Polytechnic Institute and State University, VA., U.S.A., Nov. 1982.

11. Ashton, J. e. and Whitney, J. M., *Theory of Laminated Plates* , Technomic Publishing, Stanford, CT, 1970.

12. Young, D., "Vibration of Rectangular Plates By the Ritz Method," *J. of Applied Mechanics*, Vol. 17, 1950, pp. 488-494.

13. Henneke, E. G. II, Reifsnider, K. L., and Stinchcomb, W. W., "Thermography-- An NDI Method for Damage Detection," *J. of Metals*, Sept. 1979, pp. 11-15.

14. Reifsnider, K. L., Henneke, E. G. II, and Stinchcomb, W. W., "The Mechanics of Vibrothermography," *The Mechanics of Nondestructive Testing*, W. W. Stinchcomb, Ed., Plenum Press, New York, 1980, pp.249-276.

15. Reifsnider, K. L. and Henneke, E. G. II, "Stress Related Thermal Emission," *Thermal Stresses in Severe Environments*, by D. P. H. Hasselman and R. A. Heller, Eds., Plenum Press, New York, 1980, pp. 709-726.

16. Whitcomb, J. D., "Thermographic Measurement of Fatigue Damage," *Composite Materials: Testing and Design* (Fifth Conference), ASTM STP 674, S. W. Tsai, Ed., American Society for Testing and Materials, 1979, pp. 502-516.

17. Henneke, E. G. II and Jones, T. S., "Detection of Damage in Composite Materials by Vibrothermography," *Nondestructive Evaluation and Flaw Criticality of Composite Materials*, ASTM STP 696, R. B. Pipes, Ed., American Society for Testing and Materials, 1979, pp. 83-95.

18. Jones, T. S., "Thermographic Detection of Damaged Regions in Fiber-Reinforced Composite Materials," M.S. Thesis, Virginia Polytechnic Institute and State University, Blacksburg, VA. USA, 1977.

19. Carslaw, H. S. and Jaeger, J. C., *Conduction of Heat in Solids*, Oxford University Press, London, 1947.

20. Russell, S. S., private communication.

21. Thomson, W. (Lord Kelvin), "On the Dynamical Theory of Heat, with Numerical Results Deduced from Mr. Joule's Equivalent of Thermal Unit, and M. Regnult's Observations on Steam," *Transactions of the Royal Society of Edinburgh*, Vol. 20, 1853, pp. 261-285.

22. Thomson, W. (Lord Kelvin), "On the Thermo-Elastic and Thermomagnetic Properties of Matter," *Quaterly J. of Mathematics*, Vol. 1, 1857, pp. 57-77.

23. Biot, M. A. "Thermoelasticity and Irreversible Thermodynamics," *J. Appl. Phys.*, Vol. 27, 1956, pp. 240-253.

24. Bakis, C. E. and Reifsnider, K. L., "Thermoelastic Micromechanics of Laminated Fiber Composites," to be published.

25. AGA Thermovision 780 Operating Manual, Pine Brook, NJ, 1980.

26. Highsmith, A. L. and Reifsnider, K. L., "Stiffness-Reduction Mechanisms in Composite Laminates," *Damage in Composite Materials*, ASTM STP 775, K. L. Reifsnider, Ed., American Society for Testing and Materials, 1982, pp. 103-117.

27. Tsai, S. W. *Composite Design 1986*, United States Air Force Materials Laboratory, Think Composite: Dayton, Paris, and Tokyo.

28. Kasen, M. B. "Mechanical and Thermal Properties of Filamentary-Reinforcedstructural Composites at Cryogenic Temperatures. 1: Glass-Reinforced Composites," *Cryogenics*, June 1975, pp. 327-349.

Appendix A. Software for Calculating the Natural Frequencies of a Rectangular Mid-plane Symmetric Anisotropic Plate

The computer code found in Appendix A is intended to calculate the natural frequencies of a rectangular mid-plane symmetric anisotropic laminate using Rayleigh-Ritz approximation discussed in section 2.1. The software was written to solve the eigenvalue problem defined by Eq. (2.1.27). This program forms a matrix M_{pq} which is solved by an eigenvalue solver subroutine, EIGRF. Each M_{pq} is defined Eq. (2.1.27) for each chosen k, l, i, and j, where p represents a reduced notation for each combination of k and l, and q, for a combination of i and j. The number of the terms, m and n, was chosen to be 5, and this forms a 25 × 25 matrix.

Inputing the density, the plate dimensions, the layup of the laminate plate, and the mechanical properties of the material to the program, the natural fre-

quencies of the plate can be obtained. If eigenvectors are needed for other purposes, there is also an option to print the eigenvectors, a_{ij}, along with each eigenvalue, the natural frequency. The computer code used to evaluate these eigenvalues and eigenvectors follows.

```
C-----------------------------------------------------------------------
C|                                                                      |
C|      RECTANGULAR MID-PLANE SYMMETRIC ANISOTROPIC PLATE VIBRATION     |
C|                                                                      |
C|      THIS PROGRAM FINDS THE EIGENVALUES FOR THE RAYLEIGH-RITZ        |
C|      SOLUTION FOR CLAMPED-CLAMPED MID-PLANE SYMMETRIC ANISOTROPIC    |
C|      LAMINATED PLATES.                                               |
C|                                                                      |
C-----------------------------------------------------------------------
      IMPLICIT REAL*8 (A-H,O-Z)
      DIMENSION B(5),AMATRX(25,25),R(5),IDEX(25,2)
     &,ZREAL(2,25,25),AVECT(2,25),WK(675),D1D1(5,5),D1D0(5,5)
     &,D2D1(5,5),D(3,3)
C-----------------------------------------------------------------------
C|                                                                      |
C|        INPUT THE DATA:                                               |
C|        AL: LENGTH IN X-DIRECTION.                                    |
C|        BL: LENGTH IN Y-DIRECTION.                                    |
C|        THO: DENSITY(MASS/AREA/LAYER)                                 |
C|                                                                      |
C-----------------------------------------------------------------------
      READ(5,*) AL,BL,THO
C-----------------------------------------------------------------------
C|                                                                      |
C|        SUBROUTINE DMATRX CALCULATES THE D-MATRIX OF                  |
C|        THE PLATE                                                     |
C|                                                                      |
C-----------------------------------------------------------------------
      CALL DMATRX(D,NL)
      THO=THO*NL
      PI=DARCOS(-1.D+00)
      WRITE(6,1000) THO,AL,BL
 1000 FORMAT(//,3X,'THO = ',1PD12.4//5X,'A = ',0PF6.3/5X,'B = ',F6.3)
C-----------------------------------------------------------------------
C|                                                                      |
C|        THIS PROGRAM SECTION CALCULATES THE NATURAL FREQUENCIES       |
C|        FOR CLAMPED-CLAMPED CASE                                      |
C|                                                                      |
C|        N: NUMBER OF COMPONENTS TO BE USED IN I, J, K, L              |
C|        NTYPE = 0 (IF ORTHOTROPIC)                                    |
C|              = 1 (IF ANISOTRPIC)                                     |
C|        NMODE = 0 (ONLY NATURAL FREQUENCIES WILL BE PRINTED)          |
C|              = 1 (BOTH NATURAL FREQUENCIES AND AIJ WILL BE PRINTED)  |
C|        NOUT: NUMBER OF NATURAL FREQUENCIES TO BE PRINTED             |
C|                                                                      |
C-----------------------------------------------------------------------
      READ(5,*) N,NTYPE,NMODE
      READ(5,*) NOUT
      DO 10 IK=1,N
   10 B(IK)=0.D+00
C-----------------------------------------------------------------------
C|                                                                      |
C|        SUBROUTINE BATTA CALCULATES THE CLAMPED-CLAMPED BEAM          |
C|        EIGENVALUES (BETA'S)                                          |
C|                                                                      |
C-----------------------------------------------------------------------
      CALL BATTA(B,N)
C-----------------------------------------------------------------------
C|                                                                      |
C|        CALCULATES THE COEFFICIENT OF THE DISPLACEMENT FUNCTION       |
C|        R WHERE DISPLACEMENT FUNCTION IS COSH(BETA X)                 |
C|        - COS(BETA X)) + R(SINH(BETA X) - SIN(BETA X))                |
C|                                                                      |
C-----------------------------------------------------------------------
      DO 20 IN=1,N
      TEMP=B(IN)
      R(IN)=(DCOSH(TEMP)-DCOS(TEMP))/(DSIN(TEMP)-DSINH(TEMP))
   20 CONTINUE
C-----------------------------------------------------------------------
```

```
C|
C|        CALCULATE THE INTEGRAL OF FIE PRIME I * FIE PRIME J
C|
C-----------------------------------------------------------------------
      DO 25 I=1,N
      DO 25 J=1,N
      D2D1(I,J)=0.D0
      D1D0(I,J)=0.D0
   25 D1D1(I,J)=0.D0
      DO 30 I=1,N
      DO 30 J=I,N
      CALL CD1266(I,J,R,B,T1)
      D1D1(I,J)=T1
      D1D1(J,I)=T1
      IF(NTYPE .EQ. 0) GO TO 30
      CALL CD1626(I,J,R,B,SUM1,SUM2)
      D1D0(I,J)=SUM1
      D1D0(J,I)=SUM1
      D2D1(I,J)=SUM2
      D2D1(J,I)=SUM2
   30 CONTINUE
C-----------------------------------------------------------------------
C|
C|        THIS PROGRAM SECTION FILLS UP THE MATRIX.  I AND J DETERMINE
C|        THE ROWS AND K AND L DETERMINE THE COLUMNS.
C|
C-----------------------------------------------------------------------
      NNN=N*N
      LL=0
      TWO=(2.D+00*D(1,2)+4.D+00*D(3,3))/(AL*BL)**2
      DO 50 I=1,N
      DO 50 J=1,N
      LL=LL+1
      IDEX(LL,1)=I
   50 IDEX(LL,2)=J
      DO 60 II=1,NNN
      KK=II+1
      I=IDEX(II,1)
      J=IDEX(II,2)
      ONE=D(1,1)*(B(I)/AL)**4+D(2,2)*(B(J)/BL)**4
      AMATRX(II,II)=ONE+TWO*D1D1(I,I)*D1D1(J,J)
      IF(II.EQ.NNN) GO TO 60
      DO 60 JJ=KK,NNN
      K=IDEX(JJ,1)
      L=IDEX(JJ,2)
      AMATRX(II,JJ)=TWO*D1D1(I,K)*D1D1(J,L)
      AMATRX(JJ,II)=AMATRX(II,JJ)
   60 CONTINUE
      IF(NTYPE .EQ. 0) GO TO 75
      DO 70 II=1,NNN
      DO 70 JJ=II,NNN
      I=IDEX(II,1)
      J=IDEX(II,2)
      K=IDEX(JJ,1)
      L=IDEX(JJ,2)
      AMATRX(II,JJ)=AMATRX(II,JJ)+4.D0*D(1,3)*D2D1(I,K)*D1D0(J,L)/(AL**3
     &*BL)+4.D0*D(2,3)*D1D0(I,K)*D2D1(J,L)/(BL**3*AL)
      AMATRX(JJ,II)=AMATRX(II,JJ)
   70 CONTINUE
   75 CALL EIGRF(AMATRX,NNN,NNN,2,AVECT,ZREAL,NNN,WK,IER)
      IF(IER .NE. 0) WRITE(6,2000) IER
 2000 FORMAT(///,'WARNING----------IER VALUE OF ',I3,' IN SUBROUTINE'
     &,' EIGRF')
      DO 80 LLL=1,NNN
      IF(DABS(AVECT(2,LLL)) .LE. 1.0D-25) GO TO 80
      WRITE(6,3000) LLL,AVECT(1,LLL),AVECT(2,LLL)
 3000 FORMAT(////,' WARNING-----------EIGENVALUE NUMBER',I3,
     &'  (',2D13.5,') IS COMPLEX')
   80 CONTINUE
```

```
      WRITE(6,4000)
 4000 FORMAT(//,'      CLAMPED CASE    '//9X,'FREQUENCIES'/)
      DO 100 K=1,NOUT
      ALLOW=AVECT(1,1)
      J=1
      DO 90 I=1,NNN
      TEMP=AVECT(1,I)
      IF(ALLOW .LT. TEMP) GO TO 90
      ALLOW=TEMP
      J=I
   90 CONTINUE
      F=DSQRT(ALLOW/THO)/(2.D00*PI)
      WRITE(6,5000) F
 5000 FORMAT(/,3X,'F = ',1PD12.5)
      IF(NMODE .EQ. 0) GO TO 95
      WRITE(6,5500) (ZREAL(1,II,J),II=1,NNN)
 5500 FORMAT(/,5D14.5)
   95 AVECT(1,J)=1.D+11
  100 CONTINUE
      STOP
      END
C
C-----------------------------------------------------------------------
C|                                                                     |
C|        CALCULATE CLAMPED-CLAMPED BEAM EIGENVALUES                   |
C|                                                                     |
C-----------------------------------------------------------------------
C***********************************************************************
C*                                                                     *
      SUBROUTINE BATTA(BETA,N)
C*                                                                     *
C***********************************************************************
C
      IMPLICIT REAL*8(A-H,O-Z)
      DIMENSION BETA(5)
      I=1
      TH=1.D-01
      DEL=1.D-01
   10 R1=DCOSH(TH)*DCOS(TH)-1.D+00
   20 TH=TH+DEL
      R2=DCOSH(TH)*DCOS(TH)-1.D+00
      IF(DEL .LT. 1.D-10) GO TO 40
      IF((R2*R1) .LT. 0.D+00) GO TO 30
      R1=R2
      GO TO 20
   30 TH=TH-DEL
      DEL=DEL*5.D-01
      GO TO 20
   40 BETA(I)=TH
      DEL=1.D-1
      TH=TH+DEL
      I=I+1
      IF(I .LE. N) GO TO 10
      RETURN
      END
C
C-----------------------------------------------------------------------
C|                                                                     |
C|        THIS SUBROUTINE EVALUATES THE INTEGRALS FOR THE              |
C|        COEFFICIENTS OF D12 AND D66 (BY SIMPSON'S RULE)              |
C|                                                                     |
C-----------------------------------------------------------------------
C***********************************************************************
C*                                                                     *
      SUBROUTINE CD1266(I,J,R,B,T1)
C*                                                                     *
C***********************************************************************
C
      IMPLICIT REAL*8(A-H,O-Z)
```

```
      D1(R1,X)=R1*(DCOSH(X)-DCOS(X))+DSINH(X)+DSIN(X)
      DIMENSION R(5),B(5)
      N=1.D3
      H=1./N
      A=H
      SUM=0.D+00
      DO 4 K=2,N
      ARG=B(I)*A
      ARG2=B(J)*A
      IF(MOD(K,2)) 2,2,3
    2 SUM=SUM+4.D0*D1(R(I),ARG)*D1(R(J),ARG2)
      GO TO 4
    3 SUM=SUM+2.D0*D1(R(I),ARG)*D1(R(J),ARG2)
    4 A=A+H
      T1=H*B(I)*B(J)/3.D+00*(SUM+D1(R(I),B(I))*D1(R(J),B(J)))
      RETURN
      END
C
C-----------------------------------------------------------------------
C|                                                                     |
C|       THIS SUBROUTINE EVALUATES THE INTEGRALS FOR THE               |
C|       COEFFICIENTS OF D16 AND D26 (BY SIMPSON'S RULE)               |
C|                                                                     |
C-----------------------------------------------------------------------
C**********************************************************************
C*                                                                    *
      SUBROUTINE CD1626(I,J,R,B,SUM1,SUM2)
C*                                                                    *
C**********************************************************************
C
      IMPLICIT REAL*8(A-H,O-Z)
      D0(R1,X)=R1*(DSINH(X)-DSIN(X))+DCOSH(X)-DCOS(X)
      D1(R1,X)=R1*(DCOSH(X)-DCOS(X))+DSINH(X)+DSIN(X)
      D2(R1,X)=R1*(DSINH(X)+DSIN(X))+DCOSH(X)+DCOS(X)
      DIMENSION R(5),B(5)
      N=1.D3
      H=1./N
      A=H
      SUM1=0.D+00
      SUM2=0.D+00
      DO 4 K=2,N
      ARG=B(I)*A
      ARG2=B(J)*A
      IF(MOD(K,2)) 2,2,3
    2 SUM1=SUM1+4.D0*D1(R(I),ARG)*D0(R(J),ARG2)
      SUM2=SUM2+4.D0*D2(R(I),ARG)*D1(R(J),ARG2)
      GO TO 4
    3 SUM1=SUM1+2.D0*D1(R(I),ARG)*D0(R(J),ARG2)
      SUM2=SUM2+2.D0*D2(R(I),ARG)*D1(R(J),ARG2)
    4 A=A+H
      SUM1=H*B(I)/3.D+00*(SUM1+D1(R(I),B(I))*D0(R(J),B(J)))
      SUM2=H*B(I)**2*B(J)/3.D+00*(SUM2+D2(R(I),B(I))*D1(R(J),B(J)))
      RETURN
      END
C
C-----------------------------------------------------------------------
C|                                                                     |
C|       THE FOLLOWING SOBROUTINES CALCULATE THE D-MATRIX OF THE       |
C|       PLATE                                                         |
C|                                                                     |
C-----------------------------------------------------------------------
C**********************************************************************
C*                                                                    *
      SUBROUTINE DMATRX(D,NL)
C*                                                                    *
C**********************************************************************
C
      IMPLICIT REAL*8(A-H,O-Z)
      DIMENSION Q(10,3,3),D(3,3)
```

```
      DIMENSION ANG(10),ZP(10),TH(10)
C
C-----------------------------------------------------------------------
C|                                                                      |
C|        INPUT THE DATA:                                               |
C|      - NL: NUMBER OF LAYERS.  T: THICKNESS OF EACH LAYER.            |
C|        ANG(I): ANGLES OF THE LAYUP. (DEGREE)                         |
C|                                                                      |
C-----------------------------------------------------------------------
C
      READ (5,*) NL,T
      READ (5,*) (ANG(I),I=1,NL)
      XM=NL/2.
      DO 10 I=1,NL
      ZP(I)=(I-XM-0.5D+00)*T
      TH(I)=T
   10 CONTINUE
      WRITE(6,100) (ANG(I),I=1,NL)
  100 FORMAT(///,3X,'THE STACKING SEQUENCE IS :',10(3X,F4.0))
      CALL STIFF1(Q11,Q12,Q22,Q33)
      DO 20 I=1,NL
      C=ANG(I)
   20 CALL STIFF (C,I,Q11,Q12,Q22,Q33,Q)
      DO 30 I=1,3
      DO 30 J=1,3
   30 D(I,J)=0.
      DO 40 K=1,NL
      DO 40 I=1,3
      DO 40 J=1,3
      D(I,J)=D(I,J)+Q(K,I,J)*(TH(K)*ZP(K)**2+TH(K)**3/1.2D+01)
   40 CONTINUE
      WRITE (6,200)
  200 FORMAT(//,'   THE D MATRIX IS AS FOLLOWS:' )
      WRITE (6,300) ((D(I,J),J=1,3),I=1,3)
  300 FORMAT(/,3(3X,1PD14.7))
      RETURN
      END
C
C*********************************************************************************
C*                                                                               *
      SUBROUTINE STIFF1(Q11,Q12,Q22,Q33)
C*                                                                               *
C*********************************************************************************
C
      IMPLICIT REAL*8(A-H,O-Z)
C-----------------------------------------------------------------------
C|                                                                      |
C|        INPUT THE DATA OF E1, E2, NU12, G12.                          |
C|                                                                      |
C-----------------------------------------------------------------------
      READ(5,*) E1,E2,V12,G12
      WRITE(6,100) E1,E2,V12,G12
  100 FORMAT(//,3X,'THE MATERIAL PROPERTIES ARE AS FOLLOWS: (PSI)'//
     &3X,'     E1 = ',1PD14.7,3X,'     E2 = ',D14.7/3X,'   NU12 = '
     &,D14.7,3X,'    G12 = ',D14.7//)
      V21=E2*V12/E1
      D1=1.-V12*V21
      Q11=E1/D1
      Q12=V12*E2/D1
      Q22=E2/D1
      Q33=G12
      RETURN
      END
C
C*********************************************************************************
C*                                                                               *
      SUBROUTINE STIFF(C1,I,Q11,Q12,Q22,Q33,Q)
C*                                                                               *
```

```
C*************************************************************************************
C
      IMPLICIT REAL*8(A-H,O-Z)
      DIMENSION Q(10,3,3)
      PI=DARCOS(-1.D+00)
      C=C1*PI/1.8D+02
      XM=DCOS(C)
      XN=DSIN(C)
      Q(I,1,1)=Q11*XM**4+2.D+00*(Q12+2.D+00*Q33)*(XN*XM)**2+Q22*XN**4
      Q(I,1,2)=(Q11+Q22-4.D+00*Q33)*(XN*XM)**2+Q12*(XN**4+XM**4)
      Q(I,2,2)=Q11*XN**4+2.D+00*(Q12+2.D+00*Q33)*(XN*XM)**2+Q22*XM**4
      Q(I,1,3)=(Q11-Q12-2.D+00*Q33)*XN*XM**3+(Q12-Q22+2.D+00*Q33)*XN
     &**3*XM
      Q(I,2,1)=Q(I,1,2)
      Q(I,2,3)=(Q11-Q12-2.D+00*Q33)*XN**3*XM+(Q12-Q22+2.D+00*Q33)*XN
     &*XM**3
      Q(I,3,1)=Q(I,1,3)
      Q(I,3,2)=Q(I,2,3)
      Q(I,3,3)=(Q11+Q22-2.D+00*Q12-2.D+00*Q33)*(XN*XM)**2+Q33*(XN**4
     &+XM**4)
      RETURN
      END
```

Appendix B. Finite Difference Heat Transfer Analysis

The computer coding found in Appendix B is intended to simulate the heat image generated at the vibrothermal peak frequency during a vibrothermographic test of a composite panel. It was written based upon the heat transfer analysis stated in section 2.2. An explicit finite difference approach was used to solve this heat transfer problem, and the scheme used was presented in Ref. 18.

This program was written for any layup and damage location and the nodal points can be defined as necessary and required. The heat generation is assumed to be either a constant heat input or proportional to either the displacement field or the strain field for each mode of the local resonant vibration. Which of this three to use is dependent upon the heat generation mechanism assumed. For a panel specimen, the region to be analyzed can be a small part of the panel, as long as the boundary of that region is at room temperature. The computer code used to calculate the temperature follows.

```
C-----------------------------------------------------------------------
C
C              THERMAL CONDUCTION IN COMPOSITES
C
C THIS PROGRAM IS DESIGNED TO BE USED AS A MODEL OF THE HEAT CONDUCTION
C PROBLEM SEEN WHEN A DAMAGE REGION IN A COMPOSITE IS UNDER A RESONANCE
C CONDITION.  SOLUTION OF THE HEAT CONDUCTION PROBLEM IS THROUGH AN
C EXPLICIT FINITE DIFFERENCE APPROACH
C
C-----------------------------------------------------------------------
      IMPLICIT REAL*8 (A-H,O-Z)
      REAL*8 KTH,K1,K2,K3
      DIMENSION TN(40,40),T(40,40),TD(40,40),
     &TU(40,40),TNEW(10,40,40),TOLD(10,40,40),
     &THET(10),KTH(3,3,10),RX(10),RY(10),
     &RXY(10),RU(10),RD(10),LHOT(10),Q(10,40,40),
     &IHOT(10,100),JHOT(10,100),POS(40,40,2),B(5),R(5)
C-----------------------------------------------------------------------
C
C INPUT AND CONDITION MATERIAL AND GRID PROPERTIES
C
C NS = 0 SYMMETRIC TO DELAMINATION, N = 1/2 OF THE NO. OF LAYERS
C    = 1 NOT SYMMETRIC TO DELAMINATION, N = NO. OF LAYERS
C MODE = 0, HEAT INPUT IS UNIFORM
C        1, HEAT INPUT IS PROPORTIONAL TO A FUNCTION INPUTED
C XT, YT: TOTAL LENGTH IN X AND Y DIRECTION
C MX, MY: TOTAL NO. OF NODE IN X AND Y DIRECTION
C NBNDYT, NBNTYB, NBNTYL, NBNTYR
C = 1, HEAT CONVECTION BOUNDARY CONDITION
C = 2, BOUNDARY TEMPERATURE IS ROOM TEMPERATURE
C TR: ROOM TEMPERATURE
C NF: MAX NO OF ITERATION TO BE PERFORM
C ERR: CHECK FOR THE STEADY STATE
C
C-----------------------------------------------------------------------
      READ(5,*) N,NS
      READ(5,*) XT,YT,MX,MY,MODE
      READ(5,*) NBNDYT,NBNDYB,NBNDYL,NBNDYR,TR
      DX=XT/(MX-1)
      DY=YT/(MY-1)
      DO 20 I=1,MX
      DO 20 J=1,MY
      POS(I,J,1)=(I-1)*DX
      POS(I,J,2)=(J-1)*DY
   20 CONTINUE
      READ(5,*) NF,ERR
      DO 30 I=1,3
      DO 30 J=1,3
      DO 30 K=1,N
   30 KTH(I,J,K)=0.D0
      DO 40 K=1,N
      DO 40 I=1,MX
      DO 40 J=1,MY
      Q(K,I,J)=0.D0
   40 TOLD(K,I,J)=TR
      READ(5,*) THK,K1,K2,K3,H,RHO,CP
      WRITE(6,230) THK,DX,DY,K1,K2,K3,H,RHO,CP
  230 FORMAT(//,23X,'THK',14X,'DX',14X,'DY',/,23X,'(CM)',12X,'(CM)',
     &12X,'(CM)',//,15X,3(1PD16.5),///,24X,'K1',14X,'K2',14X,'K3',/,17X,
     &'(CAL/C-CM-SEC)',2X,'(CAL/C-CM-SEC)',2X,'(CAL/C-CM-SEC)',//,15X,3D
     &16.5,///,24X,'H',14X,'RHO',14X,'CP',/,16X,'(CAL/C-CM**2-SEC)',3X,'
     &(G/CM**3)',7X,'(CAL/C-G)',//,15X,3D16.5)
      C1=THK*DX*DY*RHO*CP
C-----------------------------------------------------------------------
C
C INPUT LAYUP AND HEAT GENERATION INFORMATION
C
C THET: THE ANGLE OF EACH LAYUP
C QHEAT: THE COEFFICIENT OF THE HEAT INPUT
```

```
C LHOT: THE NUMBER OF DAMAGED GRID POINTS IN EACH LAYER
C IHOT AND JHOT: LOCATION OF THE NODE OF THE DAMAGE IN EACH LAYER
C
C-----------------------------------------------------------------------
      READ(5,*) (THET(I),I=1,N),QHEAT,(LHOT(K),K=1,N)
      DO 50 K=1,N
      IF(LHOT(K) .NE. 0) THEN
      LH=LHOT(K)
      READ(5,*)(IHOT(K,L),JHOT(K,L),L=1,LH)
      END IF
   50 CONTINUE
      WRITE(6,250) (THET(I),I=1,N)
  250 FORMAT(//,20X,'LAYUP',5X,4(F8.1)/)
C-----------------------------------------------------------------------
C
C FORM THERMAL CONDUCTIVITY MATRICES AND THERMAL RESISTANCES
C
C-----------------------------------------------------------------------
      PI=DARCOS(-1.D0)
      DO 60 I=1,N
      THET(I)=PI/180.D0*THET(I)
      C=DCOS(THET(I))
      S=DSIN(THET(I))
      KTH(1,1,I)=C*C*K1+S*S*K2
      KTH(1,2,I)=C*S*K1-C*S*K2
      IF(DABS(KTH(1,2,I)) .LT. 1.D-10) KTH(1,2,I)=1.D-50
      KTH(2,1,I)=KTH(1,2,I)
      KTH(2,2,I)=S*S*K1+C*C*K2
      KTH(3,3,I)=K3
      RX(I)=DX/(KTH(1,1,I)*DY*THK)
      RY(I)=DY/(KTH(2,2,I)*DX*THK)
      RXY(I)=2.D0/(KTH(1,2,I)*THK)
      RU(I)=THK/(KTH(3,3,I)*DX*DY)
   60 RD(I)=RU(I)
      RU(1)=1.D0/(H*DX*DY)
      IF(NS .NE. 0) THEN
      RD(N)=RU(1)
      ENDIF
      RC=1.D0/(H*THK*DX)
      WRITE(6,270)
  270 FORMAT(///,13X,'LAYER',11X,'KXX',15X,'KYY',15X,'KXY',15X,'KZZ',//)
      DO 70 I=1,N
   70 WRITE(6,280)I,KTH(1,1,I),KTH(2,2,I),KTH(1,2,I),KTH(3,3,I)
  280 FORMAT(15X,I1,3X,4(1PD18.6)/)
      WRITE(6,240) QHEAT
  240 FORMAT(//10X,'THE HEAT GENERATION COEFFICIENT OF THE DAMAGE SITES
     &IS',1PD8.2,' CAL/SEC',/)
C-----------------------------------------------------------------------
C
C CALCULATE THE TIME INCREMENT TO BE USED IN THE ITERATIONS
C AND THE HEAT GENERATION AT DAMAGE SITE FOR EACH LAYER
C
C-----------------------------------------------------------------------
      CALL DTAU(C1,RC,RX,RY,RU,RD,DT,N)
      DO 75 K=1,N
      NHOT=LHOT(K)
      IF(NHOT .NE. 0) THEN
      CALL THOT(Q,NHOT,IHOT,JHOT,QHEAT,MODE,K)
      END IF
   75 CONTINUE
C-----------------------------------------------------------------------
C
C NIT IS THE TOTAL NUMBER OF ITERATIONS PERFORMED AT STEADY STATE
C
C-----------------------------------------------------------------------
      NIT=1
C-----------------------------------------------------------------------
C
C CALCULATE NEW TEMPERATURE PATTERNS
```

```
C                                                                       |
C-----------------------------------------------------------------------
  80  DO 130 II=1,N
      K=N-II+1
      DO 100 I=1,MX
      DO 100 J=1,MY
      T(I,J)=TOLD(K,I,J)
      IF(K .EQ. 1) THEN
      TU(I,J)=TR
      ELSE
      TU(I,J)=TOLD(K-1,I,J)
      END IF
      IF(K .EQ. N) THEN
      IF(NS .NE. 0) THEN
      TD(I,J)=TR
      ELSE
      TD(I,J)=T(I,J)
      ENDIF
      ELSE
      TD(I,J)=TOLD(K+1,I,J)
      END IF
 100  CONTINUE
      CALL COMCON(TN,T,RX(K),RY(K),RXY(K),RU(K),RD(K),RC,TU,TD,Q,
     &DT,C1,K,MX,MY,TR)
      DO 120 I=1,MX
      DO 120 J=1,MY
 120  TNEW(K,I,J)=TN(I,J)
 130  CONTINUE
      IF(NIT .GE. NF) THEN
      WRITE(6,300) NIT
 300  FORMAT(//5X,'IT HASN''T REACHED THE STEADY STATE AFTER',I5,
     &' ITERATIONS.'//)
      WRITE(6,200)
 200  FORMAT(//38X,'SURFACE TEMPERATURE PATTERN',///)
      WRITE(6,210) ((TNEW(1,I,J),J=1,MY),I=1,MX)
 210  FORMAT(10X,10F8.3//)
      STOP
      END IF
      DO 140 K=1,N
      DO 140 I=1,MX
      DO 140 J=1,MY
      IF((TNEW(K,I,J)-TOLD(K,I,J)) .GT. ERR) GO TO 150
 140  CONTINUE
      TIME=DT*NIT
      WRITE(6,200)
      DO 185 I=1,MX
      DO 185 J=1,MY
 185  WRITE(6,290) POS(I,J,1),POS(I,J,2),TOLD(1,I,J)
      IF(NS .NE. 0) THEN
      DO 187 I=1,MX
      DO 187 J=1,MY
 187  WRITE(7,290) POS(I,J,1),POS(I,J,2),TOLD(N,I,J)
 290  FORMAT(10X,3F8.3)
      ENDIF
      WRITE(6,220) DT,NIT,TIME
 220  FORMAT(///,10X,'DT=',1PD13.6//'IT REACHES STEADY STATE AFTER',
     &I5,' ITERATIONS',//'TOTAL TIME =',D13.6,' SEC'/)
      STOP
 150  DO 160 K=1,N
      DO 160 I=1,MX
      DO 160 J=1,MY
 160  TOLD(K,I,J)=TNEW(K,I,J)
 170  NIT=NIT+1
      GO TO 80
      END
C
C*************************************************************************************
C                                                                                    *
      SUBROUTINE COMCON(TN,T,RX,RY,RXY,RU,RD,RC,TU,TD,Q,
```

```
     &DT,C1,K,MX,MY,TR)
C                                                                              *
C*******************************************************************************
C
      IMPLICIT REAL*8 (A-H,O-Z)
      DIMENSION TN(40,40),T(40,40),TD(40,40),TU(40,40),Q(10,40,40)
      C=C1
      C2=C/2.D0
      C4=C/4.D0
C-------------------------------------------------------------------------
C                                                                        |
C SOLVE FOR NEW TEMPERATURES AT THE CORNERS                              |
C                                                                        |
C-------------------------------------------------------------------------
      C=C4
      IF(NBNDYT .EQ. 2  .AND.  NBNDYL .EQ. 2) THEN
      TN(1,1)=TR
      ELSE
      TN(1,1)=T(1,1)+DT/C*((TR-T(1,1))/2.D0/RC
     &+(T(1,2)-T(1,1))/2.D0/RY+(T(2,1)
     &-T(1,1))/2.D0/RX+(TU(1,1)-T(1,1))/4.D0/RU
     &+(TD(1,1)-T(1,1))/4.D0/RD+Q(K,1,1))
      END IF
      IF(NBNDYT .EQ. 2  .AND.  NBNDYR .EQ. 2) THEN
      TN(1,MY)=TR
      ELSE
      TN(1,MY)=T(1,MY)+DT/C*((T(1,MY-1)-T(1,MY))/2.D0/RY
     &+(TR-T(1,MY))/2.D0/RC+(T(2,MY)
     &-T(1,MY))/2.D0/RX+(TU(1,MY)-T(1,MY))/4.D0/RU
     &+(TD(1,MY)-T(1,MY))/4.D0/RD+Q(K,1,MY))
      END IF
      IF(NBNDYL .EQ. 2  .AND.  NBNDYB .EQ. 2) THEN
      TN(MX,1)=TR
      ELSE
      TN(MX,1)=T(MX,1)+DT/C*((TR-T(MX,1))/2.D0/RC
     &+(T(MX,2)-T(MX,1))/2.D0/RY+(T(MX-1,2)
     &-T(MX,1))/2.D0/RX+(TU(MX,1)-T(MX,1))/4.D0/RU
     &+(TD(MX,1)-T(MX,1))/4.D0/RD+Q(K,MX,1))
      ENDIF
      IF(NBNDYB .EQ. 2  .AND.  NBNDYR .EQ. 2) THEN
      TN(MX,MY)=TR
      ELSE
      TN(MX,MY)=T(MX,MY)+DT/C*((T(MX,MY-1)-T(MX,MY))/2.D0/RY
     &+(TR-T(MX,MY))/2.D0/RC+(T(MX-1,MY)
     &-T(MX,MY))/2.D0/RX+(TU(MX,MY)-T(MX,MY))/4.D0/RU
     &+(TD(MX,MY)-T(MX,MY))/4.D0/RD+Q(K,MX,MY))
      END IF
C-------------------------------------------------------------------------
C                                                                        |
C SOVLE FOR NEW TEMPERATURES ALONG THE SIDES                             |
C                                                                        |
C-------------------------------------------------------------------------
      MMX=MX-1
      MMY=MY-1
      C=C2
      DO 60 I=2,MMX
      IF(NBNDYL .EQ. 2) THEN
      TN(I,1)=TR
      ELSE
      TN(I,1)=T(I,1)+DT/C*((TR-T(I,1))/RC
     &+(T(I,2)-T(I,1))/RY+(T(I+1,1)+T(I-1,1)
     &-2.D0*T(I,1))/2.D0/RX+(TU(I,1)-T(I,1))/2.D0/RU
     &+(TD(I,1)-T(I,1))/2.D0/RD+(T(I-1,2)
     &-T(I+1,2))/2.D0/RXY+Q(K,I,1))
      END IF
      IF(NBNDYR .EQ. 2) THEN
      TN(I,MY)=TR
      ELSE
      TN(I,MY)=T(I,MY)+DT/C*((T(I,MY-1)-T(I,MY))/RY
```

```
     &+(TR-T(I,MY))/RC+(T(I+1,MY)+T(I-1,MY)
     &-2.D0*T(I,MY))/2.D0/RX+(TU(I,MY)-T(I,MY))/2.D0/RU
     &+(TD(I,MY)-T(I,MY))/2.D0/RD+(T(I+1,MY-1)
     &-T(I-1,MY-1))/2.D0/RXY+Q(K,I,MY))
      END IF
  60  CONTINUE
      DO 80 I=2,MMY
      IF(NBNDYT .EQ. 2) THEN
      TN(1,I)=TR
      ELSE
      TN(1,I)=T(1,I)+DT/C*((T(1,I-1)+T(1,I+1)
     &-2.D0*T(1,I))/2.D0/RY+(T(2,I)-
     &T(1,I))/RX+(TU(1,I)-T(1,I))/2.D0/RU+(TD(1,I)
     &-T(1,I))/2.D0/RD+(T(2,I-1)-T(2,I+1))
     &/2.D0/RXY+Q(K,1,I))
      END IF
      IF(NBNDYB .EQ. 2) THEN
      TN(MX,I)=TR
      ELSE
      TN(MX,I)=T(MX,I)+DT/C*((T(MX,I-1)+T(MX,I+1)
     &-2.D0*T(MX,I))/2.D0/RY+(T(MX-1,I)
     &-T(MX,I))/RX+(TU(MX,I)-T(MX,I))/2.D0/RU
     &+(TD(MX,I)-T(MX,I))/2.D0/RD+(T(MX-1,I+1)-T(MX-1,I-1))
     &/2.D0/RXY+Q(K,MX,I))
      END IF
  80  CONTINUE
C-----------------------------------------------------------------------
C                                                                       |
C SOLVE FOR NEW TEMPERATURES IN THE INTERIOR OF THE LAYER               |
C                                                                       |
C-----------------------------------------------------------------------
      C=C1
      DO 90 I=2,MMX
      DO 90 J=2,MMY
  90  TN(I,J)=T(I,J)+DT/C*((T(I,J+1)+T(I,J-1)
     &-2.D0*T(I,J))/RY+(T(I+1,J)+T(I-1,J)-2.D0
     &*T(I,J))/RX+(TU(I,J)-T(I,J))/RU+(TD(I,J)
     &-T(I,J))/RD+(T(I-1,J+1)+T(I+1,J-1)-T(I-1,J-1)
     &-T(I+1,J+1))/RXY+Q(K,I,J))
      RETURN
      END
C
C*************************************************************************
C                                                                       *
      SUBROUTINE DTAU(CP,RC,RX,RY,RU,RD,DTIM,N)
C                                                                       *
C*************************************************************************
C
      IMPLICIT REAL*8 (A-H,O-Z)
      DIMENSION RX(10),RY(10),RU(10),RD(10),SR(10),DT(10)
      DO 10 I=1,N
      SR(I)=1.D0/RC+1.D0/RX(I)+1.D0/RY(I)+.5D0/RU(I)+.5D0/RD(I)
  10  DT(I)=CP/2.D0/SR(I)
      DTIM=DT(1)
      DO 20 I=2,N
      IF(DTIM .GT. DT(I)) DTIM=DT(I)
  20  CONTINUE
C-----------------------------------------------------------------------
C                                                                       |
C TO AVOID STABILITY PROBLEMS, WORK WITH ONLY EIGHTY PER CENT OF THE    |
C CALCULATED TIME INTERVAL                                              |
C                                                                       |
C-----------------------------------------------------------------------
      DTIM=.8D0*DTIM
      RETURN
      END
C
C*************************************************************************
C                                                                       *
```

```
      SUBROUTINE THOT(Q,NHOT,IHOT,JHOT,QHEAT,MODE,K)
C                                                                              *
C*******************************************************************************
C
      IMPLICIT REAL*8(A-H,O-Z)
      DIMENSION Q(10,40,40),IHOT(10,100),JHOT(10,100)
C-------------------------------------------------------------------------------
C                                                                              |
C PROVIDE FOR HEAT GENERATION AT THE DAMAGED SITES                             |
C                                                                              |
C-------------------------------------------------------------------------------
      IF(MODE .EQ. 0) THEN
      DO 10 I=1,NHOT
   10 Q(K,IHOT(K,I),JHOT(K,I))=QHEAT
      ELSE
      READ(5,*) (Q(K,IHOT(K,I),JHOT(K,I)),I=1,NHOT)
      DO 20 I=1,NHOT
      Q(K,IHOT(K,I),JHOT(K,I))=DABS(QHEAT*Q(K,IHOT(K,I),JHOT(K,I)))
   20 CONTINUE
      ENDIF
      RETURN
      END
```

The vita has been removed from the scanned document